This dissertation has been
microfilmed exactly as received 68-15,390

TOKARZ, Frank Joseph, 1937-
LATERAL-TORSIONAL BUCKLING OF ARCHES.

The Ohio State University, Ph.D., 1968
Engineering, civil

University Microfilms, Inc., Ann Arbor, Michigan

LATERAL-TORSIONAL BUCKLING

OF ARCHES

DISSERTATION

Presented in Partial Fulfillment of the Requirements for the Degree Doctor of Philosophy in the Graduate School of The Ohio State University

By

Frank Joseph Tokarz, B.S.,M.S.

****

The Ohio State University
1968

Approved by

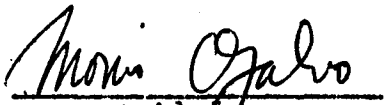

Adviser
Department of Civil Engineering

ACKNOWLEDGMENTS

This dissertation was made possible through an Engineering Fellowship provided by the American Iron and Steel Institute and a Research Assistantship provided by the Civil Engineering Department of The Ohio State University to whom I am gratefully indebted. I am also indebted to The Ohio State University Computer Center for donating the computer time required for the theoretical computations.

I wish to express my appreciation to my adviser, Dr. M. Ojalvo, for suggesting the problem considered in this dissertation and for his advice and criticism throughout the course of this study.

Thanks are extended to Messrs. A. V. Bernardo, E. E. Egbert and A. S. Holbein, all members of the Civil Engineering Department Machine Shop, for their assistance in the construction of the equipment used in the experimental investigations.

Finally, I want to thank my wife, Suzanne, for typing this manuscript and for her patience and encouragement throughout this program of graduate study.

VITA

1937	Born on September 23, Shadyside, Ohio
1960	B.S. Civil Engineering The Ohio State University, Columbus, Ohio
1960-1961	Design Engineer, General Dynamics/Astronautics San Diego, California
1961-1964	Structural Analyst, Boeing Airplane Company Renton, Washington
1964	M.S. Civil Engineering University of Washington, Seattle, Washington
1964	Structural Analyst, Ling-Temco-Vought Grand Praire, Texas
1965	Structural Analyst, Douglas Aircraft Company Long Beach, California
1965-1968	Research Assistant and A.I.S.I. Fellowship Recipient, The Ohio State University, Columbus, Ohio

FIELD OF STUDY

Major Field: Structural Engineering

Studies in Structural Engineering. Professors M. Ojalvo, S. Sergev and B.J.Hartz

Studies in Engineering Mechanics. Professor P.E. Korda

Studies in Mathematics. Professors S. Drobot, R.G. Helsel and H.D. Colson

TABLE OF CONTENTS

		Page
ACKNOWLEDGMENTS		ii
VITA		iii
LIST OF TABLES		v
LIST OF ILLUSTRATIONS		vi
NOMENCLATURE		xi
Chapter		
I	INTRODUCTION	1
II	EXPERIMENTAL TESTS Test Set-up Model Arches End Supports Restraints Application of Loads Testing Procedure	9
III	EXPERIMENTAL RESULTS Calculation of Buckling Loads Discussion of Results	26
IV	THEORETICAL SOLUTIONS OF BUCKLING LOADS	37
V	COMPARISON OF THEORETICAL AND EXPERIMENTAL BUCKLING LOADS	48
VI	SUMMARY AND CONCLUSIONS	51
APPENDIX A	TEST DATA	55
APPENDIX B	" $\bar{\beta}$ " TEST	91
BIBLIOGRAPHY		98

LIST OF TABLES

Table		Page
1.	Lateral-torsional buckling loads obtained from the free standing arch tests.....	30
2.	Lateral-torsional buckling loads obtained from the restrained arch tests.....	31
3.	Some theoretical and experimental lateral-torsional buckling loads for comparison.....	49

LIST OF ILLUSTRATIONS

Figure		Page
1.	General arrangement of testing equipment....	10
2.	Test set-up for free standing arches subjected to vertical loads.....	12
3.	Test set-up for free standing arches subjected to tilt loads.....	12
4.	Test set-up for uniformly restrained arches.	13
5.	Test set-up for crown restrained arches (rigid restraining bar).....	13
6.	Arrangement showing fixed end supports for restrained arch tests.....	16
7.	Arrangement showing hinged end supports for restrained arch tests.....	16
8.	Profile view of displaced arch centerline indicating coordinate system.....	17
9.	Round restraining bar shown in both undeflected and laterally deflected positions.	18
10.	Typical hanger to arch attachment.....	20
11.	Sketches illustrating load application for free standing arch tests.....	21
12.	Sketches illustrating vertical loads application for restrained arch tests.....	22
13.	Typical load-deflection and Southwell plots used to predict lateral-torsional buckling loads (Test No. 1).....	28

Figure		Page
14.	Free standing arch subjected to vertical loads shown in a deflected position.....	33
15.	Free standing arch subjected to tilt loads shown in a deflected position.....	33
16.	Crown restrained arches (rigid restraining bar) subjected to vertical loads shown in a deflected position.....	34
17.	Uniformly restrained arches subjected to vertical loads shown in a deflected position.....	34
18.	Diagram illustrating the deflected shapes of the arch in Test No. 13 at three stages of loading.....	35
19.	Actual deflected position of the arch in Test No. 13 at maximum applied load, Q = 2.76 pounds/inch.....	35
20.	Drawing illustrating the positive sense of forces, curvatures and twist, displacements and axes on a displaced segment of the member.....	39
21.	Load-deflection and Southwell plots for Test No. 1.....	56
22.	Load-deflection and Southwell plots for Test No. 2	57
23.	Load-deflection and Southwell plots for Test No. 3	58
24.	Load-deflection and Southwell plots for Test No. 4	59
25.	Load-deflection and Southwell plots for Test No. 5	60
26.	Load-deflection and Southwell plots for Test No. 6	61

Figure		Page
27.	Load-deflection and Southwell plots for Test No. 7	62
28.	Load-deflection and Southwell plots for Test No. 8	63
29.	Load-deflection and Southwell plots for Test No. 9	64
30.	Load-deflection and Southwell plots for Test No. 10	65
31.	Load-deflection and Southwell plots for Test No. 11	66
32.	Load-deflection and Southwell plots for Test No. 12	67
33.	Load-deflection plots for Test No. 13	68
34.	Load-deflection and Southwell plots for Test No. 14	69
35.	Load-deflection and Southwell plots for Test No. 15	70
36.	Load-deflection and Southwell plots for Test No. 16	71
37.	Load-deflection and Southwell plots for Test No. 17	72
38.	Load-deflection and Southwell plots for Test No. 18	73
39.	Load-deflection and Southwell plots for Test No. 19	74
40.	Load-deflection and Southwell plots for Test No. 20	75
41.	Load-deflection and Southwell plots for Test No. 21	76

Figure		Page
42.	Load-deflection and Southwell plots for Test No. 22	77
43.	Load-deflection and Southwell plots for Test No. 23	78
44.	Load-deflection and Southwell plots for Test No. 24	79
45.	Load-deflection and Southwell plots for Test No. 25	80
46.	Load-deflection and Southwell plots for Test No. 26	81
47.	Load-deflection and Southwell plots for Test No. 27	82
48.	Load-deflection and Southwell plots for Test No. 28	83
49.	Load-deflection and Southwell plots for Test No. 29	84
50	Load-deflection and Southwell plots for Test No. 30	85
51.	Load-deflection and Southwell plots for Test No. 31	86
52.	Load-deflection and Southwell plots for Test No. 32	87
53.	Load-deflection and Southwell plots for Test No. 33	88
54.	Load-deflection and Southwell plots for Test No. 34	89
55.	Load-deflection and Southwell plots for Test No. 35	90
56.	Theoretically calculated deflection, slope of deflection and angle of twist curves for an arch described by Test No. 25	92

Figure Page

57. Arrangement of instrumentation used to facilitate the experimental calculation of the angle of twist 94

58. Profile view of arch centerline showing rotations of Points A and B 95

NOMENCLATURE

A	Flexural stiffness of the arch cross-section about the x axis
B	Flexural stiffness of the arch cross-section about the y axis
C	Torsional stiffness of the arch cross-section about the z axis
d	Distance fron mirror to transit and graph mounted on board
D	Vertical distance between chord line joining the end supports and the neutral axis of the arch cross-section
D_b	Flexural stiffness of the restraining bar
$G, G_o, \bar{G}$	Internal couple about the x axis; final state, loaded but unbuckled state, increment as the result of buckling
$G', G'_o, \bar{G}'$	Internal couple about the y axis; final state, loaded but unbuckled state, increment as the result of buckling
$H, H_o, \bar{H}$	Height of the arch or internal couple about the z axis; final state, loaded but unbuckled state, increment as the result of buckling
H/L	Height-span ratio of arch
$K, K_o, \bar{K}$	Magnitude of applied restraint ($K=6D_b/L_b$) or externally distributed couple about the x axis; final state, loaded but unbuckled state, increment as the result of buckling
$K', K'_o, \bar{K}'$	Externally distributed couple about the y axis; final state, loaded but unbuckled state, increment as the result of buckling
KL/C	Magnitude of applied restraint in non-dimensional form

L	Arch span
L_b	Spacing between the pair of arches for the restrained tests
M	External couple supplied by restraining bar ($M=K\alpha$)
$N, N_o, \bar{N}$	Shear directed parallel to the x axis; final state, loaded but unbuckled state, increment as the result of buckling
$N'_o, N'_o, \bar{N}'$	Shear directed parallel to the y axis; final state, loaded but unbuckled state, increment as the result of buckling
Q	Uniform arch load (force per unit length of span)
QCR	Uniform lateral-torsional buckling load (force per unit length of span)
R_h (R_h^a, R_h^b)	Rotation of mirror about a horizontal axis (at points A and B, respectively)
R_v (R_v^a, R_v^b)	Rotation of mirror about a vertical axis (at points A and B, respectively)
s	Distance coordinate measured along the centriodal axis of the member
$T, T_o, \bar{T}$	Internal normal force; final state, loaded but unbuckled state, increment as the result of buckling
$u, u_o, \bar{u}$	Displacement measured parallel to the undeflected x axis; final state, loaded but unbuckled state, increment as the result of buckling
$v, v_o, \bar{v}$	Displacement measured parallel to the undeflected y axis; final state, loaded but unbuckled state, increment as the result of buckling
$w, w_o, \bar{w}$	Displacement measured parallel to the undeflected z axis; final state, loaded but unbuckled state, increment as the result of buckling
x, y, z	Orthogonal reference axes associated with the deflected curve

$X, X_o, \bar{X}$	Externally distributed load parallel to the x axis; final state, loaded but unbuckled state, increment as the result of buckling
$Y, Y_o, \bar{Y}$	Externally distributed load parallel to the y axis; final state, loaded but unbuckled state, increment as the result of buckling
$Z, Z_o, \bar{Z}$	Externally distributed load parallel to the z axis; final state, loaded but unbuckled state, increment as the result of buckling
α	Rotation of the ends of the restraining bars
$\beta, \beta_o, \bar{\beta}$ (β^a, β^b)	Angle of twist of the arch cross-section about the z axis; final state, loaded but unbuckled state, increment as the result of buckling (at the points A and B, respectively)
k', k'_o	Curvatures about the x axis for the deflected and the undeflected curves, respectively
k', k'_o	Curvatures about the y axis for the deflected and the undeflected curves, respectively
Δ	Lateral deflection of the model arch (measured at the crown of the arch unless specified otherwise)
Δ_v, Δ_h	Changes from the undeflected arch readings of the reflected positions of the "dots" on the graph paper in the vertical and horizontal directions, respectively
$\lambda, \lambda_{cr}, \Delta\lambda$	Buckling parameter ($\lambda = QL^3/A$), buckling parameter associated with the lateral-torsional buckling load, increment of buckling parameter
$\theta, \theta_o, \bar{\theta}$	Externally distributed couple about the z axis; final state, loaded but unbuckled state, increment as the result of buckling
(ϕ^a, ϕ^b)	Arctangent of the slope of the undeflected arch (at points A and B, respectively)
τ, τ_o	Twist about the z axis for the deflected and the undeflected curves, respectively

CHAPTER I

INTRODUCTION

A member which has the shape of a plane curve in its undeformed state may buckle out of its plane when a system of planar loads are applied to it. Because this buckling usually produces twist about the longitudinal axis as well as lateral deflection, it is called "lateral-torsional buckling". Henceforth, any reference to buckling or stability will imply the aforementioned buckling behavior. The load that is required to maintain the member in such a deflected and twisted position is called the critical or lateral-torsional buckling load.

Such members are susceptible toward lateral-torsional buckling when (1) the member is not laterally supported along its length and (2) the flexural stiffness of the member about its principal axis in the plane of the member is small in comparison with the flexural stiffness about the other principal axis.

Lateral-torsional buckling may occur long before member stresses due to flexure and/or thrust exceed the proportional limit of the material. A member designed to meet a specific

stress requirement does not usually fail should the allowable stresses be moderately exceeded. However, should the buckling load be exceeded the same member would either fail catastrophically or develope unacceptably large deflections. It is for this reason that buckling loads should be known precisely.

Hencky[1*] and Timoshenko[2] derived theoretical solutions for buckling of circular rings with uniform radial loads. Buckling equations are derived from the equilibrium equations of a displaced segment of the ring. In Hencky's deriviation, the radial loads are assumed to change direction during buckling so that they are always directed towards the center of initial curvature. Timoshenko assumed that the directions of the loads do not change during buckling and that they are displaced laterally only.

Timoshenko[3] developed theoretical solutions for the buckling of circular bars with equal end couples. Solutions were obtained using the approach discussed in the previous paragraph.

Goldberg and Bodganoff[4] presented a theory of buckling for circular rings of constant I cross-section subjected to a uniform radial loading. Buckling solutions are obtained from a set of derived differential equations.

*Superscribed number indicates the corresponding reference in Bibliography.

Ostlund[5] presented a method for investigating the lateral stability of a connected pair of arches. The arches and connecting members are treated in the theory as a space frame made of straight line segments. His investigations included experimental work.

Stussi[6] presented a method for the determination of the buckling loads of parabolic arches subjected to uniform vertical loads. He established a numerical procedure for determining rotations and displacements at successive points on the arch and used this procedure in conjunction with the method of Engesser-Vianello to obtain natural frequencies and buckling loads. The theoretical results were substantiated by tests.

Godden[7] determined the buckling loads of tied arch ribs of parabolic profile. The tied arch ribs are comprised of an arch, vertical hangers having no bending stiffness, and of a laterally rigid bar extending between the two end supports. The hangers are tied to the arch at their upper ends and to the rigid bar at their lower ends. As the arch deflects the hangers become inclined. The arches are assumed to be loaded with horizontal thrust at the end supports, and the distance between end supports is allowed to shorten as the arch deflects laterally. It is also assumed that the hangers developed a uniform tension per unit length of span equal to the horizontal thrust multiplied by $8H/L^2$. H and L

are the height and span of the arch, respectively. The theoretical solutions are based on Rayleigh's Principal and are substantiated experimentally. In the experimental work, the arches were loaded as the theory implied, i.e. by a horizontal loads at a movable end support.

Fukasawa[8] developed theoretical solutions for the buckling of circular arches subjected to uniform radial loads (which may or may not change direction as the arch deflects laterally). He used the potential energy approach to obtain solutions. The warping-torsion of the cross-section is considered. Experimental work is included in his investigation.

Layrangues[9,10] determined the buckling loads of free standing circular arches and of pairs of circular arches which were connected by a continuous system of bracing. The arches were subjected to uniform radial and uniform lateral loads. Equilibrium equations expressed in terms of deformations and force-displacement relations were established and solved. The solutions were then examined to determine what value of radial loading would make either the deformations or the internal forces approach infinity in magnitude. This value was defined as the critical buckling load.

Dabrowski[11] developed theoretical solutions for the buckling of arches, either circular with radial hangers or parabolic with vertical hangers. In the latter case, a constant normal force and a constant mean radius of curvature

were assumed. Loads were applied through hangers having bending stiffness. The theoretical solutions were obtained by developing and solving two governing differential equations. These two equations were derived for a curved bar uniformly loaded in its plane.

References 1 through 11 include all contributions to the subject of lateral-torsional buckling of curved members known to the writer. The present status may be summarized as follows: a limited number of theoretical solutions based upon a linear theory of buckling are available. Experimental verification is limited to the works of Stussi, Godden, Ostlund, and Fukasawa. It was felt that additional theoretical solutions should be developed and that these and older solutions should be verified by an extensive program of testing.

The primary objectives of this dissertation are:

(1) TO CONDUCT EXPERIMENTAL INVESTIGATIONS OF ARCHES FOR THE PURPOSE OF DETERMINING LATERAL-TORSIONAL BUCKLING LOADS.

(2) TO OBTAIN THEORETICAL SOLUTIONS FOR LATERAL-TORSIONAL BUCKLING LOADS.

(3) TO COMPARE SOME OF THE EXPERIMENTAL RESULTS WITH AVAILABLE SOLUTIONS BASED UPON THE LINEAR THEORY OF BUCKLING.

In the following discussion certain terms will be used to describe the manner of loading, the end supports, and the

restraints. The definitions of these terms are found in Chapter II where they first appear.

Thirty-five tests are reported. In Tests No. 1 thru No. 13 the arches are free standing. In Tests No. 14 thru No. 35 they are restrained.

A free standing arch is one which is supported only at its ends. A restrained arch has external restraint supplied to the arch between its end supports.

The free standing tests can be divided according to the manner of load application. In Tests No. 1 thru 7 the load is always vertical. In Tests No. 8 thru No. 13 the load which is originally vertical and in the original plane of the arch, tilts with the onset of lateral displacement.

All restrained arch tests were conducted with vertical loading. Tests No. 14 thru No. 26 have a single lateral restraining bar at the crown of the arch, whereas in Tests No. 27 thru No. 35 the arches have fifteen equally spaced lateral bars.

Two types of end supports are employed in the arch tests. These are fixed end supports and hinged end supports.

The lateral deflection of the model arch is observed in each test and the critical buckling load is predicted by means of either a Southwell plot or a load-deflection plot. The plots are discussed later in detail.

The tests explore the effects of the following factors: (1) the shape of the arch, (2) the height-span ratio (H/L) of the arch, (3) the flexural stiffness of the restraining bars, (4) the distribution of restraint, (5) the type of end supports, and (6) the type of loading.

Restrained arches with tilt loading simulate actual bridge arches with lateral bracing between them and a stiff roadway above or below the arches.

Theoretical solutions for the lateral buckling loads of parabolic arches are developed* from three of Kirchhoff's six equations of equilibrium for naturally curved and twisted rods. The solutions obtained are for free standing parabolic arches and arches laterally restrained at the crown only. The loads considered are uniform vertical and uniform tilt loads. Solutions are obtained for both fixed and hinged type end supports.

A pair of governing equations are used for the theoretical solutions. The following assumptions and approximations are made.

(1) The arches are made of a linear elastic material.

(2) The proportional limit of the arch is never exceeded.

(3) Displacements occuring in the loaded arches are small so that internal forces just prior to the onset of

*Refer to footnote on page 37.

buckling may be computed on the basis of the undeformed shape.

(4) The displacement of the arch at buckling are subjected to the condition that the centerline is inextensible.

(5) Initial radii of curvature are large compared to cross-sectional dimensions so that flexural-curvature and torsional-twist relationships are analogous to the Bernoulli-Euler relationships are applicable.

(6) The flexural and torsional stiffnesses of the cross-section are constant throughout the arch.

(7) In the undeformed state the member has no twist about the logitudinal axis and one principal axis of the cross-section is in the pre-buckling plane of the arch.

(8) The contribution to the torsional stiffness arising from warping torsional restraint is negligible.

(9) The centroid and shear center coincide.

Tables 1 and 2 summarize all of the experimental values obtained for the buckling loads.

Table 3 provides a comparison of experimental and theoretical results. The theoretical solutions obtained by this author are based upon Equations (9) of Chapter IV.

A special test was conducted to verify the variation of the angle of twist ($\bar{\beta}$) based on the theoretical considerations of Chapter IV. Refer to Appendix B.

CHAPTER II

EXPERIMENTAL TESTS

Test Set-up

The general arrangement of testing equipment is shown in Figure 1. The frame was of welded construction using 3 and 4 inch structural steel channels and angles. It was a rigid assembly which provided a means of securing the prescribed arch end support conditions and also permitted the hanging of cannisters from the arch into a water tank below. When the tank was filled with water to a predetermined level it provided a necessary depth of water so that the bottom of the loading cannisters could be submerged approximately 13 inches. This depth was roughly equivalent to 3 pounds of bouyancy force on each hanger. The centrifigal water pump shown has a control valve to regulate output. The bouyancy force on the cannisters could be decreased slowly and evenly on all hangers by pumping water out of the tank.

A line of sight from a transit was utilized to observe the lateral deflection of the model arch. Readings were taken on a scale mounted on the frame perpendicular to the plane of the arch and very near to the point at which the magnitudes of deflection were desired. The deflections were

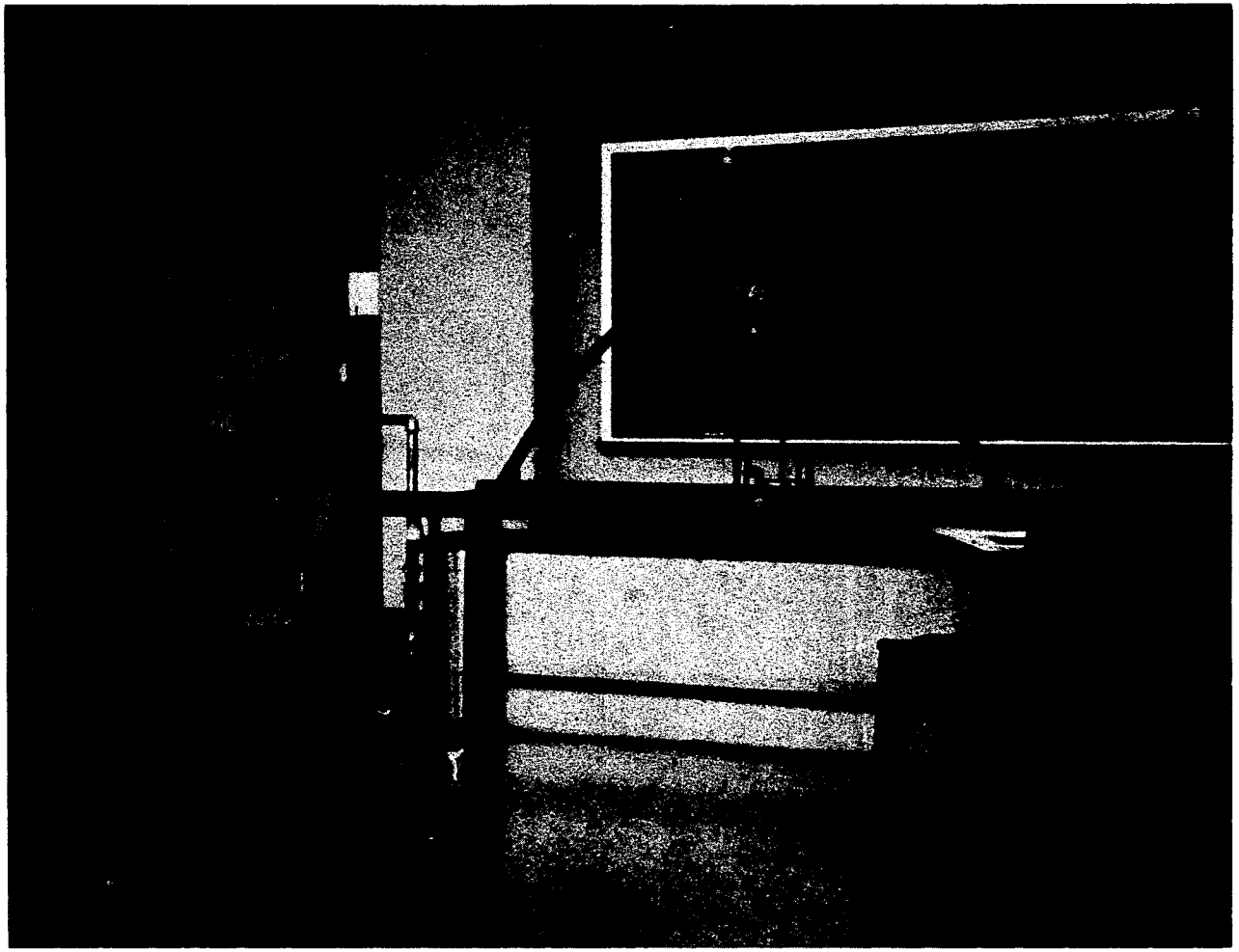

Fig. 1.--General arrangement of testing equipment

measured to the nearest 1/100 of an inch.

In order to determine the hanger loads both the water level in the tank and the weight of lead shot in the cannisters had to be known. The lead shot was weighed on a balance-scale. The water level was read on a scale clamped to the inside wall of the water tank. The least division on the scale was a 16th of an inch which corresponded to approximately 1/100 of a pound of bouyancy force. The lead shot was weighed with equal precision.

The basic test set-up is considered to simulate a free standing arch subjected to vertical hanger loads. It is illustrated by Figure 2. In order to have a capability for tilt loading, the basic test set-up was modified by placing a pair of immovable steel bars (7.16 inches in diameter) at the elevation of the model arch end supports. These bars prevented the hanger wires from displacing laterally at this elevation. The arch was free to move laterally as the hanger loads were increased, thus forcing the hangers to become inclined or tilted. Refer to Figures 3 and 15.

Although in all of the restrained arch tests, the arches were loaded with vertical loads, the basic test set-up again was subjected to alteration to provide the prescribed restraint. To accomplish this, identical arches connected by restraining bars were tested in pairs as shown in Figures 4 and 5. The type of restraint supplied is illustrated by

Fig. 2.--Test set-up for free standing arches subjected to vertical loads

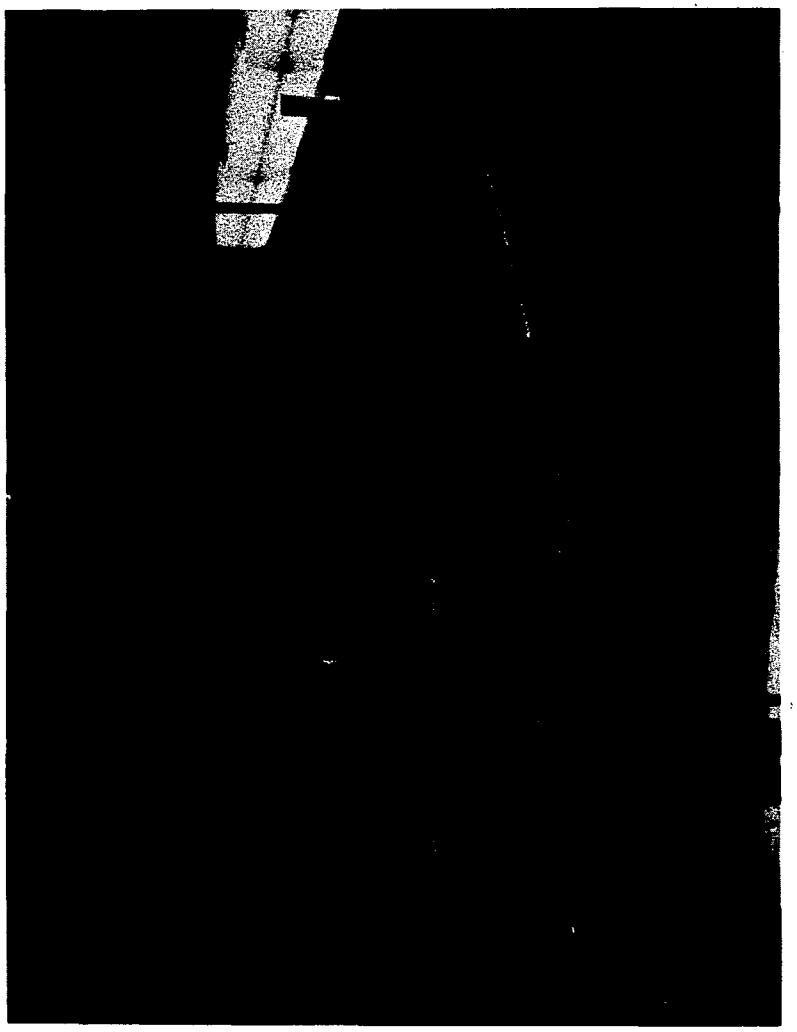

Fig. 3.--Test set-up for free standing arches subjected to tilt loads

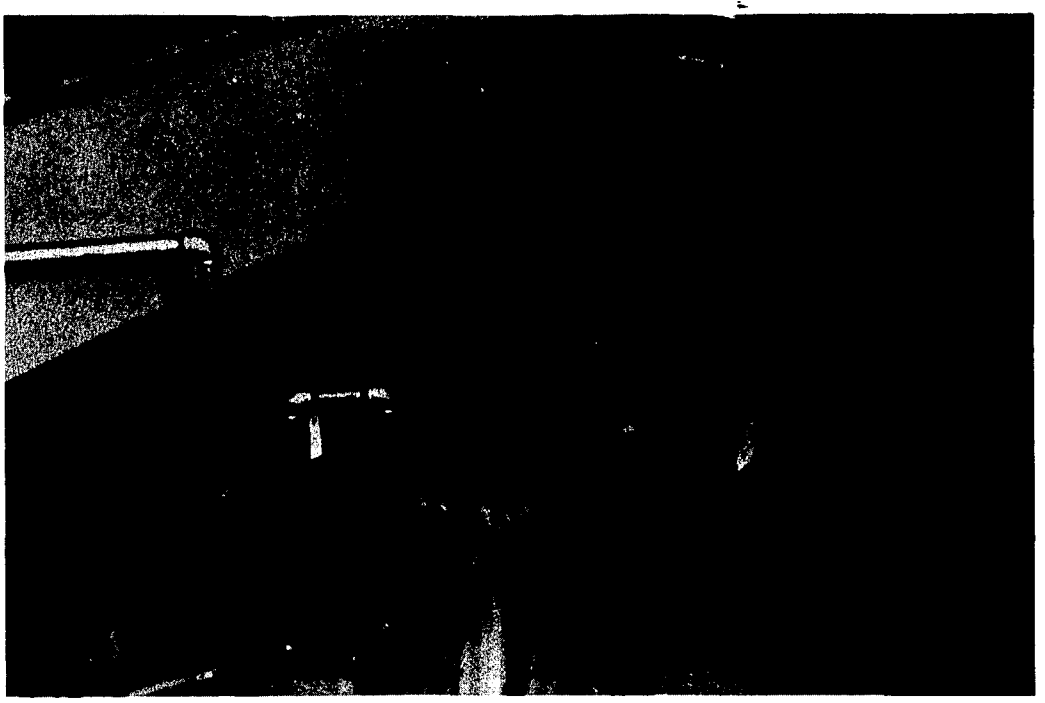

Fig. 4.--Test set-up for uniformly restrained arches

Fig. 5.--Test set-up for crown restrained arches (rigid restraining bar)

the sketch in Figure 9.

Model Arches

All model arches were made from 2024-T3 aluminum alloy sheets. This alloy was selected for its machineability. Tensile tests were made on specimens cut from the sheets from which the arches were fabricated. The tensile modulus of elasticity and Poisson's ratio were found to be 10,720,000 pounds per square inch and 0.32, respectively.

The model arches tested were either of parabolic or circular profile. They had a constant cross-section whose thickness was 0.192 inches and whose depth was 1.5 inches. The arches had a span of approximately 60 inches. Height-span ratios tested were 0.2, 0.3, and 0.4.

Along the centerline of the model arches holes were drilled to facilitate attachment of the load hangers and the restraint bars. Flexural tests were conducted on specimens having similiar hole arrangements and it was found that the holes had a negligible effect on the flexural stiffnesses.

A study of the model arches with the above configurations revealed that for all tests that - (1) the stress levels prior to buckling were well below the proportional limit of the material, (2) in-plane deflections prior to buckling were negligible and (3) no in-plane buckling was possible prior to the onset of out-of-plane buckling.

End Supports

The model arches were supported at their extremities by either fixed end supports or by hinged end supports. The end support fixtures were either bolted or securely clamped to the frame. Figures 6 and 7 illustrate these supports.

The boundary conditions imposed by the end supports can best be explained by referring to Figure 8. Both types of support prohibited translation along the x,y and z axes. The fixed end supports prohibit rotations about the x,y and z axes, however the hinge end supports prohibit rotation about the z axis only. The latter support was constructed by cutting a v-notch into a gimble which was held in place by bearings at the gimble supports. A knife-edge fitting attached to the model arch rested in the v-notch. The bearings allowed rotation about the y axis; the knife-edge fitting resting in the v-notch permitted rotation about the x axis while prohibiting rotation about the z axis (provided the knife-edge remains in the apex of the v-notch).

Restraints

As previously mentioned, tests were conducted upon two types of laterally restrained arches. They will be referred to as crown restrained and uniformly restrained. The crown restrained arches had a lateral bar connecting the pair of arches at the crown only, whereas the uniformly restrained

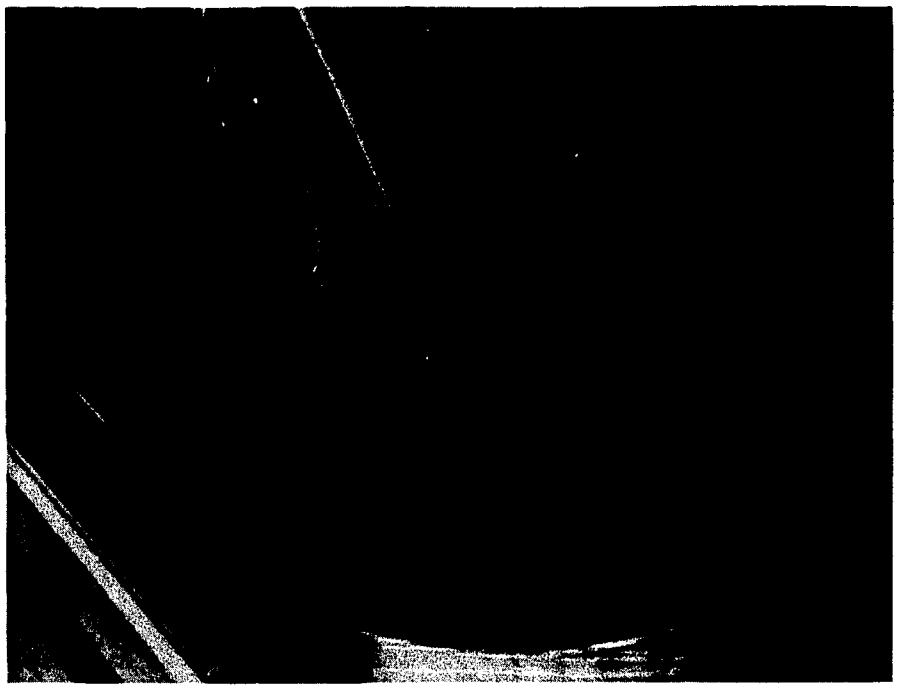

Fig. 6.--Arrangement showing fixed end supports for restrained arch tests

Fig. 7.--Arrangement showing hinged end supports for restrained arch tests

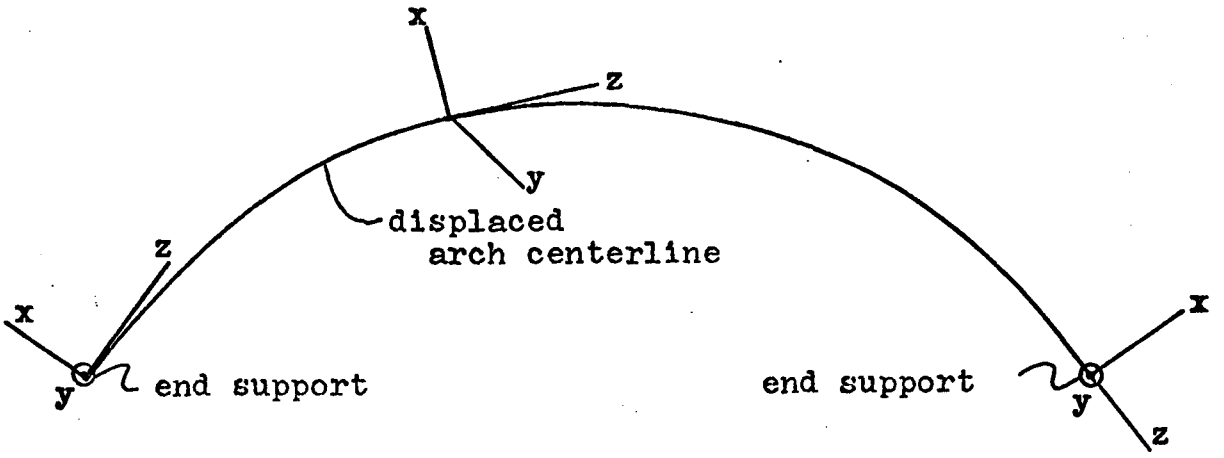

Fig. 8.--Profile view of displaced arch centerline indicating coordinate system

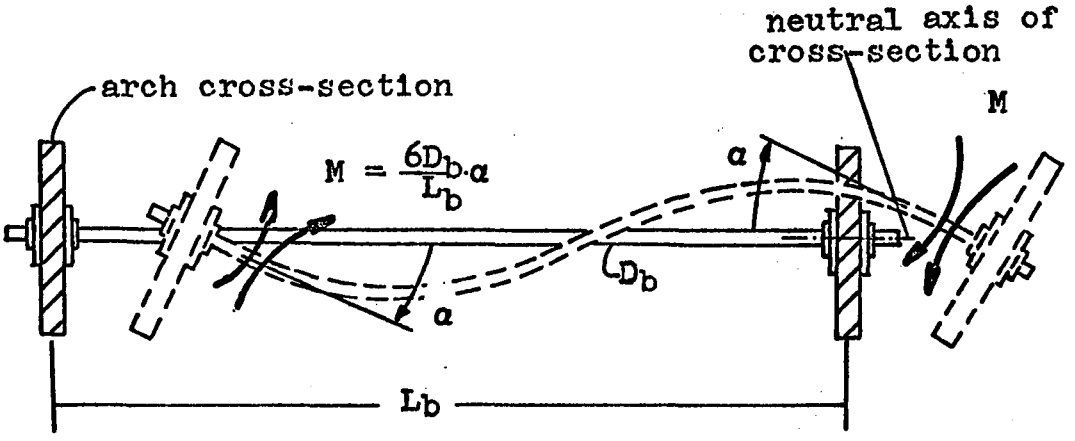

Fig. 9.--Round restraining bar shown in both undeflected and laterally deflected positions

arches had 15 equally spaced restraining bars connecting the pair of arches. Figures 4 and 5 illustrate these.

Refer to Figure 8. The lateral restraining bars in the above mentioned tests inhibit only rotations about the displaced x and z axes. Rotations about the y axis and all other displacements were not inhibited.

All of the restraining bars had a solid round cross-section except the rigid which appears in Figure 5.

The restraint supplied by a lateral bar comes about in the following manner. Two identical arches were positioned parallel to each other and connected by a bar (perpendicular to the original planes of the arches). The load was then applied to the pair of arches as shown in Figure 12 with one-half of the hanger load being applied to each arch. As the arches deflected laterally the round restraining bar deflected as illustrated by Figure 9. The rigid restraining bar, which was used only in crown restrained tests, did not deflect or permit any rotation of the arch cross-section as the arches deflected laterally. By assuming that the in-plane displacements of the arches are identical, the flexural stiffness of the round bars are calculated to be $K=6D_b/L_b$. In the crown restrained tests, the round bar supplies a twisting moment to the arch of $K(\bar{\beta})$, where $\bar{\beta}$ is the angle of twist of the arch cross-section about the longitudinal axis.

It was convenient to express the flexural stiffness of the bars in the non-dimensional form, KL/C, in which C is the torsional rigidity of the arch cross-section and L is the arch span.

All of the bars were made of 2024-T3 aluminum. The round bars had diameters of 3/32, 1/8, 5/32 and 3/16 inches. Flexural tests were conducted to determine the magnitude of the restraints (KL/C). It was found that for bar diameters of 3/32, 1/8, 5/32 and 3/16 inches, KL/C equaled 0.19, 0.47 0.86, and 2.00 respectively. For the rigid bar KL/C is infinite.

Application of Loads

In all tests the loads were applied to the model arches through 14 equally spaced hangers as shown in Figures 11 and 12.

The upper end of each hanger was attached to the arch so that the hanger imparted only a concentrated load through the centroid of the cross-section. To accomplish this the following arrangement was used and is illustrated by Figure 10.

A hole was countersunk from both sides of the model arch producing a circular knife-edge of 0.09 inches in diameter on the centerline of the cross-section's thickness. The lower most point of the knife-edge was on the neutral

axis. The hanger, made of 0.062 inch diameter wire, was designed so that at the maximum rotation of the cross-section the only contact between the hanger and the cross-section would be at the knife-edge. In the foregoing manner, the point of load application was established at the neutral axis and acting through the shear-center of the cross-section.

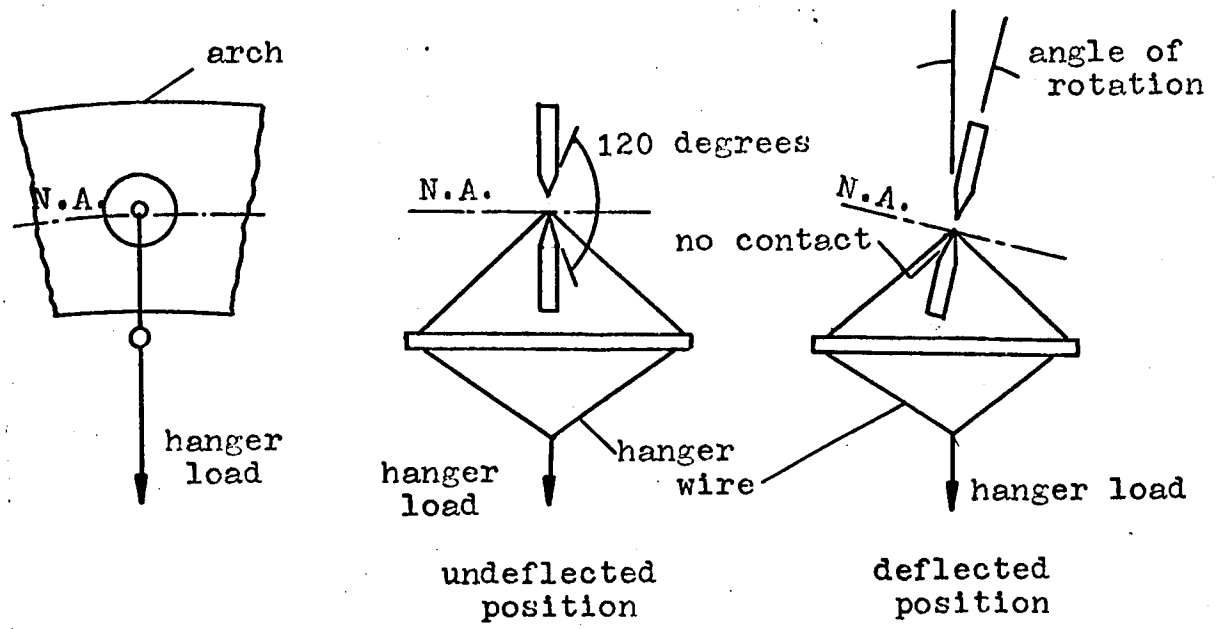

Fig. 10.--Typical hanger to arch attachment.

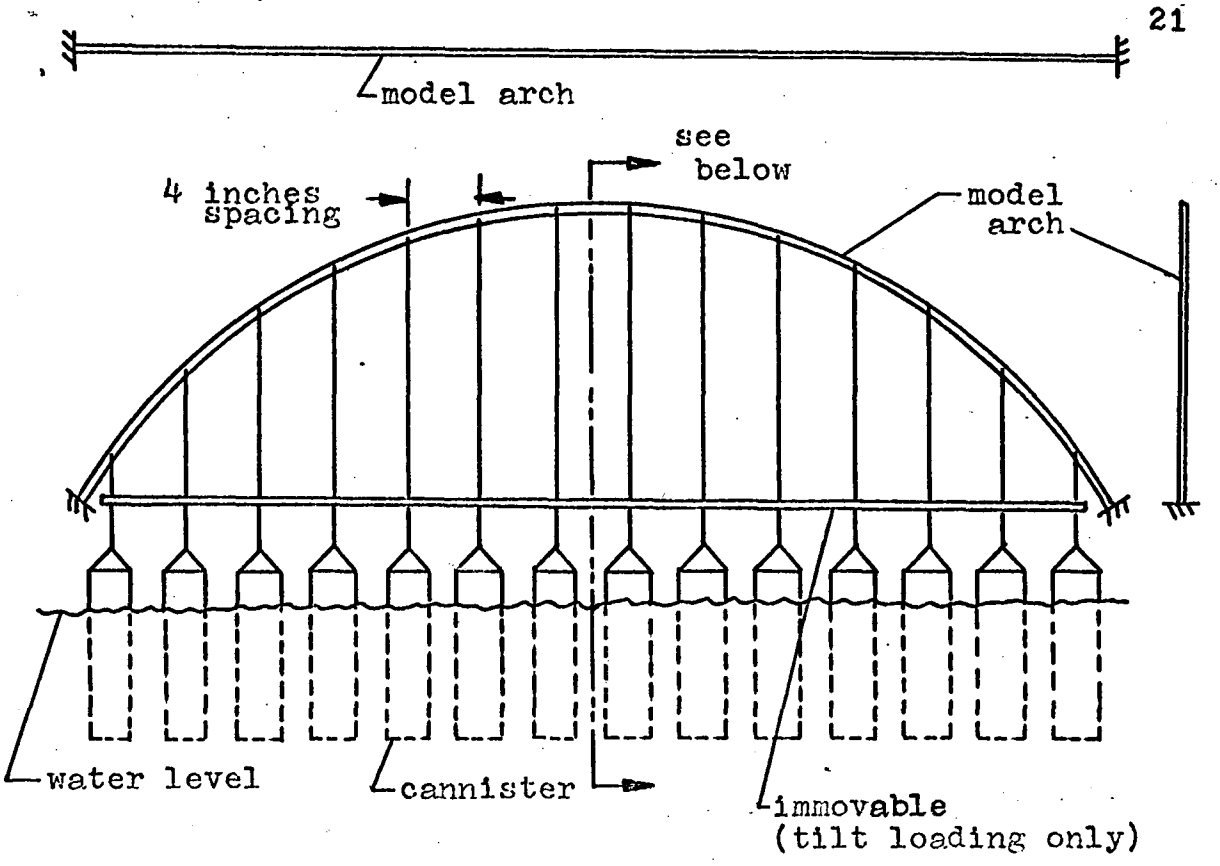

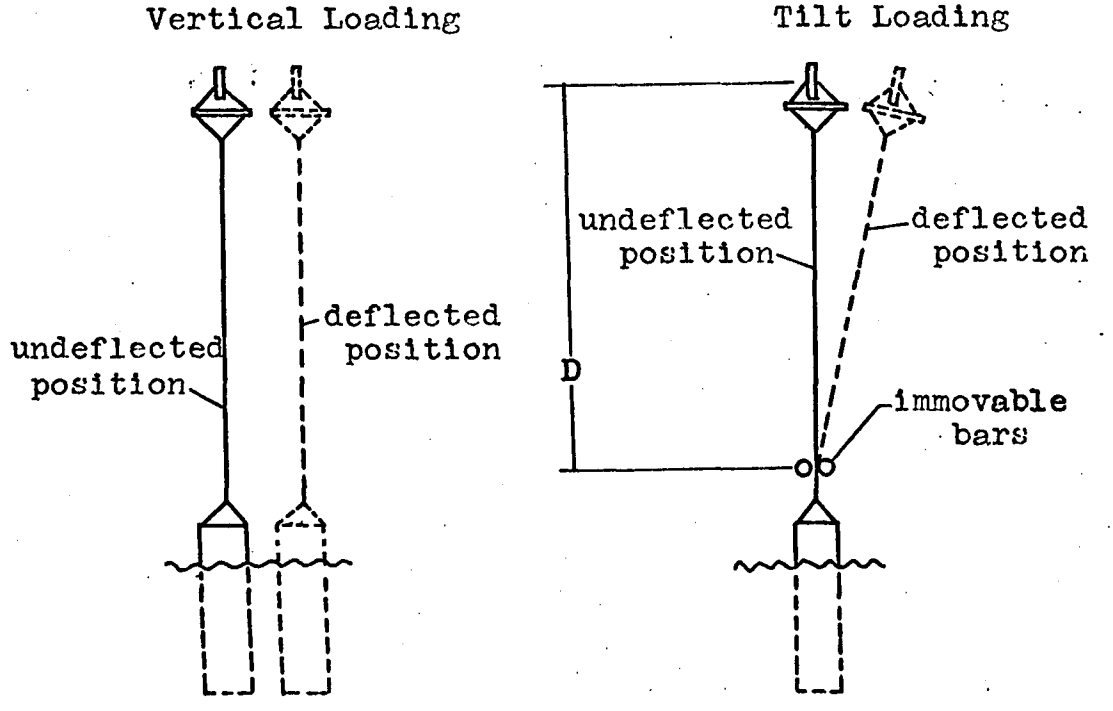

Fig. 11.-- Sketches illustrating vertical and tilt load application for free standing arch tests

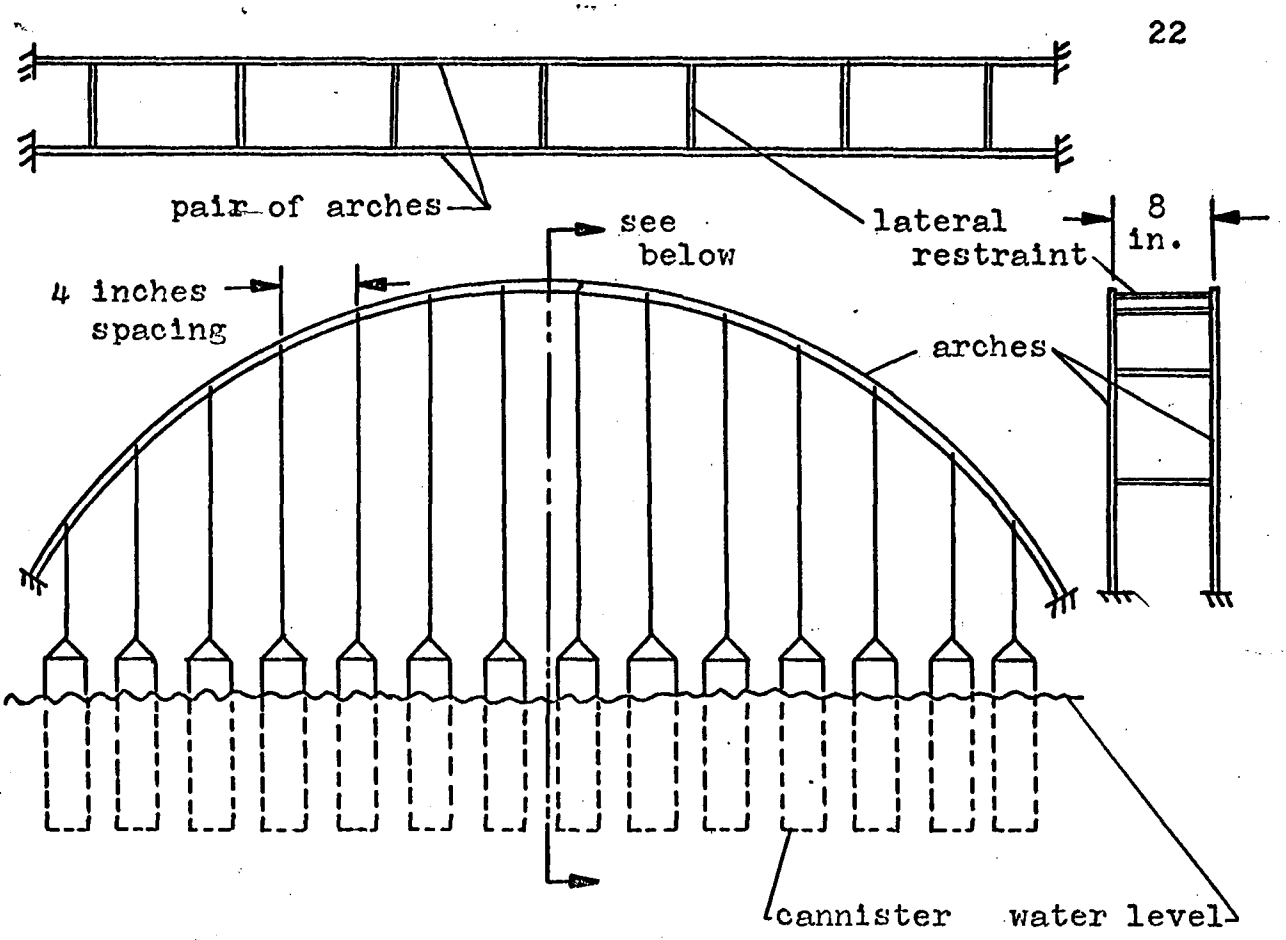

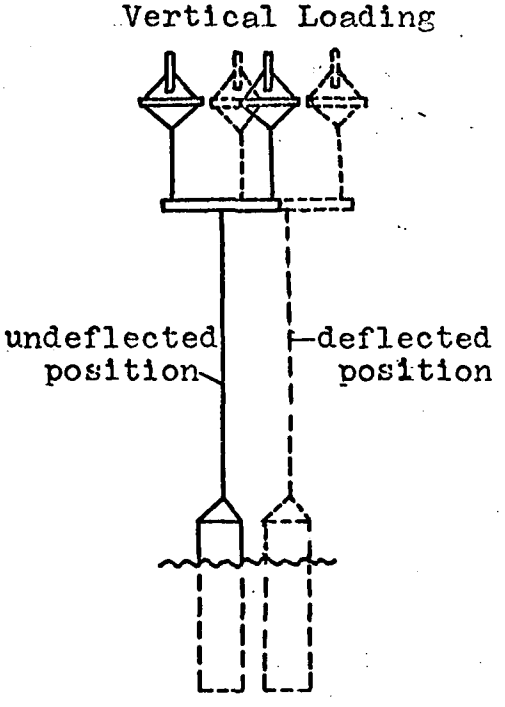

Fig. 12.--Sketch illustrating vertical load application for restrained arch tests

The lower end of the hanger was attached to a cannister which could be partially emersed in water.

The equivalent uniform load (Q) was computed by dividing the hanger load by the horizontal spacing between hangers (4 inches).

The total load over a 4 inch horizontal section of arch is equal to the weight of the cannister, the hanger, the 4 inch portion of the arch plus the weight of the lead shot added to the cannister minus the bouyancy force on the cannister due to the volume of water it displaces. All cannisters were of 3 inch diameter.

The hangers imparted either vertical loads or tilt loads to the model arches as shown in Figure 11. In tests where vertical loading was desired the hangers and cannisters were free to displace laterally as the arch deflected, thus the hanger remained vertical throughout the entire test. In tests where tilt loading was desired, two immovable bars were placed along the chord line joining the two end supports. These bars prevented lateral displacement of the wires perpendicular to the original plane of the arch and forced the hanger wires to tilt. A tilt hanger imparts both a vertical load (approximately equal to the hanger load) and a horizontal load equal to the hanger load multiplied by the tangent of the angle of tilt of the wires.

Testing Procedure

In general, the basic objective of all testing was to observe and record the lateral deflection at the crown of the model arch and the corresponding applied hanger loads. The lowest of the buckling loads were predicted from this data. The following test procedure was adopted.

The arch along with its prescribed end supports was attached to the frame aligning the arch in a vertical plane as closely as possible. Any error in alignment causes lateral deflection with each increase in the hanger loads.

The datum for measurement of deflection was taken as the arch position when the hanger loads were zero.

Equal hanger loads were applied to the arch. They were made equal by calculating the bouyancy force of each cannister and then adding lead shot into the cannister until the desired hanger load was obtained.

At the beginning of a test, increments of load were applied by the addition of equal amounts of lead shot to the cannisters. As the hanger loads were increased the plot of lateral deflection (Δ) versus uniform load (Q) was drawn. From this plot it was observed that at some point (occuring at a deflection of approximately 0.3 of an inch) the deflections became very sensitive to load increments.

At this point the method of loading was changed. All further load increments were added by lowering the water

level in the tank and thereby reducing the bouyancy force on the cannisters. This mode of loading was continued until approximately 1.2 inches of lateral deflection of the arch was observed for the arch tests with height-span ratios of 0.4 and 0.9 of an inch for the arch tests with height-span ratios of 0.2. It was felt that this range of deflection would permit the accurate prediction of the buckling loads.

As a check against possible slippage at the end supports and as a check to see that the proportional limit of the arch material was not exceeded, the hanger loads were reduced. The water was first restored to its original level (it had been lowered to increase bouyancy force on the hangers) and deflection readings taken. The cannisters were next removed and again deflection readings were taken. A comparison was made between these values and those recorded at the start of the test. The values agreed very favorably.

CHAPTER III

EXPERIMENTAL RESULTS

Calculation of Buckling Loads

At the outset of each test an attempt was made to align the model arch and its prescribed end supports so that the arch was in a vertical plane. It was impossible to accomplish this perfectly. Any misalignment will prohibit the test loads from reaching the buckling loads as predicted by theory.

The Southwell method[12] which is a method of predicting the buckling load from deflection data was used. The method was originally derived for tests on pin-ended columns. Ariaratnam[13] proved its applicability to lateral-torsional buckling of plane frames. It is assumed that the method has validity in the present tests. Southwell showed that the load-deflection curve of an initially imperfect column is a hyperbola in the neighborhood of the smallest buckling load. The asymptote of the hyperbola is a horizontal line at the load equal to buckling load. By a suitable change of variables, this hyperbolic portion of the load-deflection curve may be converted into a straight line whose slope is the

reciprocal of the critical buckling load. The method permits a computation of the buckling load without having to actually reach it in the test.

When using the Southwell method, instead of observing the entire deflection curve of the arch, it is convenient to select one point having a representative deflection behavior. Except for Test No. 13 the deflected shape of buckling was primarily symmetrical about the crown of the arch with the maximum deflection at the crown. The lateral deflection of the crown (Δ) was therefore selected as the representative point.

In Test No. 13 the deflected shape was neither purely symmetrical nor antisymmetrical about the crown and therefore deflections at both the crown and a quarter point were observed. The critical buckling load was estimated from load-deflection data.

Figure 13 indicates a typical load-deflection plot (Δ versus Q) and a Southwell plot (Δ/Q versus Δ). It also illustrates the application of the Southwell method to the present test results.

Certain limitiations must be recognized in utilizing the Southwell plot to predict the buckling loads. When both the loads and deflections are small, the ratios (Δ/Q) are not determinable with great precision; also in this range the ratios will be highly sensitive to unavoidable imperfec-

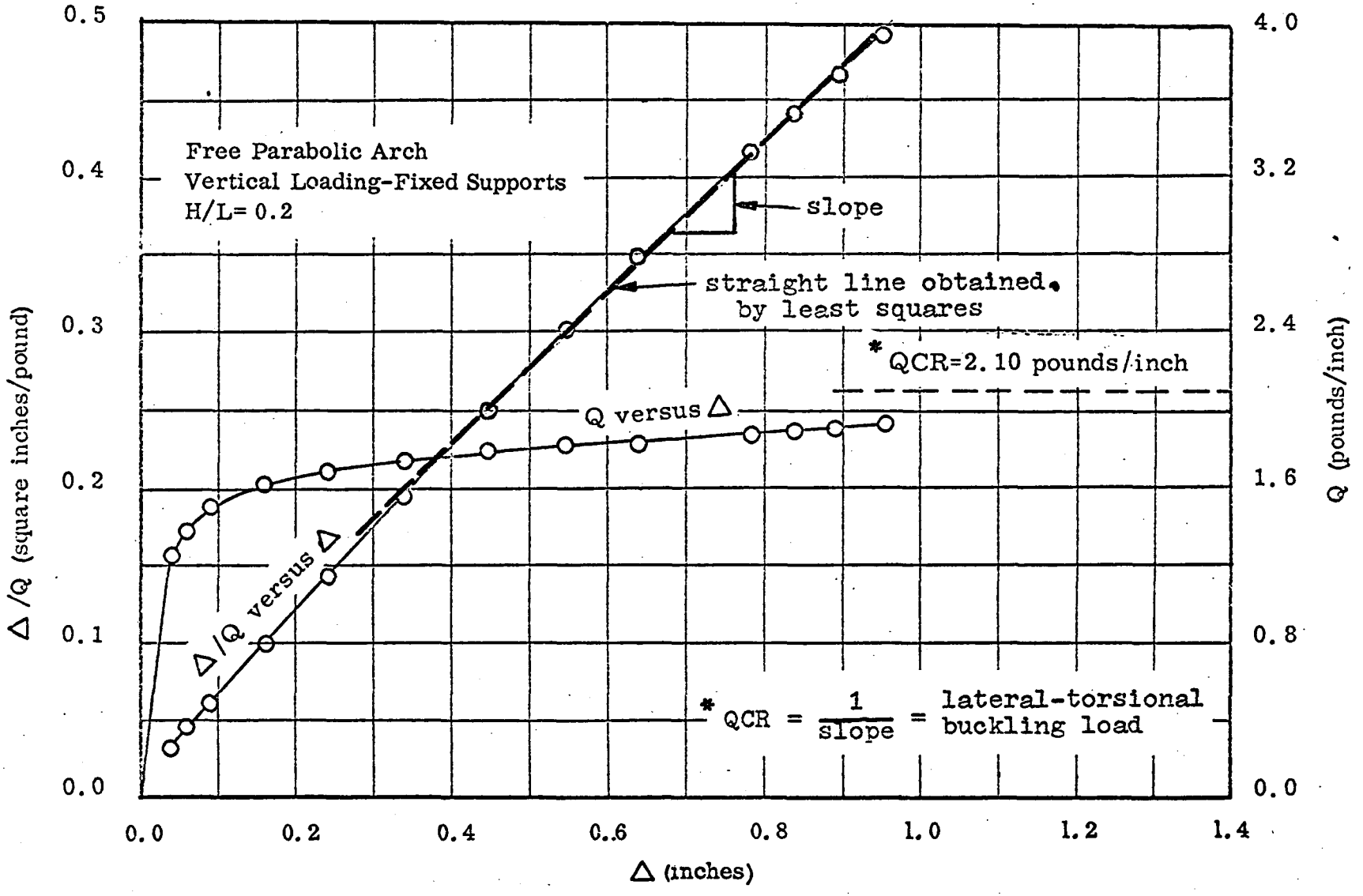

Fig. 13.--Typical load-deflection and Southwell plots used to predict lateral-torsional buckling loads (Test No. 1)

tions of alignment, workmanship, and test equipment. Therefore, a spreading of the data must be expected. At the other end of the range, the relationship between measured load and deflection ceases to be hyperbolic because deflections become so large that the material no longer is linearly elastic and/or the curvature expressions used in the flexure-curvature relationships can not be based upon small deflection theory.[12]

In nearly all of the tests, after the desired maximum lateral deflection was reached the load was removed and the model arch resumed its initial position. The exceptions were the free standing arches with hinged end supports. Because the displacements generally disappeared upon unloading and because of the results of the preliminary stress calculations, it was concluded that the arches behaved elastically.

The crown of the arch in Test No. 3 was permitted to deflect two inches laterally (0.8 to 1.2 inches more than in other tests). In the author's opinion, the fact that the Southwell plot remained a straight line supports the assumption of the applicability of small deflection theory to the problem under investigation.

Based on the above discussion, the smallest buckling load was predicted from the higher rations of Δ/Q. The buckling loads as predicted from the test results are summarized in Tables 1 and 2. The Southwell and load-deflection plots of the test results are presented in Appendix A. The

TABLE 1

LATERAL-TORSIONAL BUCKLING LOADS OBTAINED

FROM THE FREE STANDING ARCH TESTS

Free Standing Arches[a]					
Load	Test No.	Arch Profile	H/L	End Support	Test QCR (lbs/in)[b]
Vertical	1	Parabolic	0.2	Fixed	2.10
	2	Parabolic	0.3	Fixed	1.67
	3	Parabolic	0.4	Fixed	1.66
	4	Parabolic	0.2	Hinged	0.21
	5	Circular	0.4	Fixed	1.40
	6	Circular	0.2	Fixed	2.26
	7	Circular	0.2	Hinged	0.16
Tilt	8	Parabolic	0.2	Fixed	6.20
	9	Parabolic	0.4	Fixed	5.34
	10	Parabolic	0.2	Hinged	2.30
	11	Circular	0.4	Fixed	4.57
	12	Circular	0.2	Fixed	6.94
	13	Circular	0.2	Hinged	2.90

[a]In all tests the model arches had a span of 59 inches, C/A= 1.515 and A= 9500 pound inches squared.

[b]All of the lateral-torsional buckling loads (QCR) were obtained from the Southwell plots except for Test No. 13 where the load-deflection plot was used.

TABLE 2

LATERAL-TORSIONAL BUCKLING LOADS OBTAINED

FROM THE RESTRAINED ARCH TESTS

Restrained Arches[a] (Parabolic Profile and Vertical Loading)					
Type	Test No.	KL/C	H/L	End Support	Test QCR (lbs/in)[b]
Crown Restrained	14	0.19	0.2	Fixed	2.20
	15	0.19	0.4	Fixed	1.63
	16	0.47	0.2	Fixed	2.31
	17	0.47	0.4	Fixed	1.66
	18	0.86	0.2	Fixed	2.32
	19	0.86	0.4	Fixed	1.75
	20	0.86	0.2	Hinged	0.36
	21	2.00	0.2	Fixed	2.43
	22	2.00	0.4	Fixed	1.95
	23	2.00	0.2	Hinged	0.41
	24	Rigid	0.2	Fixed	3.16
	25	Rigid	0.4	Fixed	2.63
	26	Rigid	0.2	Hinged	0.62
Uniformly Restrained	27	0.19	0.2	Fixed	2.47
	28	0.19	0.4	Fixed	1.95
	29	0.19	0.2	Hinged	0.48
	30	0.47	0.2	Fixed	3.01
	31	0.47	0.4	Fixed	2.46
	32	0.47	0.2	Hinged	0.73
	33	0.86	0.2	Fixed	3.69
	34	0.86	0.4	Fixed	3.72
	35	0.86	0.2	Hinged	1.22

[a]In all tests the model arches had a span of 59 inches, C/A= 1.515 and A= 9500 pound inches squared.

[b]All of the lateral-torsional buckling loads (QCR) were obtained from the Southwell plots.

buckling loads are also shown on the load-deflection plots for comparison.

Discussion of Test Results

Figures 14 thru 17 show the arches for several tests in deflected positions.

In all tests except Nos. 12 and 13 the model arches deflected symmetrically about the crown at the arch. When the deflected shapes were symmetrical, the buckling loads were predicted from the Southwell plots.

In general, the points on these Southwell plots establish with sufficient accuracy the straight line necessary to predict the buckling loads. Some scatter of the points can be observed at small loads and small deflections. This topic was discussed in the previous section.

The deflected shapes in Tests Nos. 12 and 13 were neither purely symmetrical nor unsymmetrical. In Test No. 12 the unsymmetrical contribution to the deflected shape was small and the buckling load was therefore predicted by the Southwell plot as for the tests in which the deflections were predominately symmetrical.

In Test No. 13 the symmetrical and unsymmetrical contribution to the deflected shape were approximately equal. Because of the form of this deflected arch the deflection was observed at the crown of the arch and at a point 18 inches from one end support. Figure 18 illustrates the de-

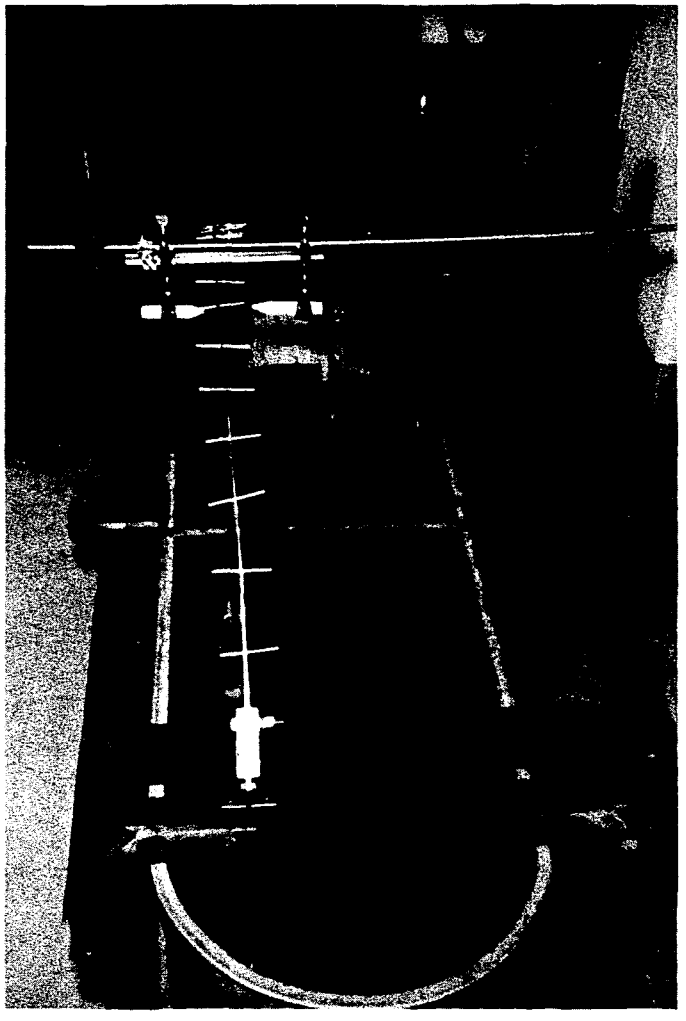

Fig. 14.--Free standing arch subjected to vertical loads shown in a deflected position

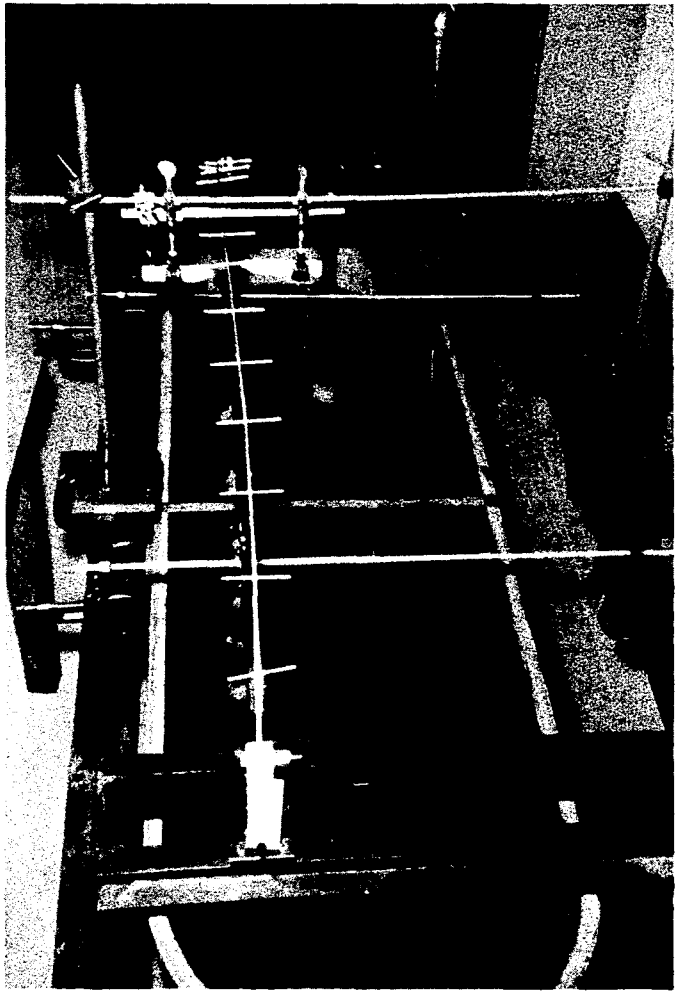

Fig. 15.--Free standing arch subjected to tilt loads shown in a deflected position

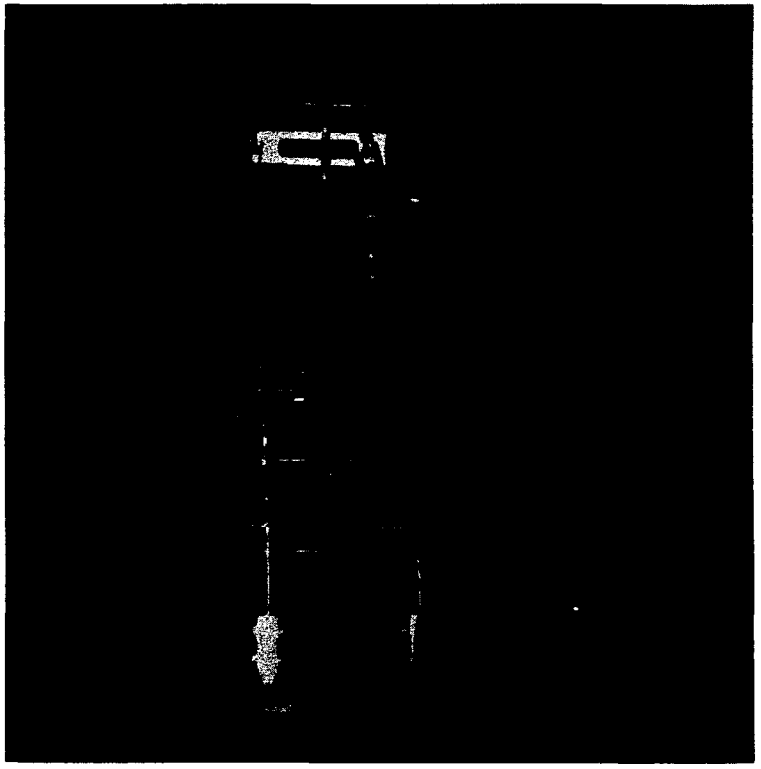

Fig. 16.--Crown restrained arches (rigid restraining bar) subjected to vertical loads shown in a deflected position

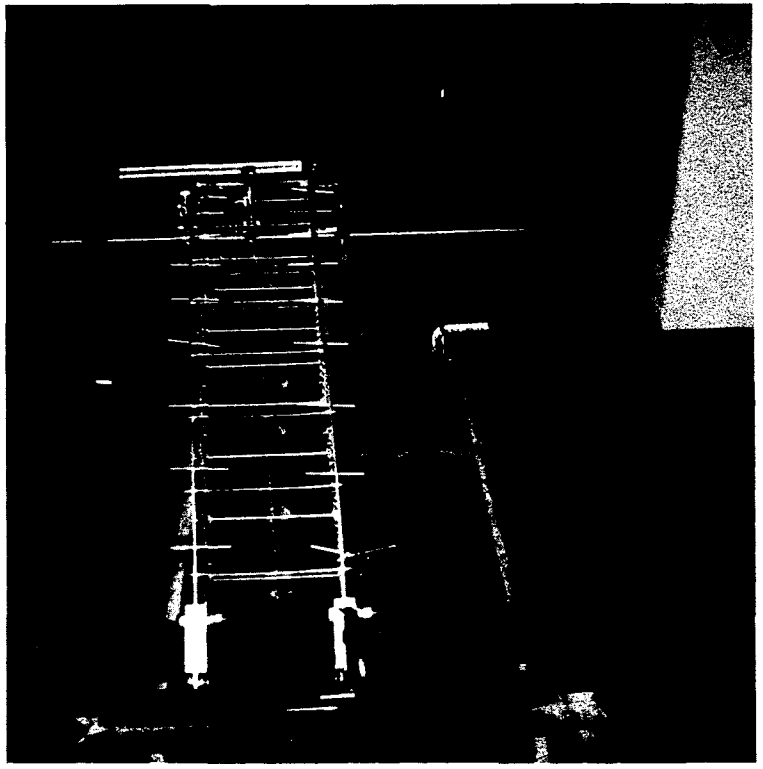

Fig. 17.--Uniformly restrained arches subjected to vertical loads shown in a deflected position

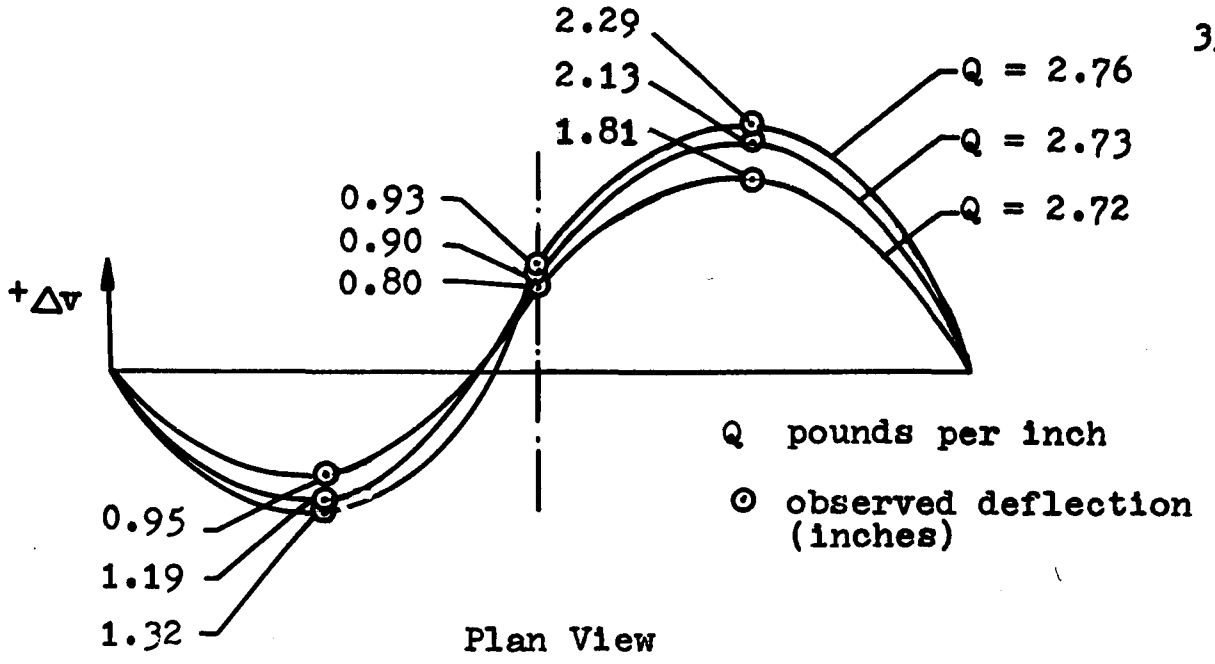

Fig. 18.--Diagram illustrating the deflected shapes of the arch in Test No. 13 at three stages of loading

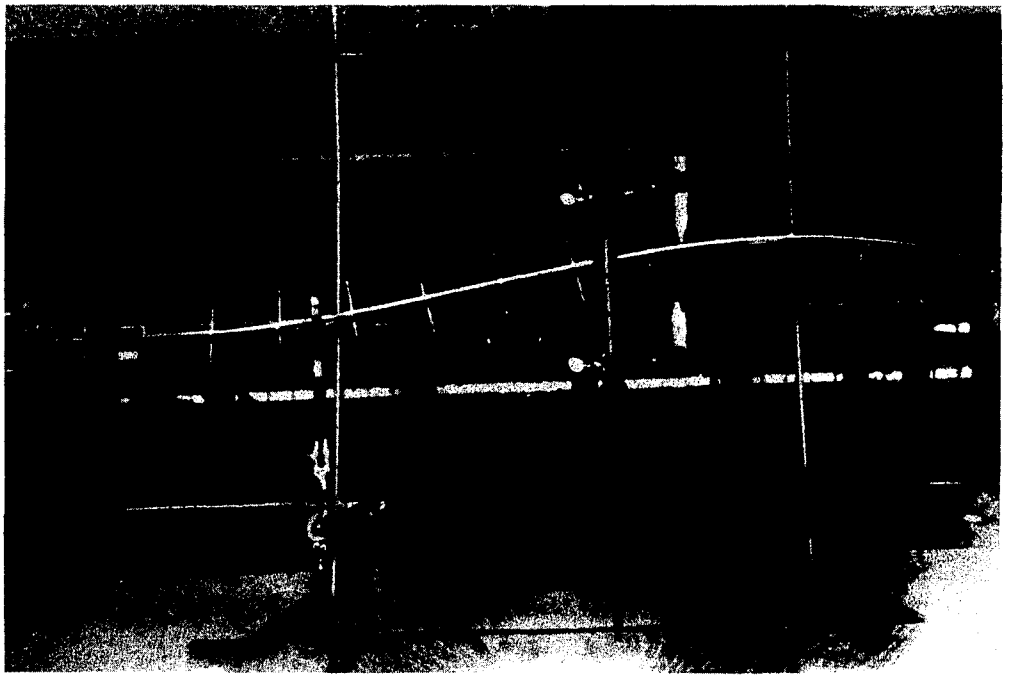

Fig. 19.--Actual deflected position of the arch in Test No. 13 at maximum applied load, Q=2.76 pounds/inch

flected shape of the arch at three stages of loading, while the actual deflected shape (at maximum applied load, Q=2.76 pounds/inch) of the arch model is shown in Figure 19.

CHAPTER IV

THEORETICAL SOLUTION OF BUCKLING LOADS

A pair of linear differential equations governing the lateral buckling of parabolic arches are developed* from three of Kirchhoff's[14] six equilibrium equations for curved and twisted rods. The smallest buckling loads and deformed shapes were obtained for free standing and laterally restrained arches (restraint at crown only). Both uniform vertical and uniform tilt loadings were investigated. Boundary conditions studied were those implied by the earlier described end supports i.e., fixed and hinged.

A linearizing technique[16] was used when combining equilibrium equations, equations relating internal couples to changes in curvature and twist, and geometric relations. Symbols are defined in the nomenclature section, and wherever possible they correspond to those given in A.E.H.Love, "A Treatise on the Mathematical Theory of Elasticity," Chapters XVIII and XXI.[14] All of the assumptions listed on

*The pair of buckling equations for the parabolic arch, equations (9), are a special case of the more general buckling equations (6). Equations (6) were derived in a seminar held at The Ohio State University under the supervision of Professor Morris Ojalvo.

pages 7 and 8 apply.

The pair of equations developed were solved by a numerical method. The computations were carried out on an IBM 7094 computer.

A segment of a small displaced length of the member is shown in Figure 20. The positive sense of the internal and external forces, curvatures and twist, displacements, and the axes are indicated. An arrow with a double head designates the positive direction in accordance with the right hand screw convention. The original curve of the parabolic arch is assumed to be in the plane formed by the x and z axes. The y axis is considered as the lateral or out-of-plane direction.

The three of Kirchhoff's six equations which govern out-of-plane deformation are

$$\begin{aligned} \frac{dN}{ds} + Tk + N\tau + Y &= 0 \\ \frac{dG}{ds} - G'\tau + Hk' - N' + K &= 0 \\ \frac{dH}{ds} - Gk' + G'k + \theta &= 0 \end{aligned} \qquad (1)$$

The equations relating internal couples to changes in curvature and twist are

$$\begin{aligned} G &= A(k - k_o) \\ G' &= B(k' - k_o') \\ H &= C(\tau - \tau_o) \end{aligned} \qquad (2)$$

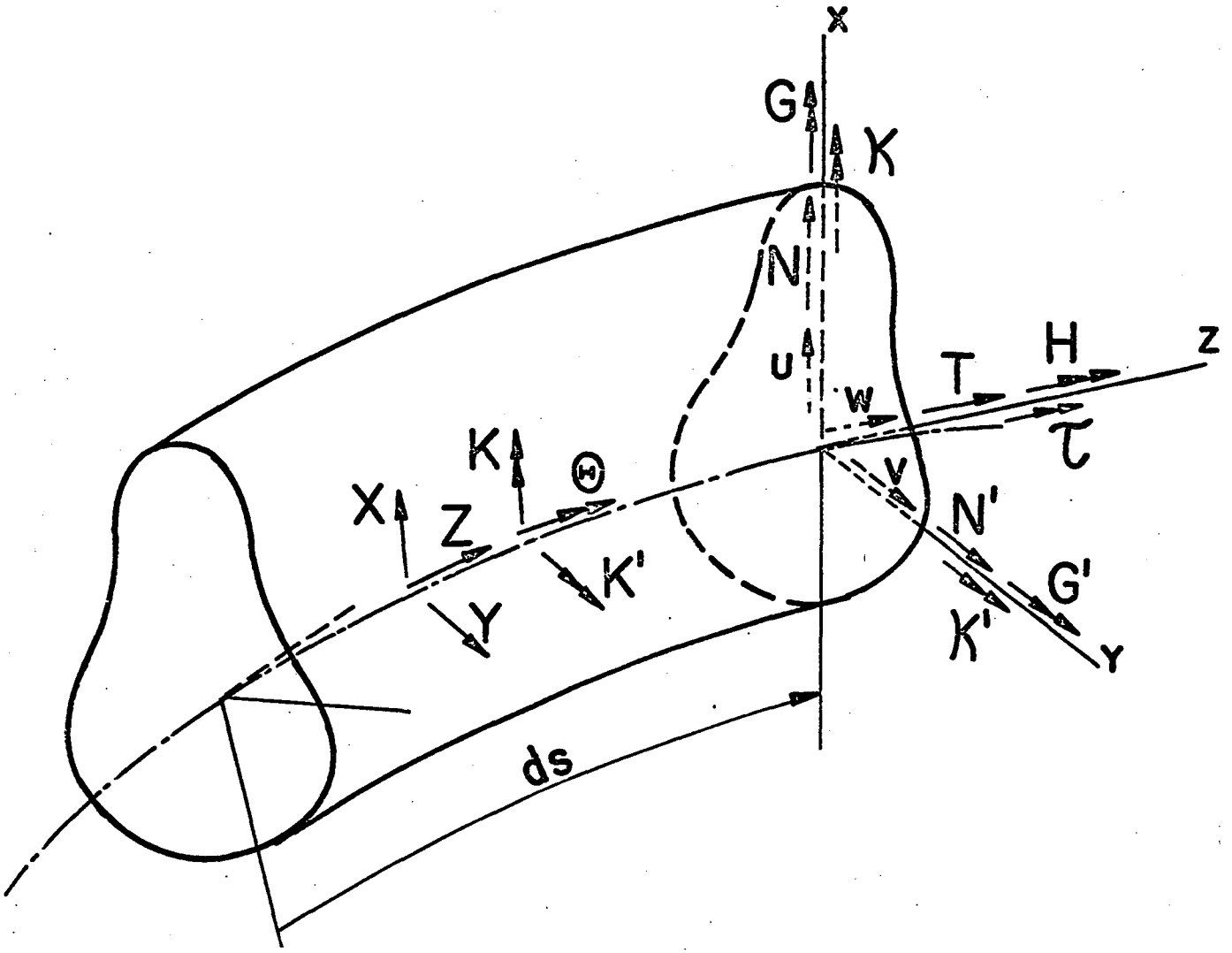

Fig. 20.--Drawing illustrating the positive sense of forces, curvatures and twist, displacements and axes on a displaced segment of the member

The geometric relations describing the final curvatures and twist in terms of initial curvatures, initial twist and displacements are

$$
\begin{aligned}
k &= k_o + \beta k_o' - \frac{d^2v}{ds^2} + \frac{d}{ds}(u\tau_o) - \frac{d}{ds}(w k_o) \\
k' &= k_o' + \beta k_o + \frac{d^2u}{ds^2} - \frac{d}{ds}(v\tau_o) + \frac{d}{ds}(w k_o') \\
\tau &= \tau_o + \frac{d\beta}{ds} + k_o\left(\frac{du}{ds} - v\tau_o + w k_o'\right) + k_o'\left(\frac{dv}{ds} + u\tau_o - w k_o\right)
\end{aligned}
\tag{3}
$$

The "linearizing technique" previously mentioned considers the displacements and both internal and external forces of the member in its buckled configuration to consist of two parts. The first part is associated with the loaded member just prior to buckling and the second part is the increment resulting from the buckling itself. The variables are

$$
\begin{aligned}
N &= N_o + \bar{N} & K &= K_o + \bar{K} \\
N' &= N_o' + \bar{N}' & K' &= K_o' + \bar{K}' \\
T &= T_o + \bar{T} & \theta &= \theta_o + \bar{\theta} \\
G &= G_o + \bar{G} & u &= u_o + \bar{u} \\
G' &= G_o' + \bar{G}' & v &= v_o + \bar{v} \\
H &= H_o + \bar{H} & w &= w_o + \bar{w} \\
X &= X_o + \bar{X} & \beta &= \beta_o + \bar{\beta} \\
Y &= Y_o + \bar{Y} & & \\
Z &= Z_o + \bar{Z} & &
\end{aligned}
\tag{4}
$$

The parts associated with the pre-buckling configuration have the subscript "o" and the incremental parts resulting from buckling are designated by a bar above the symbol.

Since buckling is considered to have occured as soon as the member exhibits a small deformation, the incremental part of the displacements and forces are considered to be infinitesimal. Thus, in the derivation of the buckling equations all terms involving products of infinitesimals are neglected.

Prior to buckling the loads and displacements are all in the original plane of the curve, therefore Y_o, K_o, H_o, N'_o, G_o, θ_o, v_o, and β_o are all equal to zero. It is assumed that the undeflected curve is in the plane containing one of the cross-section's principal axis. This implies $k_o=0$ and $\tau_o=0$. The assumption that the centerline of the member is inextensible results in

$$\frac{dw}{ds} = uk'_o \qquad (5)$$

By combining equations (1) thru (5) and observing the above mentioned considerations the following two equations defining lateral buckling of planar curved members are obtained.

$$\frac{d^4\bar{v}}{ds^4}(-A) + \frac{d^2\bar{v}}{ds^2}(T_o - G'_o k'_o + C(k'^2_o)) + \bar{Y} + \frac{d\bar{K}}{ds}$$

$$+ \frac{d\bar{v}}{ds}(N_o k'_o + G'_o \frac{d}{ds}(k'_o) - \frac{dG'_o}{ds} k_o + C\frac{d}{ds}(k'^2_o))$$

$$+ \frac{d^2\bar{\beta}}{ds^2}((A+C)k'^2_o - G'_o) + \frac{d\bar{\beta}}{ds}((2A+C)\frac{d}{ds}(k'_o) + N_o + \frac{dG'_o}{ds})$$

$$+ \bar{\beta}(A\frac{d}{ds}(k'^2_o) - T_o k'_o) = 0 \qquad (6)$$

$$\frac{d^2\bar{v}}{ds^2}((A+C)k'^2_o - G'_o) + \frac{d\bar{v}}{ds}(C\frac{d}{ds}(k'^2_o)) + \frac{d^2\bar{\beta}}{ds^2}(C) + \bar{\theta}$$

$$+ \bar{\beta}(-A(k'^3_o) + G'_o k'_o) = 0$$

G'_o , N_o and T_o are obtained from an ordinary linear stress analysis which does not consider the possibility of buckling. $\bar{Y}$ is determined from a consideration of the final directions of the loads applied to the members and the displaced y axis. $\bar{K}$ and $\bar{\theta}$ would appear where elastic restraint is applied between the end supports of the member. $\bar{\theta}$ would also appear when the loads are not applied thru the neutral axis. k'_o is determinable once the shape of the curved member is selected.

In the solution of a parabolic arch subjected to only a uniform loading (Q), the quantities G'_o , N_o , $\bar{K}$ and $\bar{\theta}$ are equal to zero. Although T_o is not easily expressible as a

function of "s" it can be calculated numerically at any section and used in that form in the numerical computations for the buckling loads. For vertical loading

$$\bar{Y} = \bar{\beta}(Q\cos^2\phi) + \frac{d\bar{v}}{ds}(Q\sin\phi\cos\phi) \tag{7}$$

and for tilt loading

$$\bar{Y} = \bar{\beta}(Q\cos^2\phi) + \frac{d\bar{v}}{ds}(Q\sin\phi\cos\phi) - \frac{\bar{v}}{D}(Q\cos\phi) \tag{8}$$

In equations (7) and (8) ϕ is defined by the arctanϕ being equal to the slope of the undeflected arch. The quantity $\bar{v}/D$ is equal to the angle of tilt of load. Refer to Figure 12. Only solutions where D is equal to the vertical distance between the chord line joined by the two end supports and arch are considered.

Finally, the equations for the solutions of lateral buckling of uniformly loaded parabolic arches are

$$\begin{aligned}&\frac{d^4\bar{v}}{ds^4}(-A) + \frac{d^2\bar{v}}{ds^2}(T_o + C(k_o')^2) + \frac{d\bar{v}}{ds}(C\frac{d}{ds}(k_o')^2)\\ &\quad + \frac{d^2\bar{\beta}}{ds^2}((A+C)k_o') + \frac{d\bar{\beta}}{ds}((2A+C)\frac{d}{ds}(k_o'))\\ &\qquad + \bar{\beta}(A\frac{d^2}{ds^2}(k_o') + k_o' T_o) + \bar{Y} = 0\end{aligned} \tag{9}$$

$$\frac{d^2\bar{v}}{ds^2}((A+C)k_o') + \frac{d\bar{v}}{ds}(C\frac{d}{ds}(k_o')) + \frac{d^2\bar{\beta}}{ds^2}(C) + \bar{\beta}(-A(k_o')^2) = 0$$

and can be used to solve for the buckling loads provided that six boundary conditions are specified. In general, three boundary conditions are available at each end of the arch.

Instead of applying the boundary conditions at both ends of the arch, they are applied at one end and at the crown. The boundary conditions

$$\bar{v} = \frac{d\bar{v}}{ds} = \bar{\beta} = 0 \tag{10}$$

or

$$\bar{v} = \frac{d\bar{v}}{ds} = 0 \tag{11}$$

$$\frac{d^2\bar{v}}{ds^2} = 0 \tag{12}$$

were used at the end supports. The boundary conditions (10) imply a fixed support while (11) and (12) imply a hinged support. Equation 12 is obtained by equating the moment about the x axis to zero.

The free standing and crown restrained arches provide the following boundary conditions at the crown of the arch respectively.

$$\frac{d\bar{\beta}}{ds} = N_o' = \frac{d\bar{v}}{ds} = 0 \tag{13}$$

and

$$\frac{d\bar{\beta}}{ds} = N'_o = 0 \tag{14}$$

$$\tfrac{1}{2}K\bar{\beta} + C\frac{d\bar{v}}{ds} = 0 \tag{15}$$

The condition (15) is obtained by equating the externally applied restraining couple ($\frac{1}{2}K\beta$) to the internal twist ($C\frac{dv}{ds}$).

A numerical method utilizing a forward integration technique was adopted to obtain the buckling loads from equations (9).

The uniform loading is incorporated in the buckling parameter, $\lambda = QL^3/A$. In general, the coefficient in (9) and boundary conditions as well, may depend on λ.

After selecting a valus of λ, equations (9) are expressed as a system of six first order differential equations. A set of initial values (at the end support) are assumed. Since three of the values have already been prescribed as boundary conditions only three missing initial values are arbitrary. With this set of values the problem becomes an initial-value problem which is solved by application of a fourth order Runge-Kutta[17] technique. This procedure is repeated by assuming two additional independent sets of initial values.

Any linear combination of these three solutions will satisfy the initial boundary conditions. Consequently, the buckling involves finding a linear combination of these three solutions satisfying the remaining boundary conditions at the crown, which gives rise to a system of three homogeneous equations with three arbitary constants.

A solutions to this system will exist only if a non-trival solution can be found. This implies that the determinate formed by the coefficients of the constants be zero.

Since some of these coefficients depend upon λ, it is highly unlikely that the initial selected value of λ will be such that the determinate will be zero. Therefore, the process is repeated with a new $\lambda = \lambda + \Delta\lambda$, where $\Delta\lambda$ is an increment of the buckling parameter, until the algebraic sign of two successive determinates changes. At this point a "false position" method[15] is used to continue the process until a sufficiently accurate $\lambda = \lambda_{cr}$ makes the determinate approximately zero.

Theoretically there are an infinite number of buckling parameters λ_{cr} which satisfy the solution. By selecting the initial λ value and the $\Delta\lambda$ small, it is possible to find the smallest buckling load.

Once the buckling parameter λ_{cr} associated with the smallest load is established, it is a relatively simply matter to determine thelateral deflection ($\bar{v}$) and angle of twist ($\bar{\beta}$) at locations along the arch. Any two of the three homogeneous equations used to establish λ_{cr} can be used to solve for two of the three arbitrary constants in terms of the third. Then the buckling shapes ($\bar{v}$ and $\bar{\beta}$) can be determined as a linear combination of the three independent solutions. The magnitudes of the shapes will be a

function of the third arbitrary constant.

Table 3 presents the theoretically determined smallest buckling loads for some of the cases for which experimental data was obtained.

CHAPTER V

COMPARISON OF THEORETICAL AND EXPERIMENTAL BUCKLING LOADS

Lateral-torsional buckling loads (QCR) to be compared are listed in Table 3. Twenty different cases are included. In the following discussion, the different cases will be identified with the test number corresponding to the experimental investigation.

The buckling loads obtained from theoretical solutions are based on the works of Stussi[6], Godden[7] and this writer. All of the experimentally predicted buckling loads are obtained from the experimental investigation herein. The Southwell method was used in all cases.

The buckling loads determined from Stussi's solutions are compared for cases 1, 2, and 3. These buckling loads are within 14 percent of those predicted from tests. In cases 1 and 3 they are lower, while in case 2 the theoretical load is higher.

Godden's theoretical solutions are for tied arch ribs (refer to page 3). He made the following assumptions: (1) the loading is applied by horizontal thrust at the end sup-

TABLE 3

SOME THEORETICAL AND EXPERIMENTAL LATERAL-TORSIONAL BUCKLING LOADS FOR COMPARISON

Arch	Load	Case or Test No.	H/L	KL/C	End Support	Test QCR lbs/in	Theoretical QCR (lbs/in)		
							Author	Stussi	Godden
Free Standing	Vertical	1	0.2	----	Fixed	2.10	1.89	1.91	----
		2	0.3	----	Fixed	1.67	1.84	1.90	----
		3	0.4	----	Fixed	1.66	1.53	1.63	----
		4	0.2	----	Hinged	0.21	0.30	----	----
	Tilt	8	0.2	----	Fixed	6.20	5.51	----	5.48
		9	0.4	----	Fixed	5.34	6.13	----	----
		10	0.2	----	Hinged	2.30	3.02	----	2.70
Crown Restrained	Vertical	14	0.2	0.19	Fixed	2.20	1.91	----	----
		15	0.4	0.19	Fixed	1.63	1.57	----	----
		16	0.2	0.47	Fixed	2.31	1.94	----	----
		17	0.4	0.47	Fixed	1.66	1.57	----	----
		18	0.2	0.86	Fixed	2.32	1.96	----	----
		19	0.4	0.86	Fixed	1.75	1.75	----	----
		20	0.2	0.86	Hinged	0.36	0.35	----	----
		21	0.2	2.00	Fixed	2.43	2.02	----	----
		22	0.4	2.00	Fixed	1.95	1.86	----	----
		23	0.2	2.00	Hinged	0.41	0.39	----	----
		24	0.2	Rigid	Fixed	3.16	2.29	----	----
		25	0.4	Rigid	Fixed	2.63	2.52	----	----
		26	0.2	Rigid	Hinged	0.62	0.57	----	----

In all cases the arches had a parabolic profile, a span of 59 inches, C/A= 1.515 and A= 9500 pound inches squared.

ports, (2) the distance between the end supports is allowed to shorten as the arch deflects laterally, and (3) the hangers have a uniform tension per inch of span equal to the horizontal thrust multiplied by $8H/L^2$. Because of these assumptions, the writer has some doubt regarding the applicability of Godden's solutions for comparison. Nevertheless, his solutions are compared for cases 8 and 10. In case 8 the buckling load that he obtained is 12 percent lower then that predicted from tests. In case 10 it is 17 percent higher.

The buckling loads determined from the theoretical solutions of Chapter IV are compared for twenty cases. With the exceptions of cases 4, 10 , and 24, these buckling loads are within 17 percent of those predicted from tests. In cases 4 and 10 they are 43 and 32 percent higher, respectively. In case 24 the theoretical load is 28 percent lower.

In general, the author's theoretical solutions predicted buckling loads that are lower than those predicted from tests. The exceptions are cases 2, 4, 9 and 10.

CHAPTER VI

SUMMARY AND CONCLUSIONS

This dissertation is a study of the lateral-torsional buckling of arches. Heretofor only a limited number of theoretical solutions were available. These solutions are based on a linear buckling theory. Experimental verification was also limited. It was therefore felt that additional theoretical solutions should be developed and that these solutions and older solutions should be verified by an extensive program of testing.

The primary objectives of this dissertation were: (1) to predict from experimental investigation the lateral-torsional buckling loads of arches, (2) to obtain theoretical solutions for lateral-torsional buckling loads of arches, and (3) to compare wherever possible the experimental results with available solutions based upon the linear theory of buckling.

The experimental investigation involved thirty-five different arch tests. The lateral deflection of the model arches was observed and recorded in each test. From this data lateral-torsional buckling loads were predicted by means of either a Southwell plot or a load-deflection plot.

The buckling loads are listed in Tables 1 and 2.

Two types of model arches were tested. These were free standing arches and restrained arches. The experimental testing considered the effects of the following factors: (1) the shape of the arch (parabolic or circular), (2) the height-span ratio of the arch, (3) the flexural stiffness of the restraining bars, (4) the type of restraint (crown or uniform), (5) the end supports (fixed or hinged), and (6) the type of loading (vertical or tilt).

Theoretical solutions for the lateral-torsional buckling loads of parabolic arches were obtained from Equations (9). These equations were developed from Kirchhoff's equations of equilibrium for naturally curved and twisted rods. The assumptions and approximations made are listed in Chapter I. A numerical method employing a forward integration technique was adopted to obtain buckling loads from Equations (9). The computations were carried out on a IBM 7094 computer.

The theoretical solutions considered: (1) free standing and crown restrained arches, (2) uniform vertical and uniform tilt loads, and (3) fixed and hinged end supports. The lateral-torsional buckling loads from these solutions which can be compared with the experimental results are listed in Table 3.

The theoretical solution of a vertically loaded parabolic arch with a rigid restraint at the crown and fixed end supports indicated a variation of the angle twist ($\bar{\beta}$) of the arch along its length which was not initially anticipated. A special test was conducted which verified this variation. Refer to Appendix B.

In Chapter III, lateral-torsional buckling loads determined from theoretical solutions are compared with some of those predicted fron the test results. Twenty different cases are included and are listed in Table 3. The Southwell method was used to predict the buckling loads from the test results in all cases. The theoretical buckling loads are taken from the works of Stussi, Godden and the author. All of the theoretical solutions are based on a linear buckling theory.

With the exception of the buckling load obtained by this author for case 4 , all of the loads based on theoretical considerations agree very favorably with those predicted from test results.

In case 4 the theoretical buckling load is 43 per cent higher than the load from tests. Because of the low magnitude of the loads involved in the test, the test results will be highly sensitive to unavoidable imperfections of alignment, workmanship and test equipment. It is therefore felt that the 43 per cent difference is not significant.

It is concluded that the experimental investigations contained herein substantiate the theoretical solutions for lateral-torsional buckling loads taken from the investigations of Stussi and this author.

APPENDIX A

TEST DATA

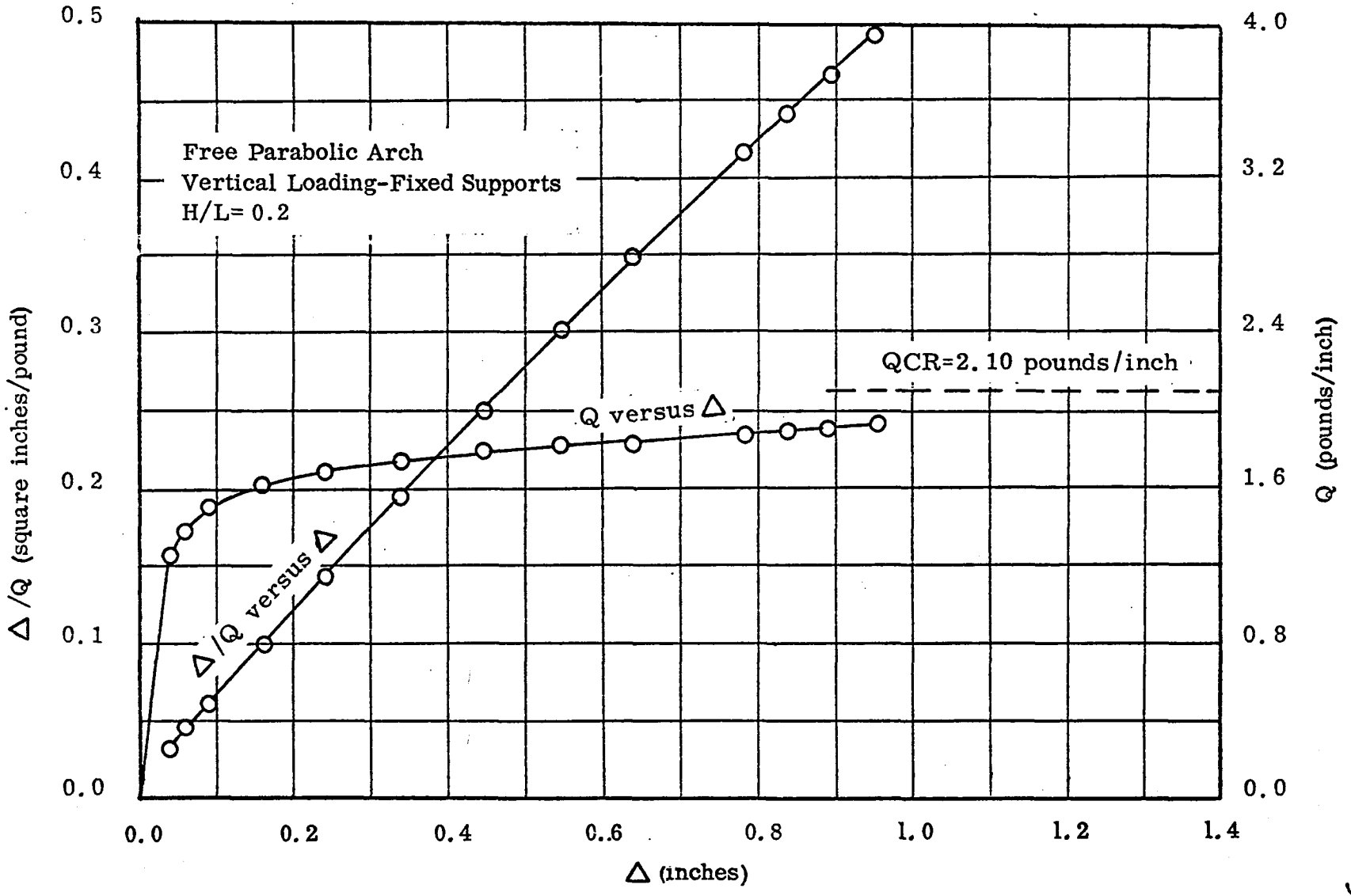

Fig. 21.--Load-Deflection and Southwell plots for Test No. 1

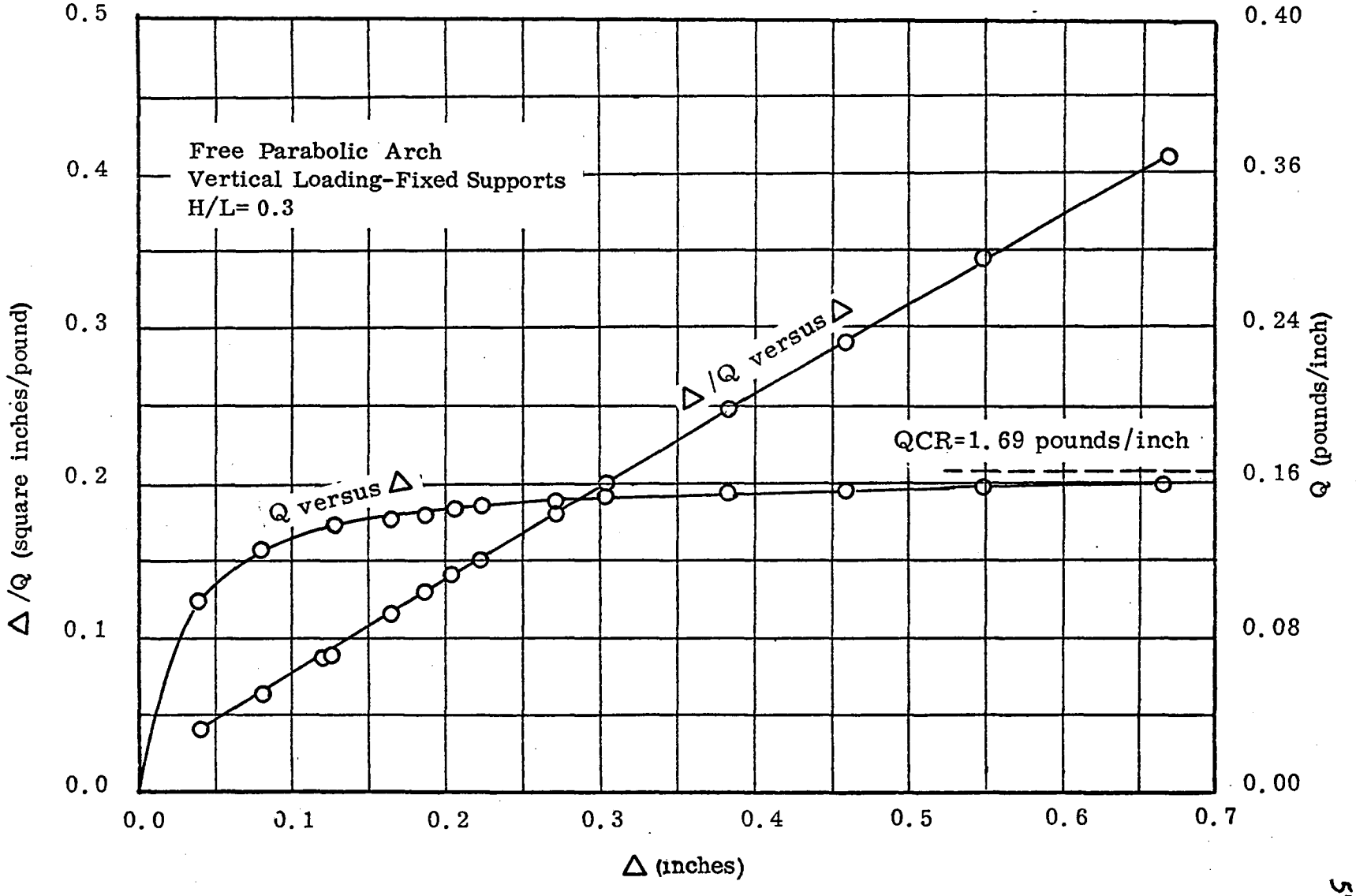

Fig. 22.-- Load-Deflection and Southwell plots for Test No. 2

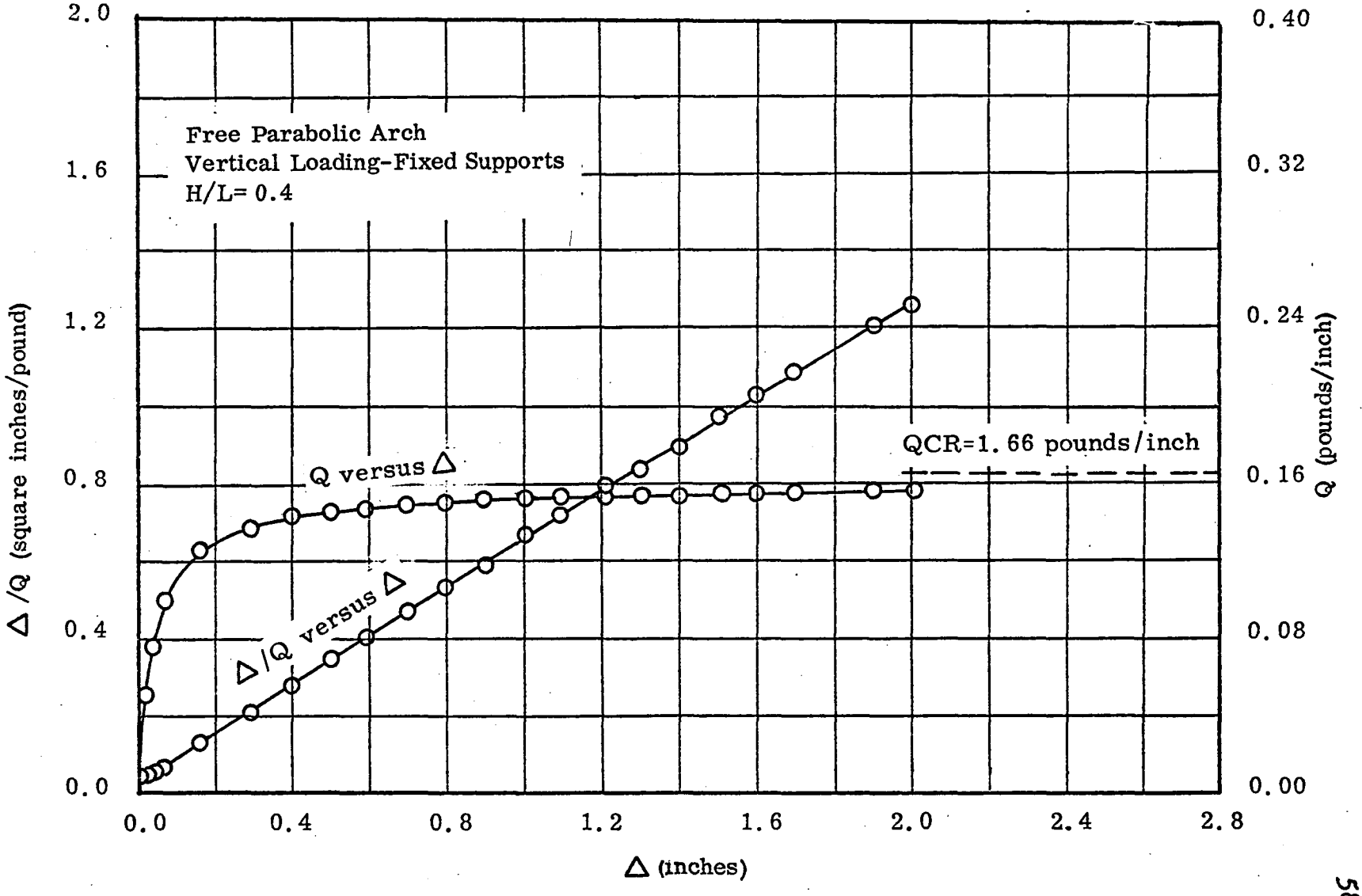

Fig. 23.--Load-Deflection and Southwell plots for Test No. 3

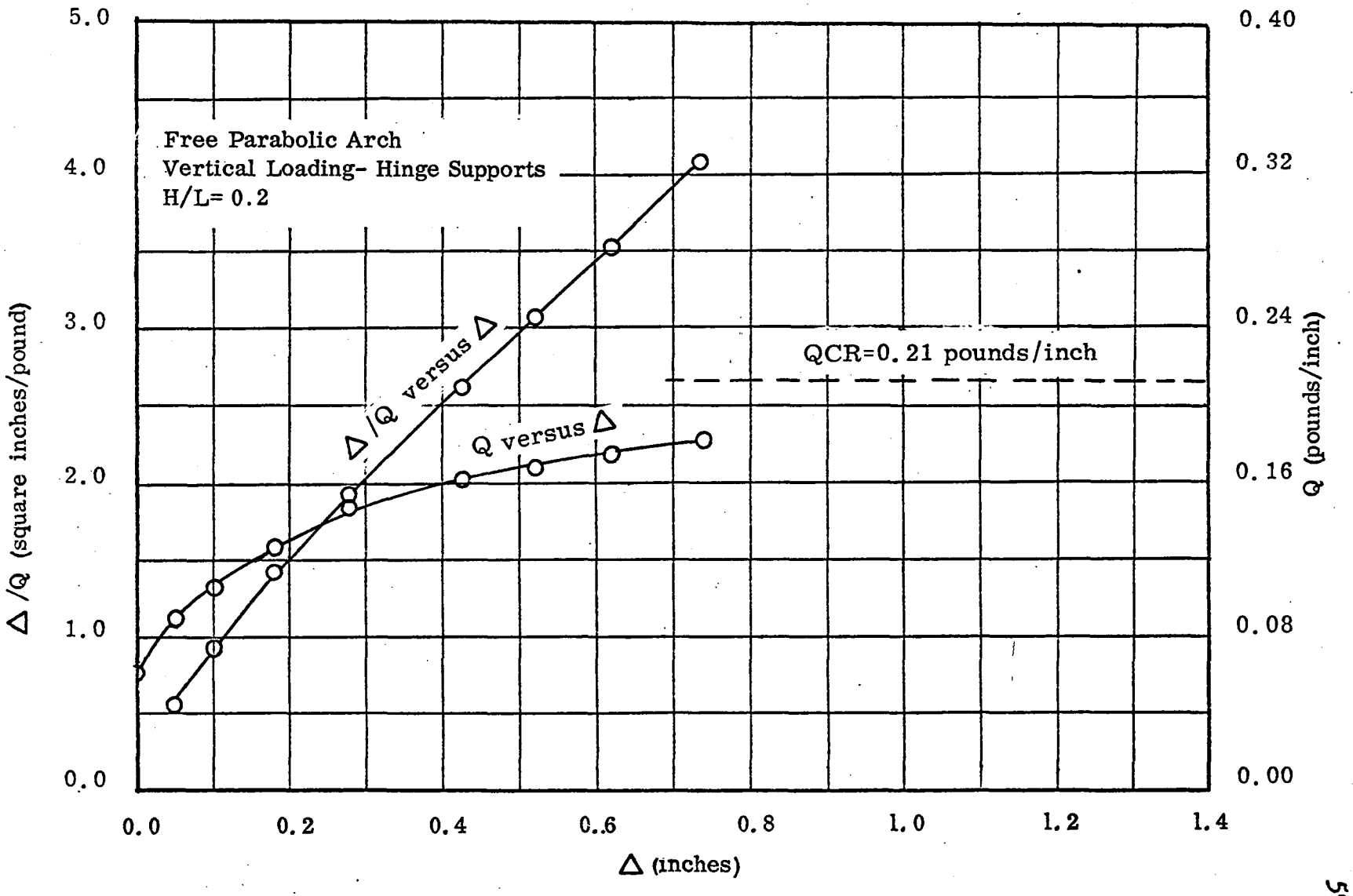

Fig. 24.-- Load-Deflection and Southwell plots for Test No. 4

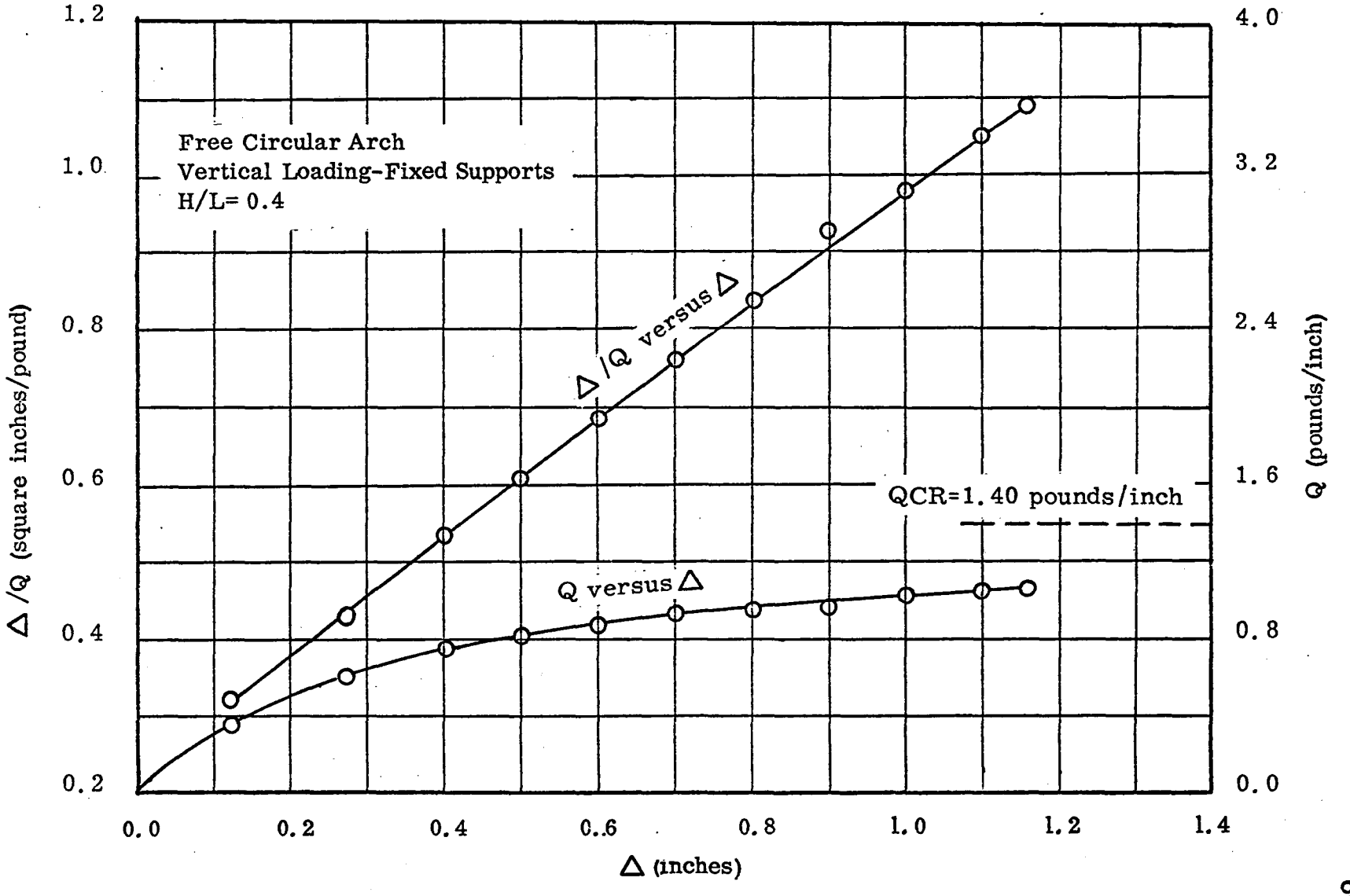

Fig. 25. -- Load-Deflection and Southwell plots for Test No. 5

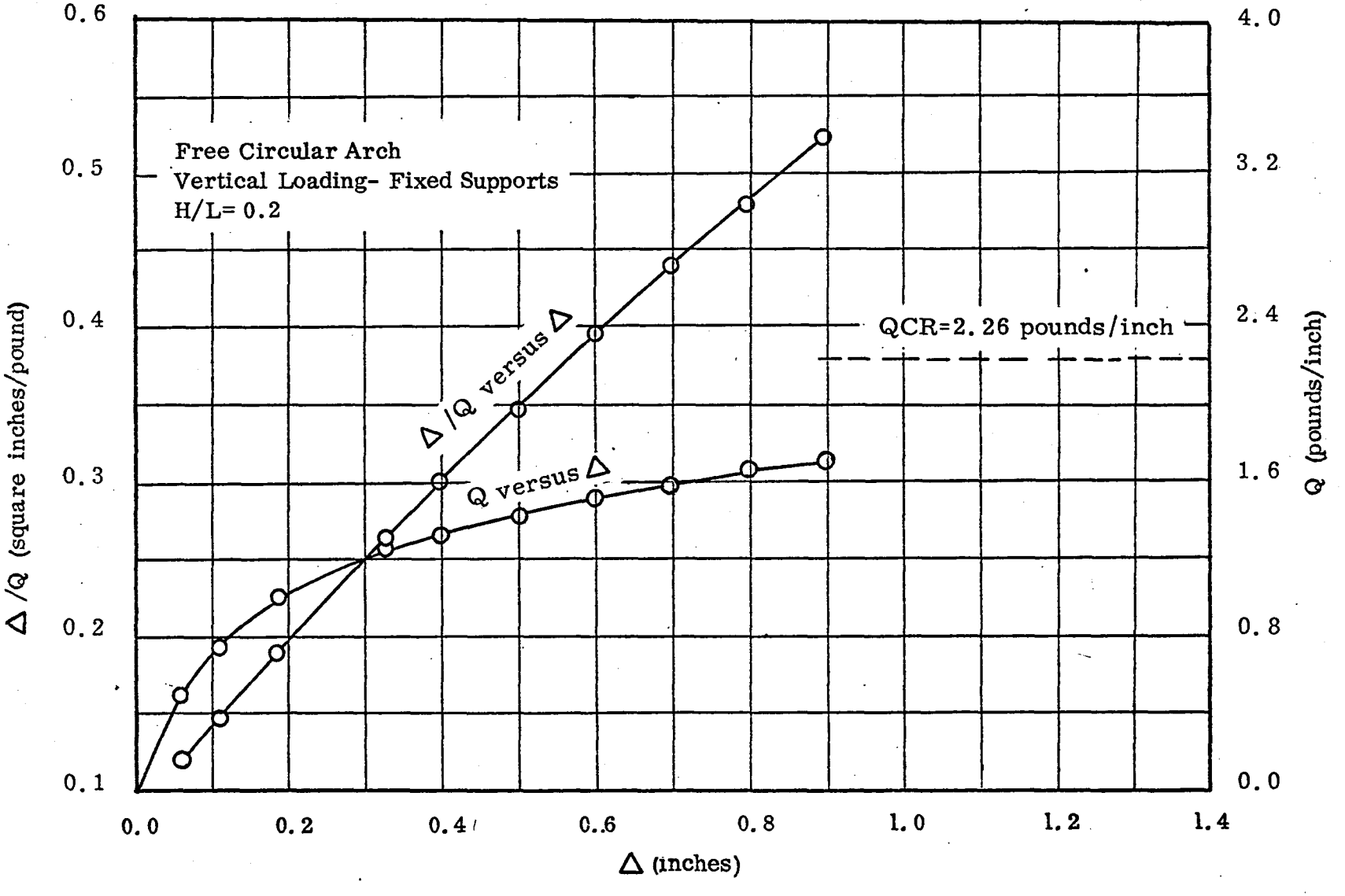

Fig. 26. --Load-Deflection and Southwell plots for Test No. 6

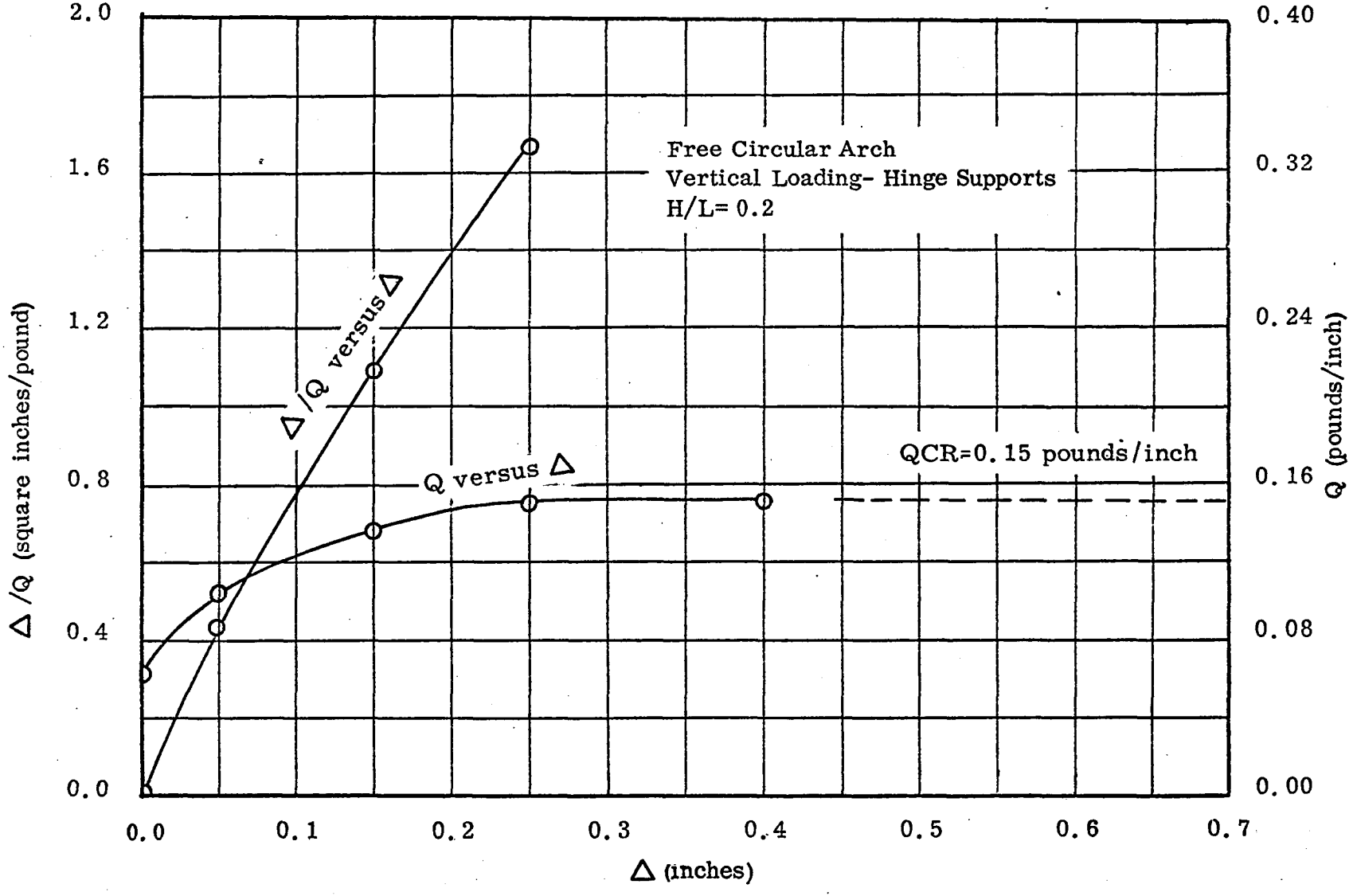

Fig. 27.-- Load-Deflection and Southwell plots for Test No. 7

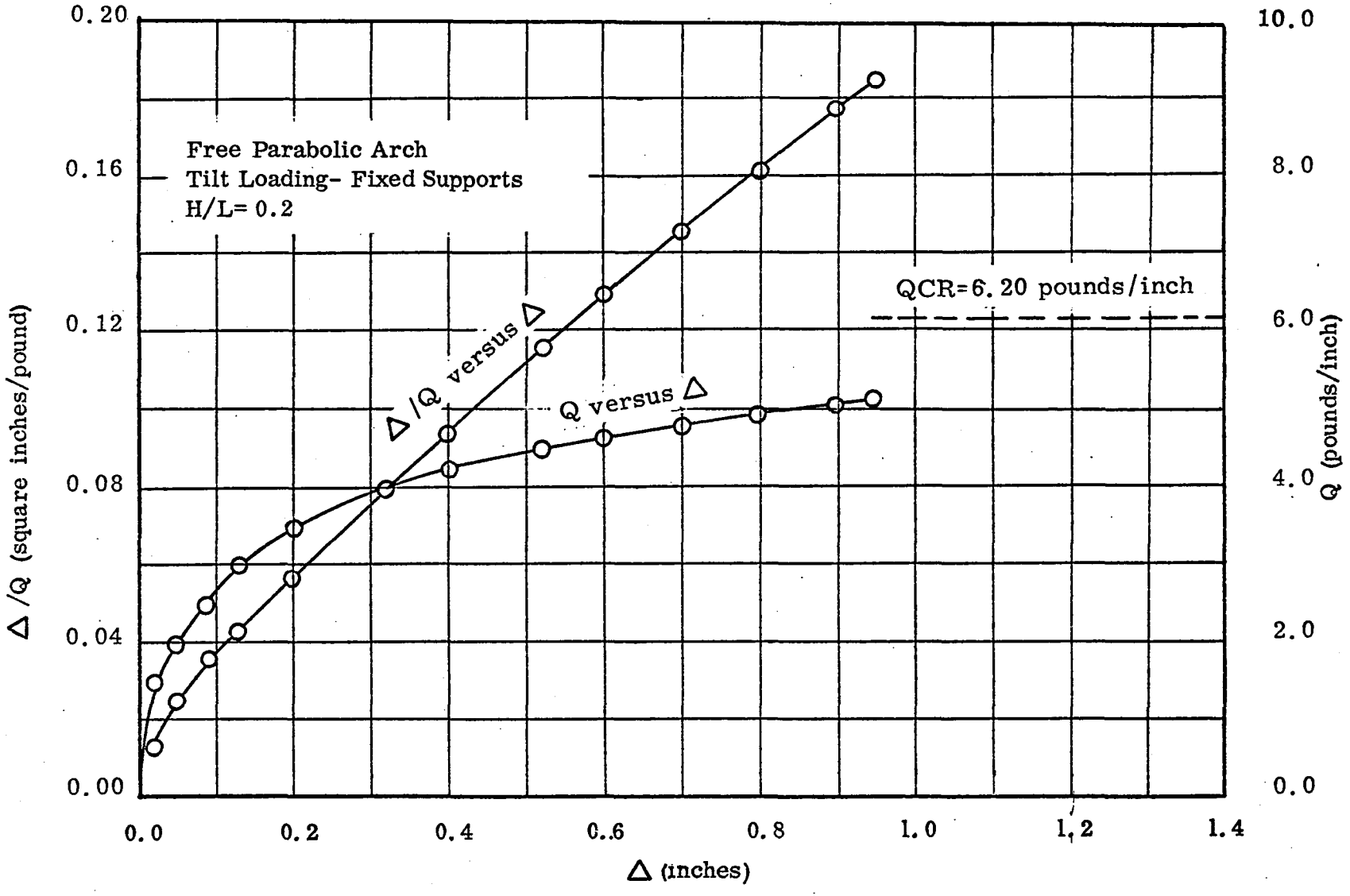

Fig. 28.--Load-Deflection and Southwell plots for Test No. 8

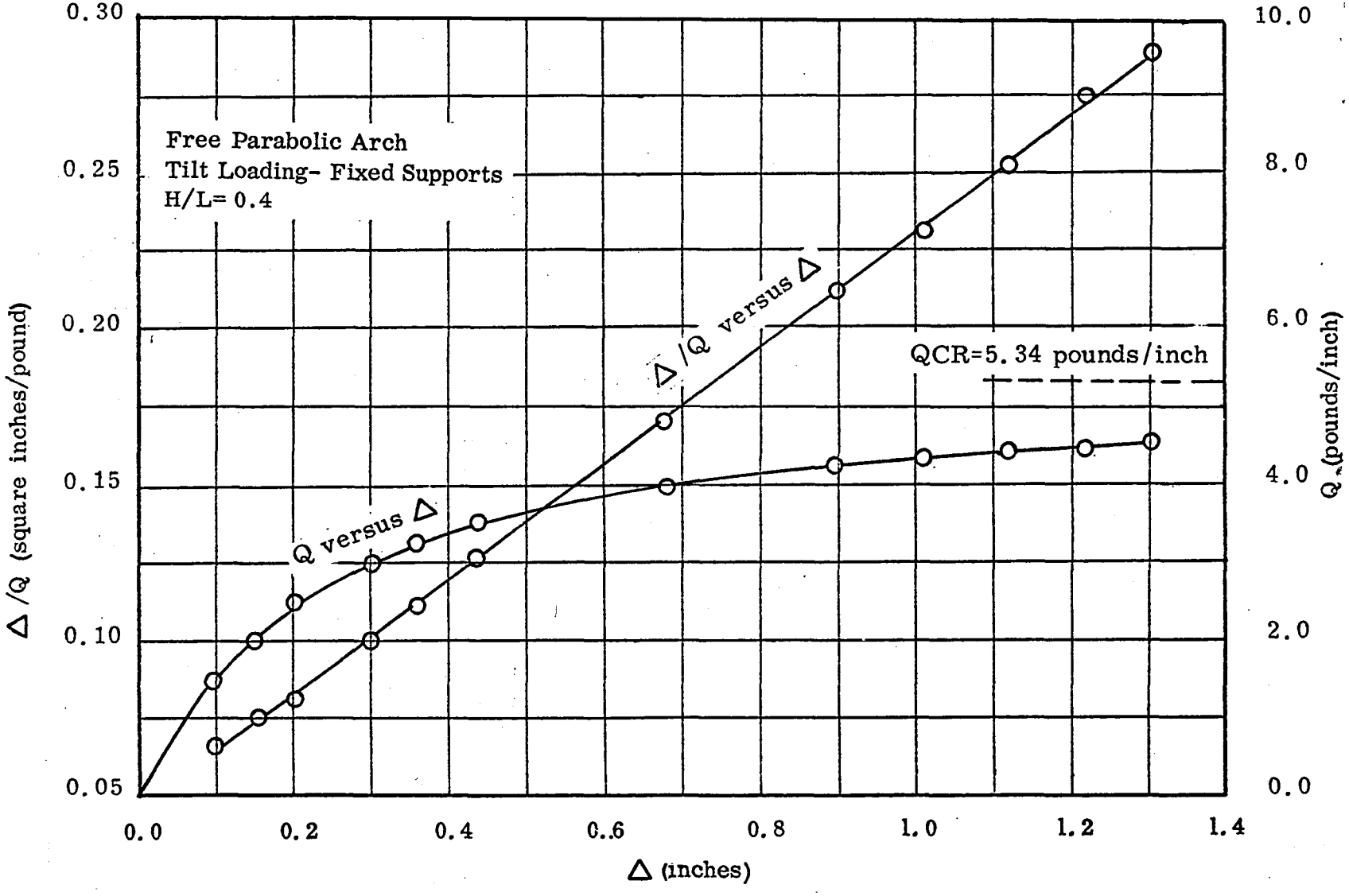

Fig. 29.--Load-Deflection and Southwell plots for Test No. 9

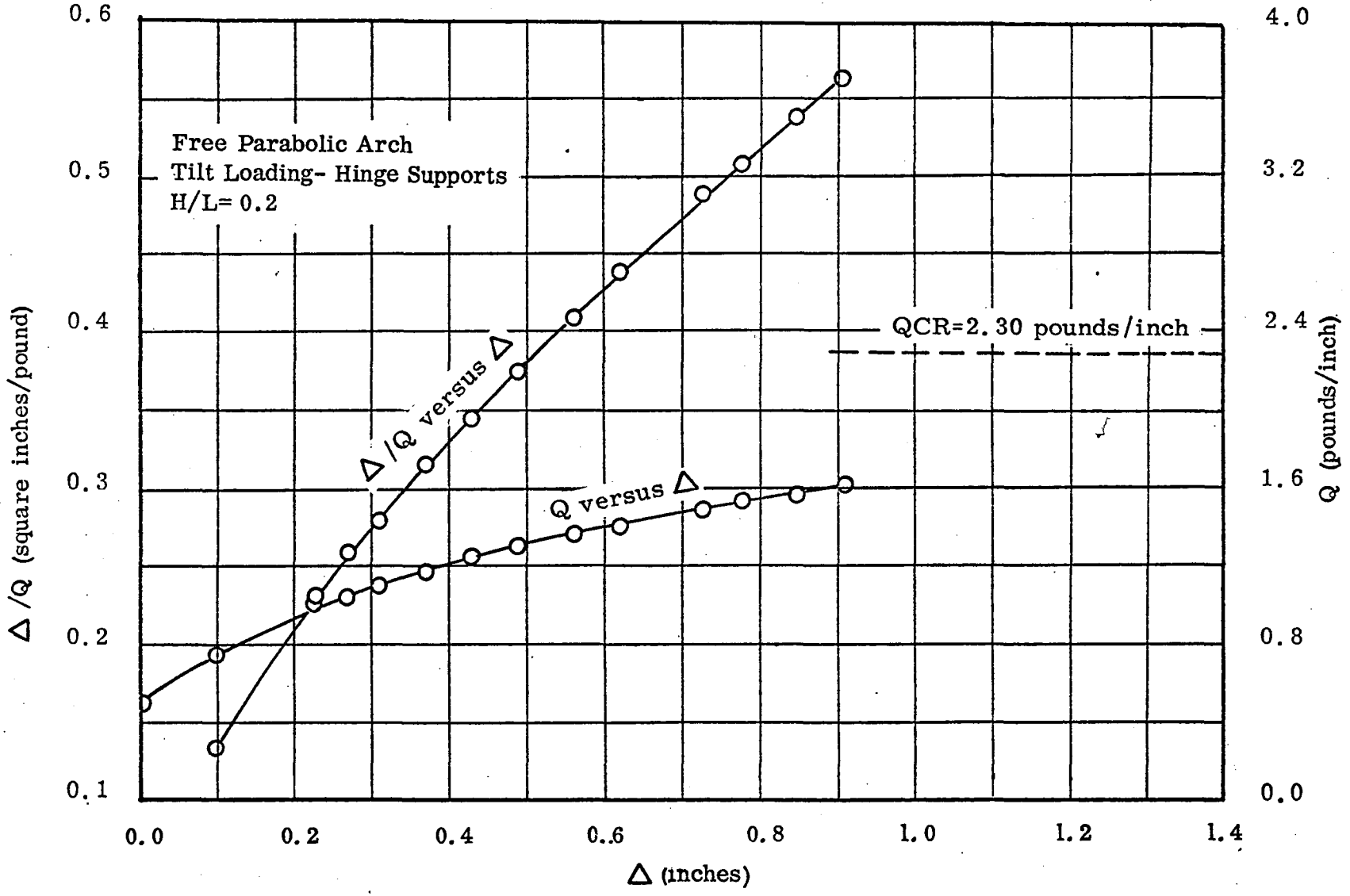

Fig. 30. -- Load-Deflection and Southwell plots for Test No. 10

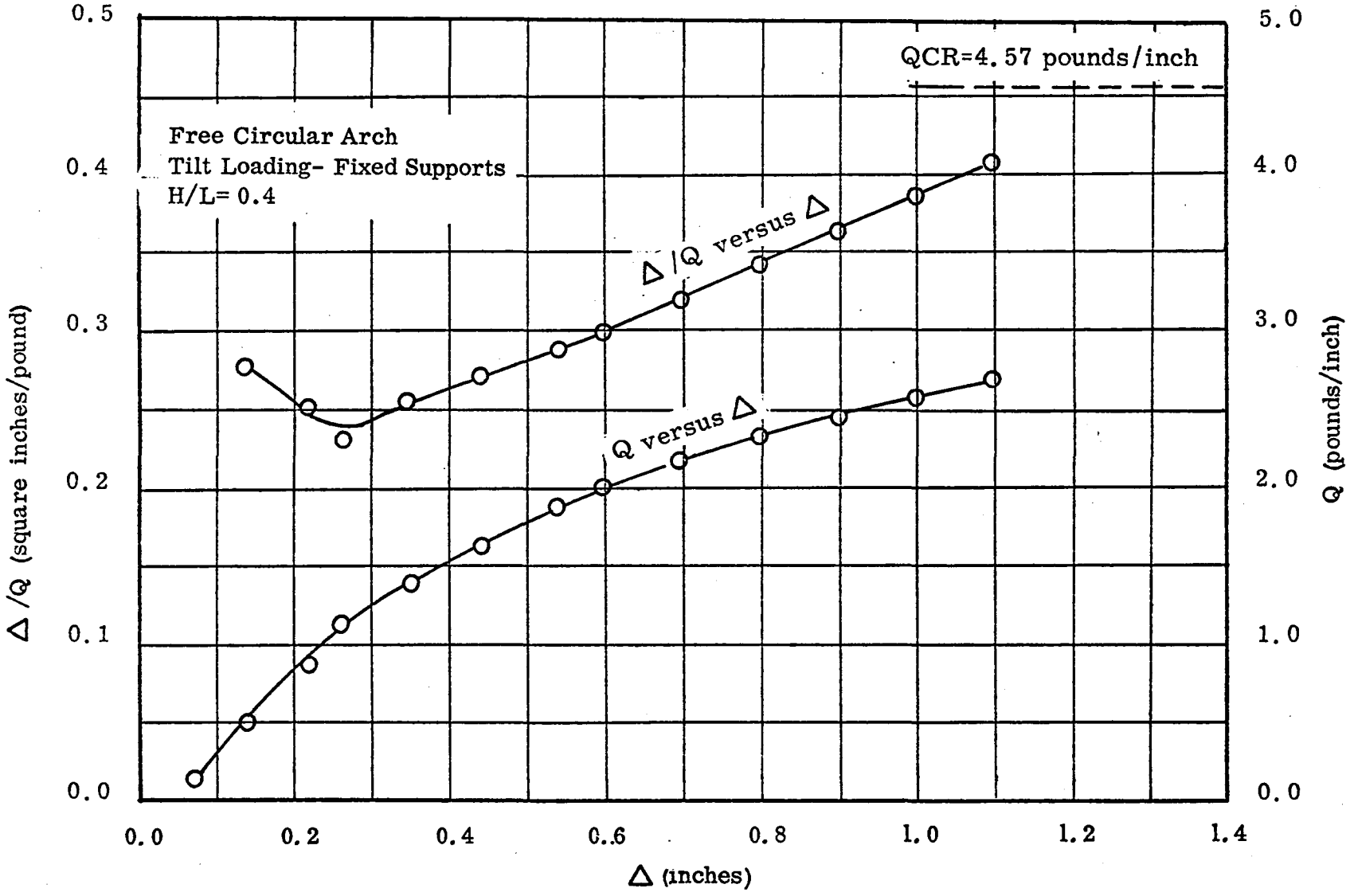

Fig. 31.-- Load-Deflection and Southwell plots for Test No. 11

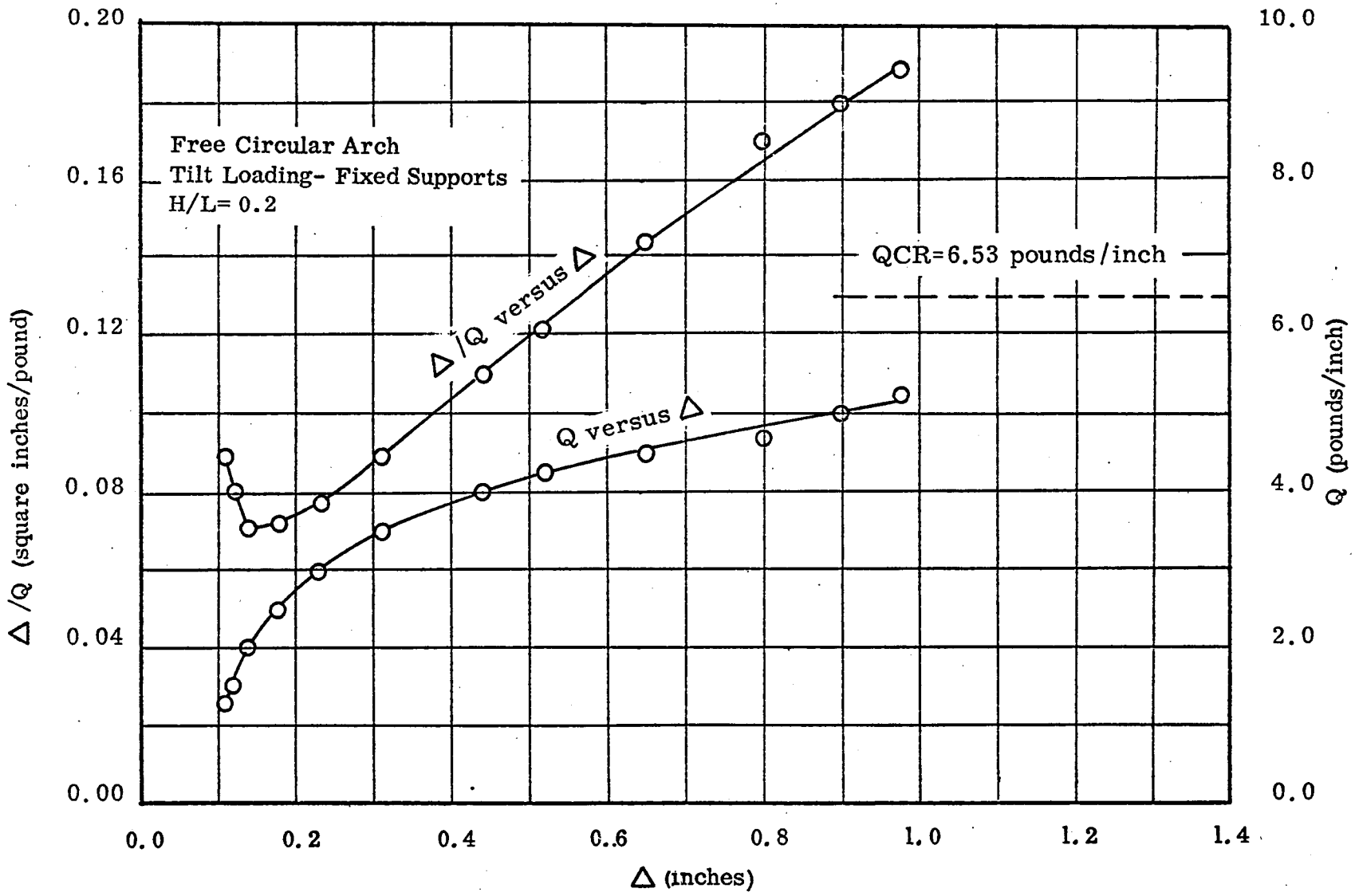

Fig. 32. -- Load-Deflection and Southwell plots for Test No. 12

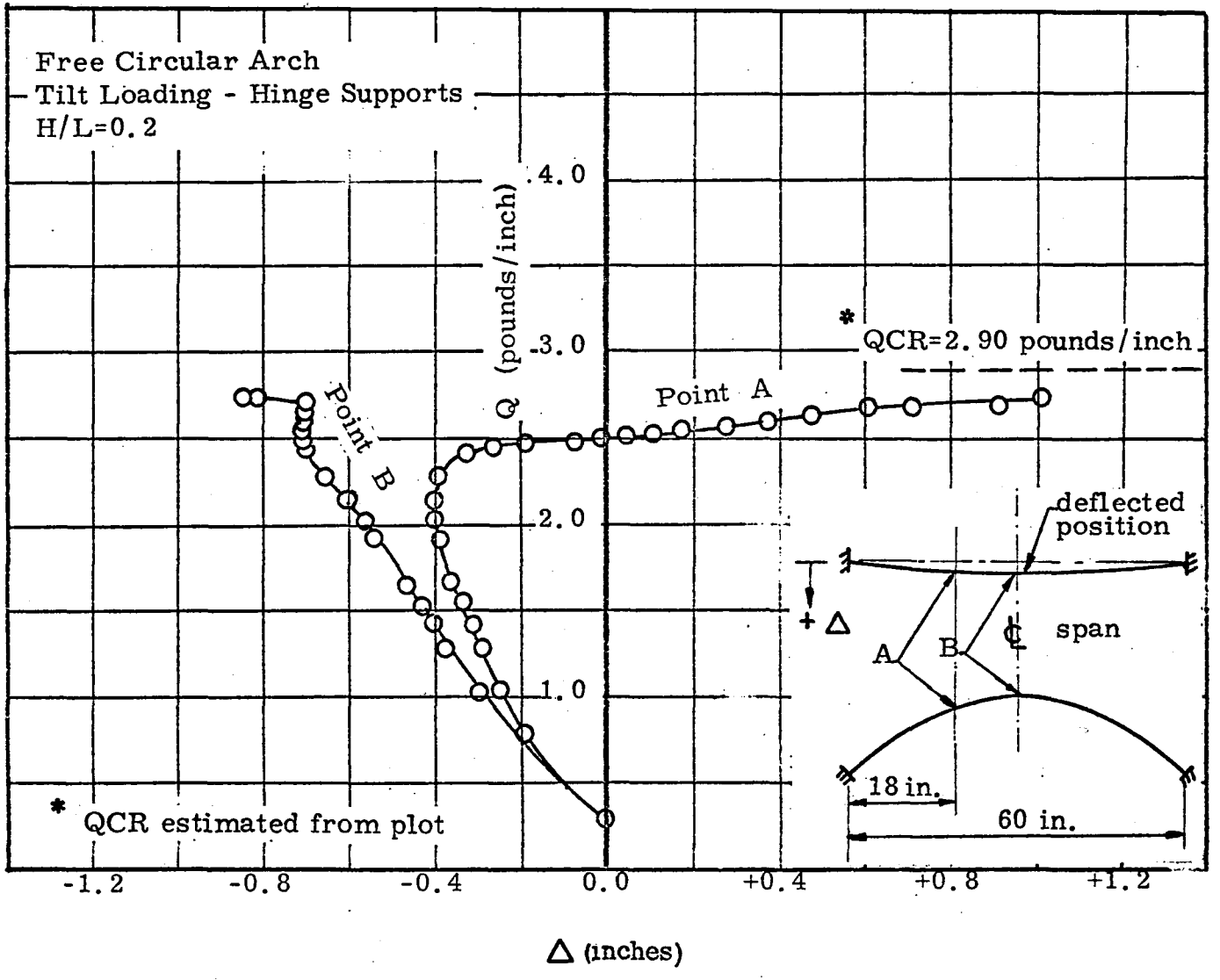

Fig. 33. -- Load-Deflection plots for Test No. 13

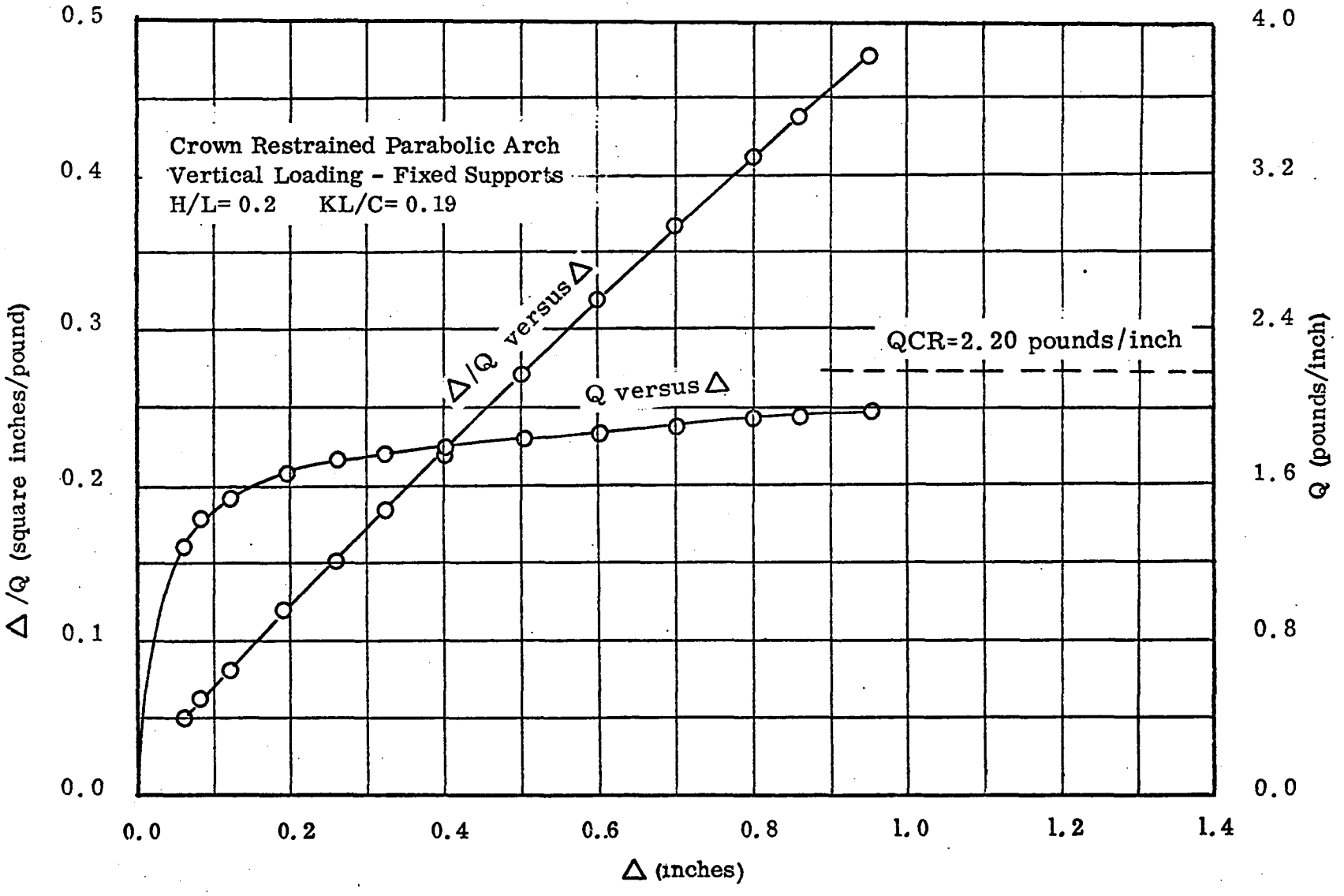

Fig. 34. -- Load-Deflection and Southwell plots for Test No. 14

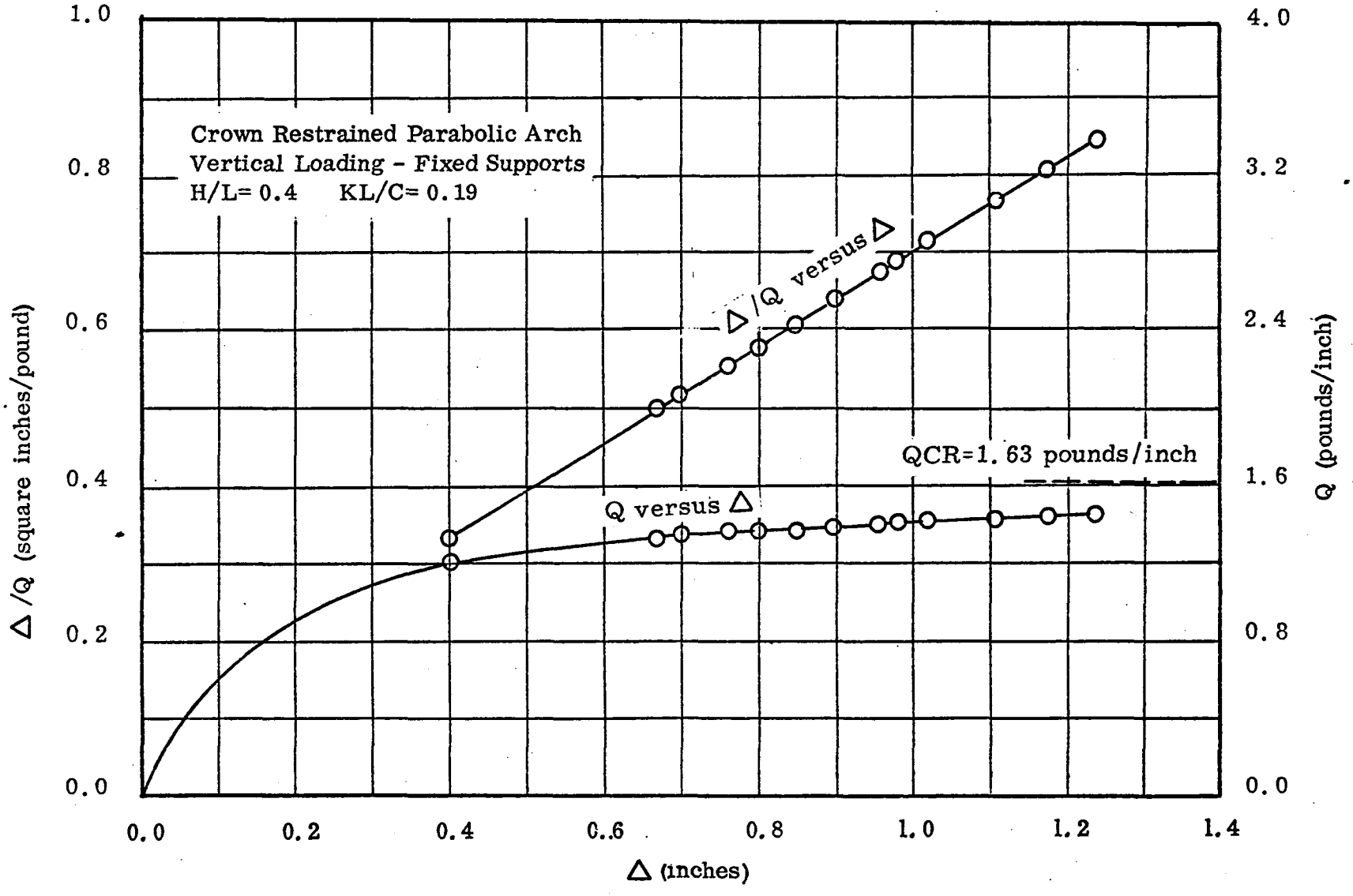

Fig. 35. --Load-Deflection and Southwell plots for Test No. 15

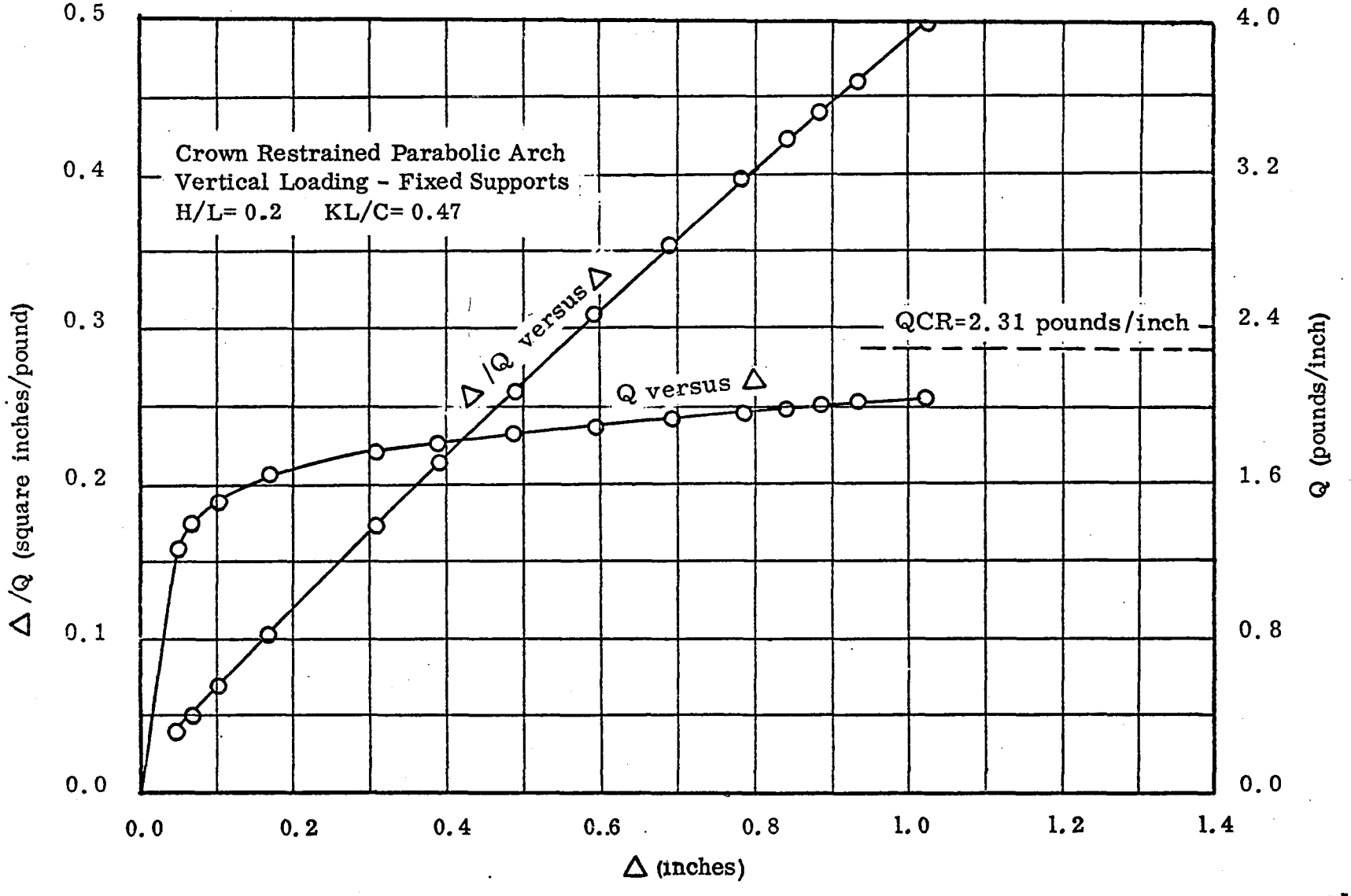

Fig. 36. --Load-Deflection and Southwell plots for Test No. 16

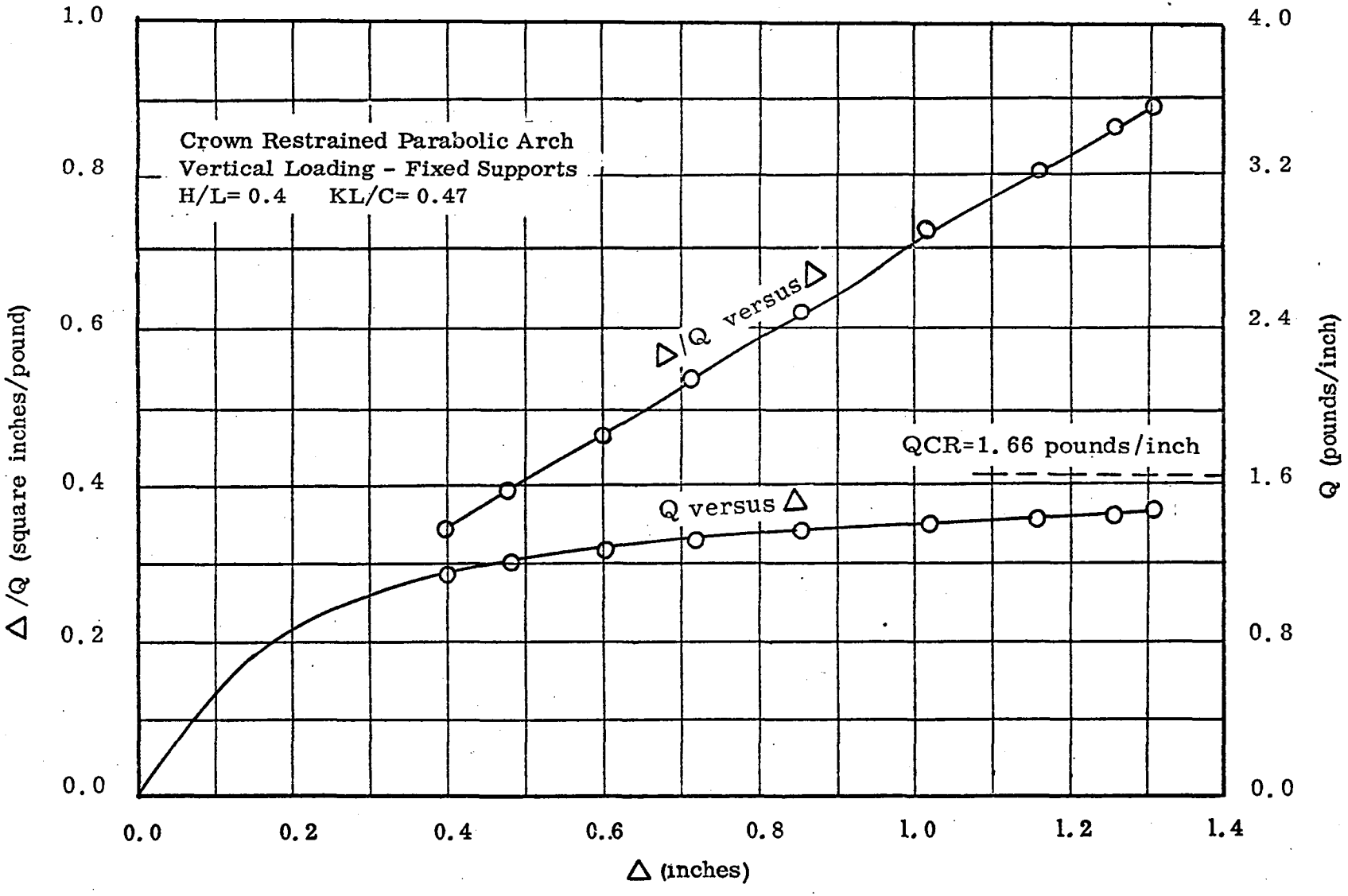

Fig. 37.--Load-Deflection and Southwell plots for Test No. 17

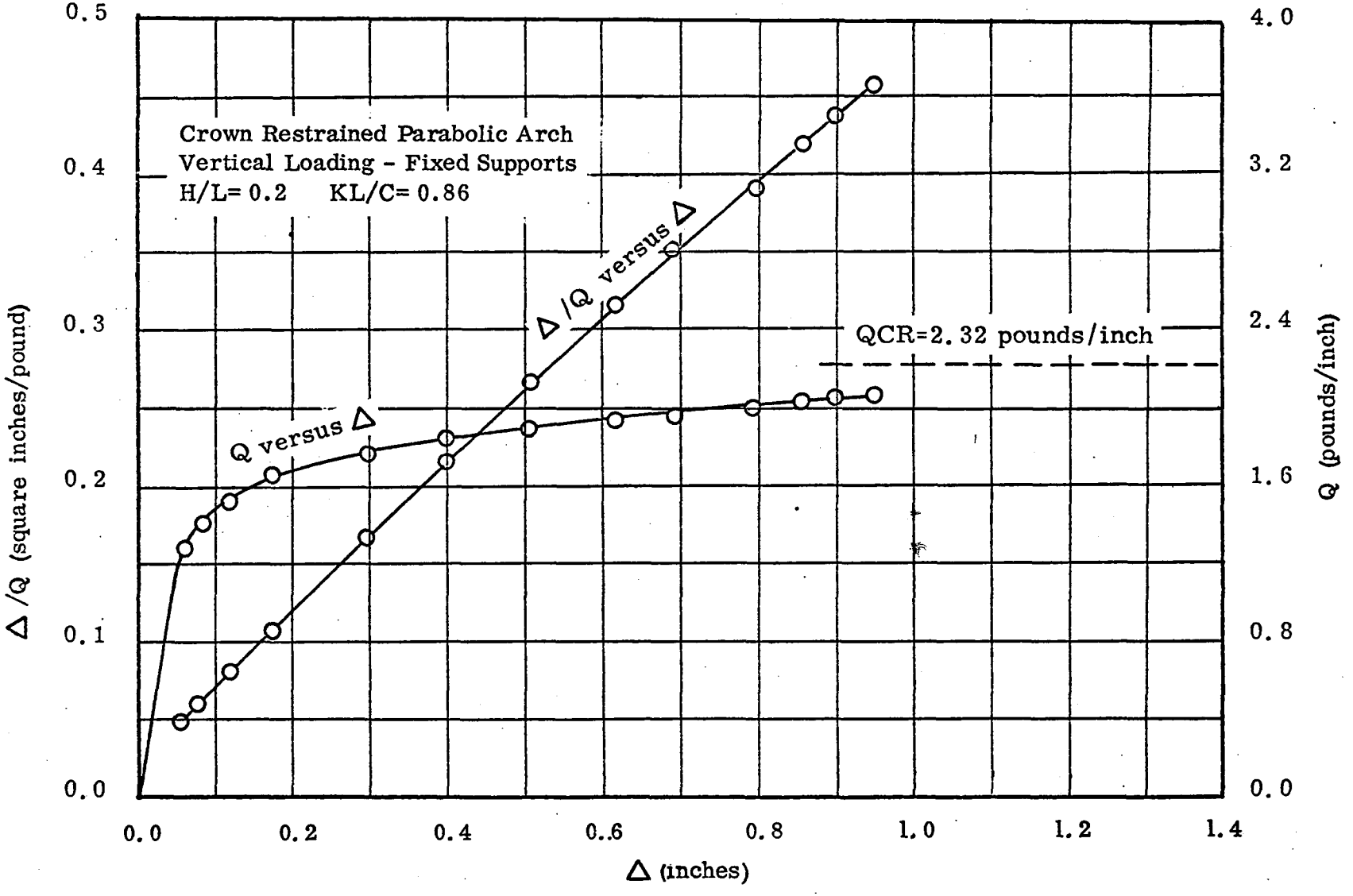

Fig. 38.--Load-Deflection and Southwell plots for Test No. 18

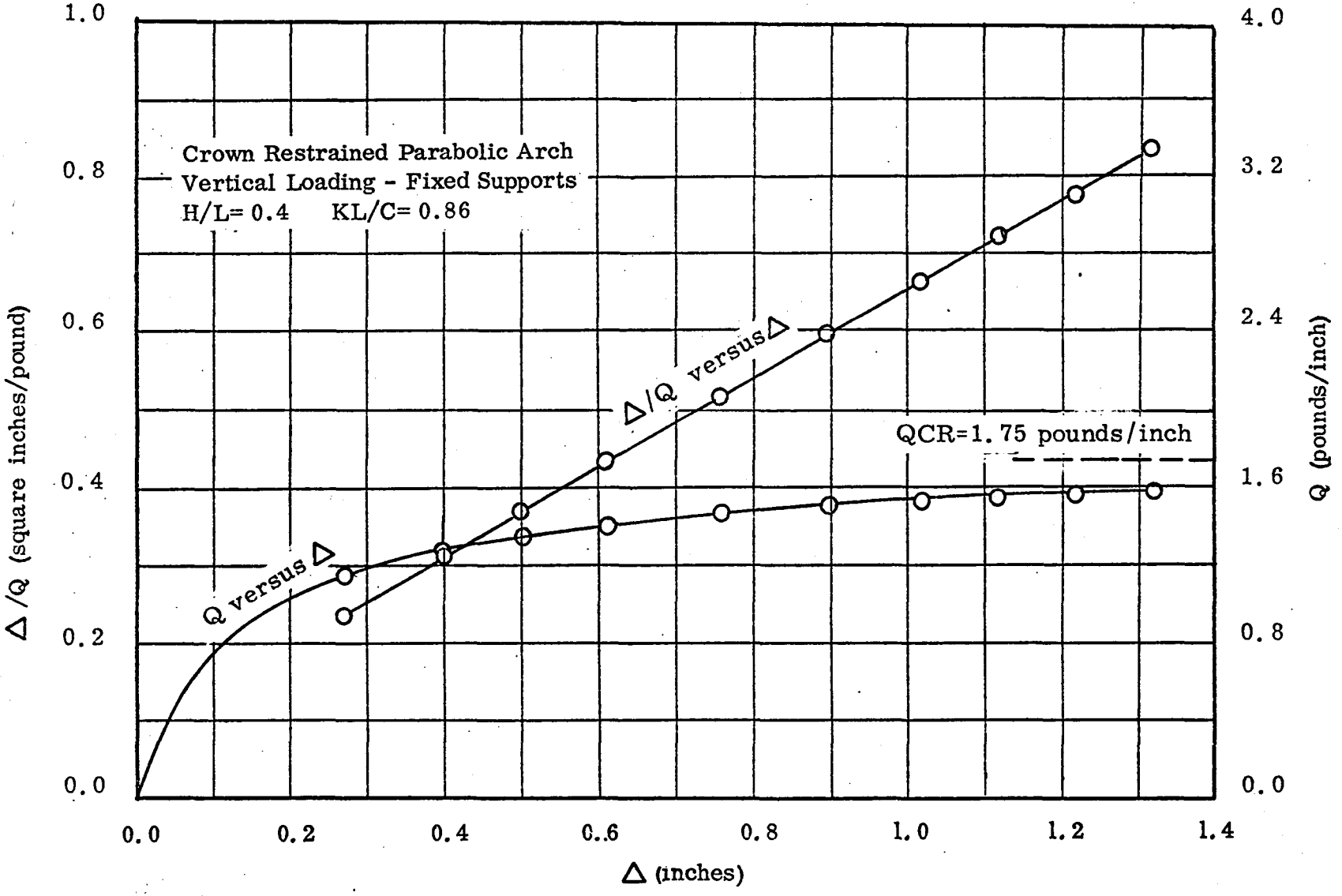

Fig. 39. -- Load-Deflection and Southwell plots for Test No. 19

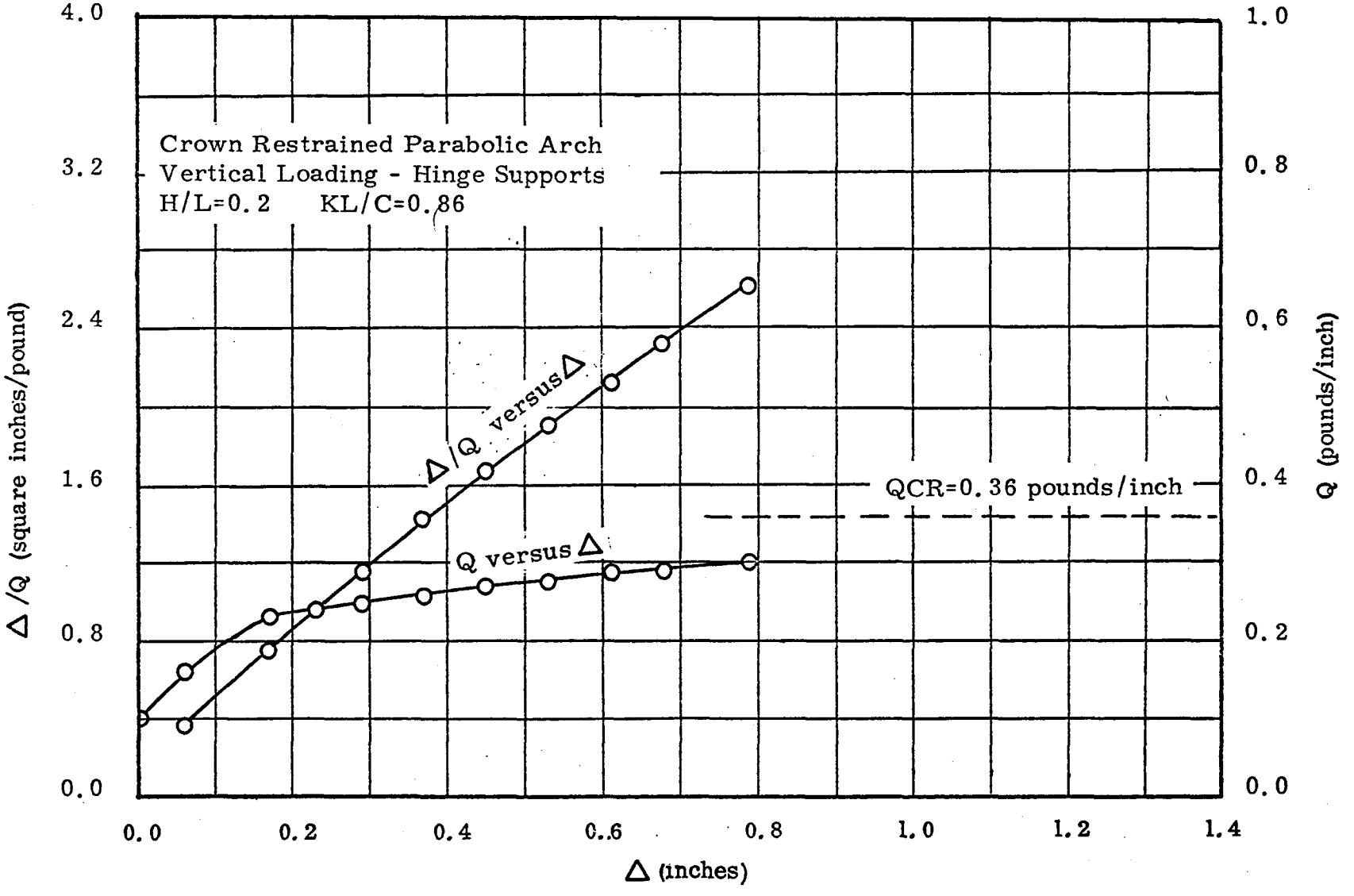

Fig. 40. -- Load-Deflection and Southwell plots for Test No. 20

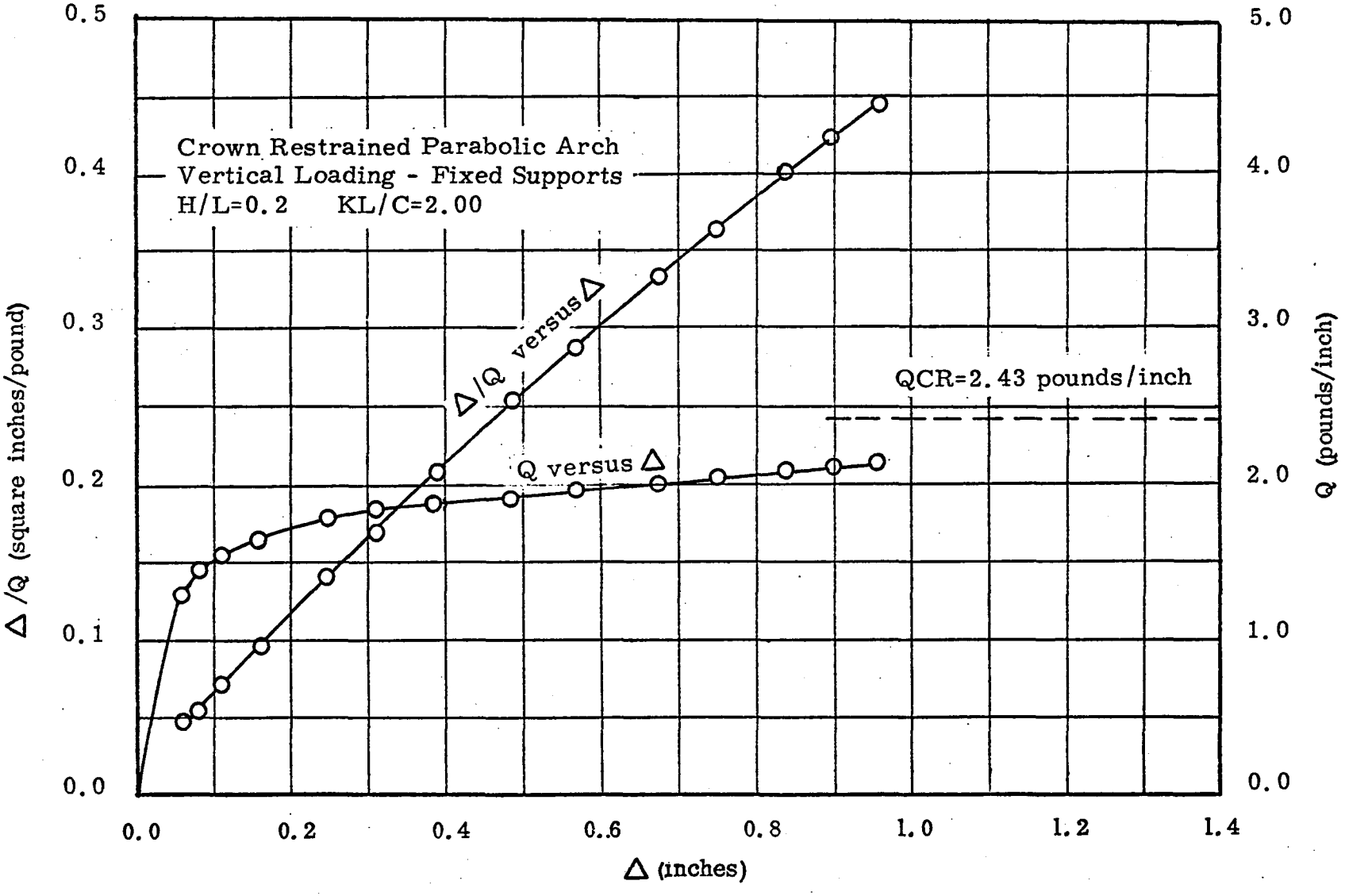

Fig. 41. -- Load-Deflection and Southwell plots for Test No. 21

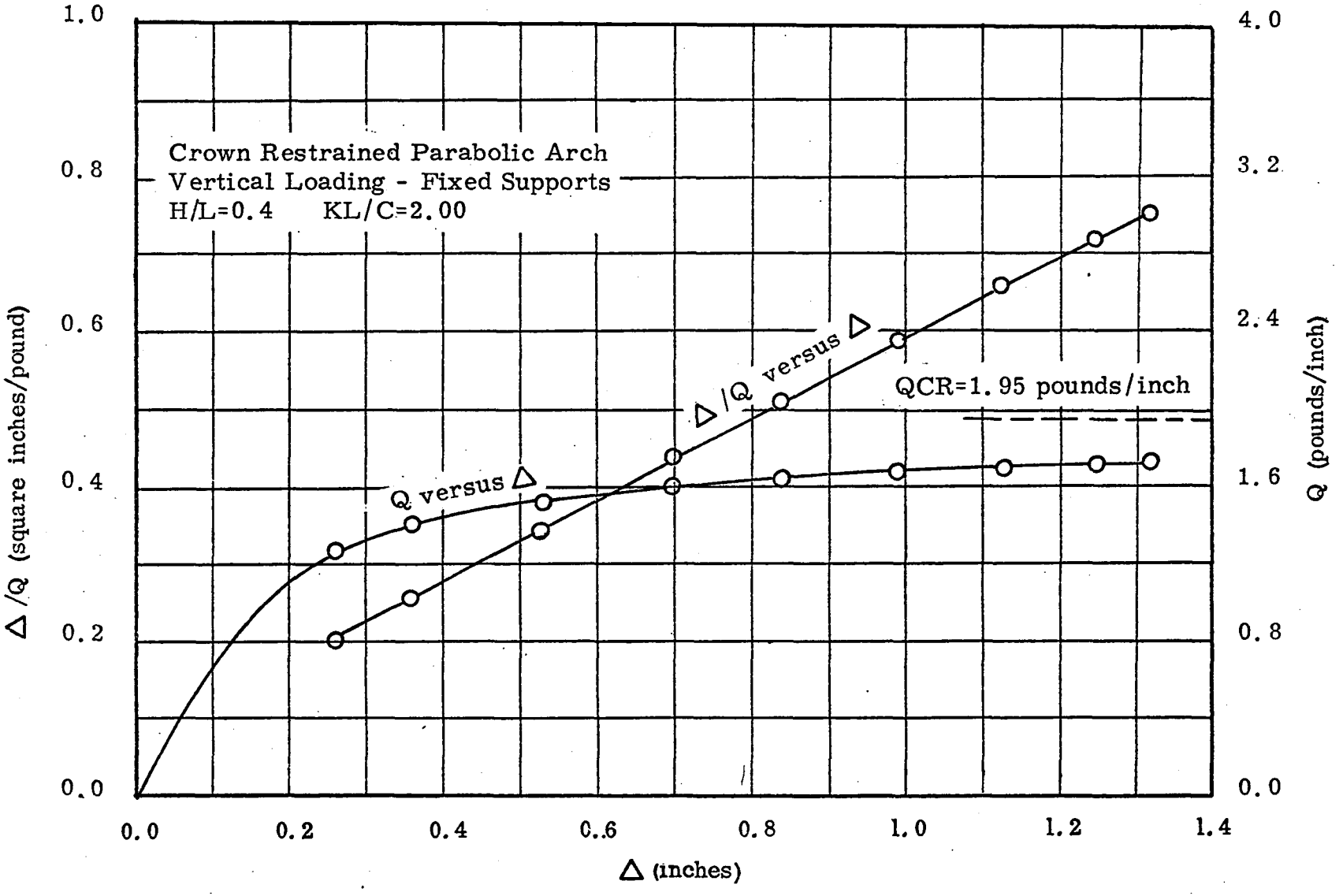

Fig. 42. -- Load-Deflection and Southwell plots for Test No. 22

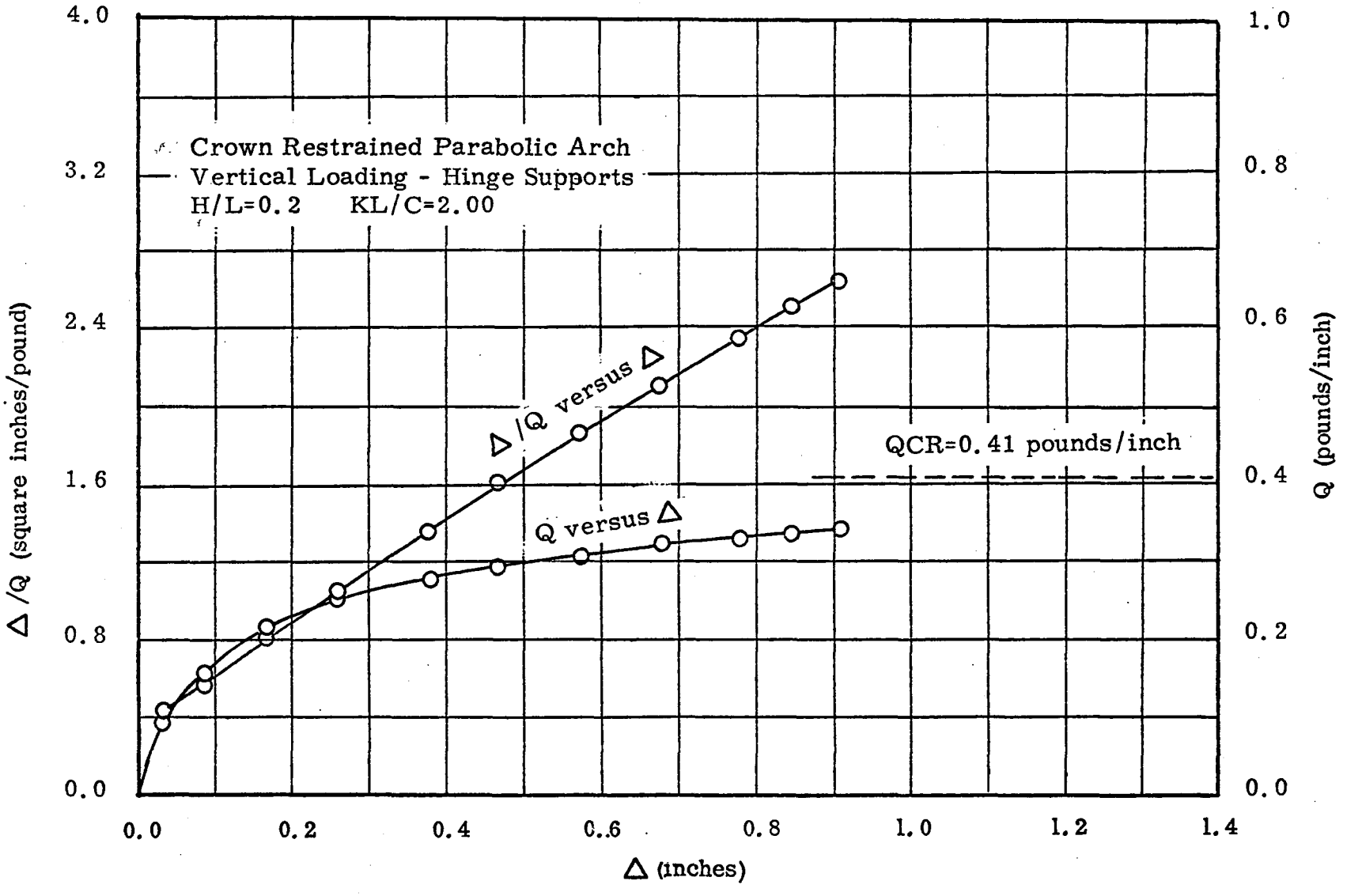

Fig. 43. -- Load-Deflection and Southwell plots for Test No. 23

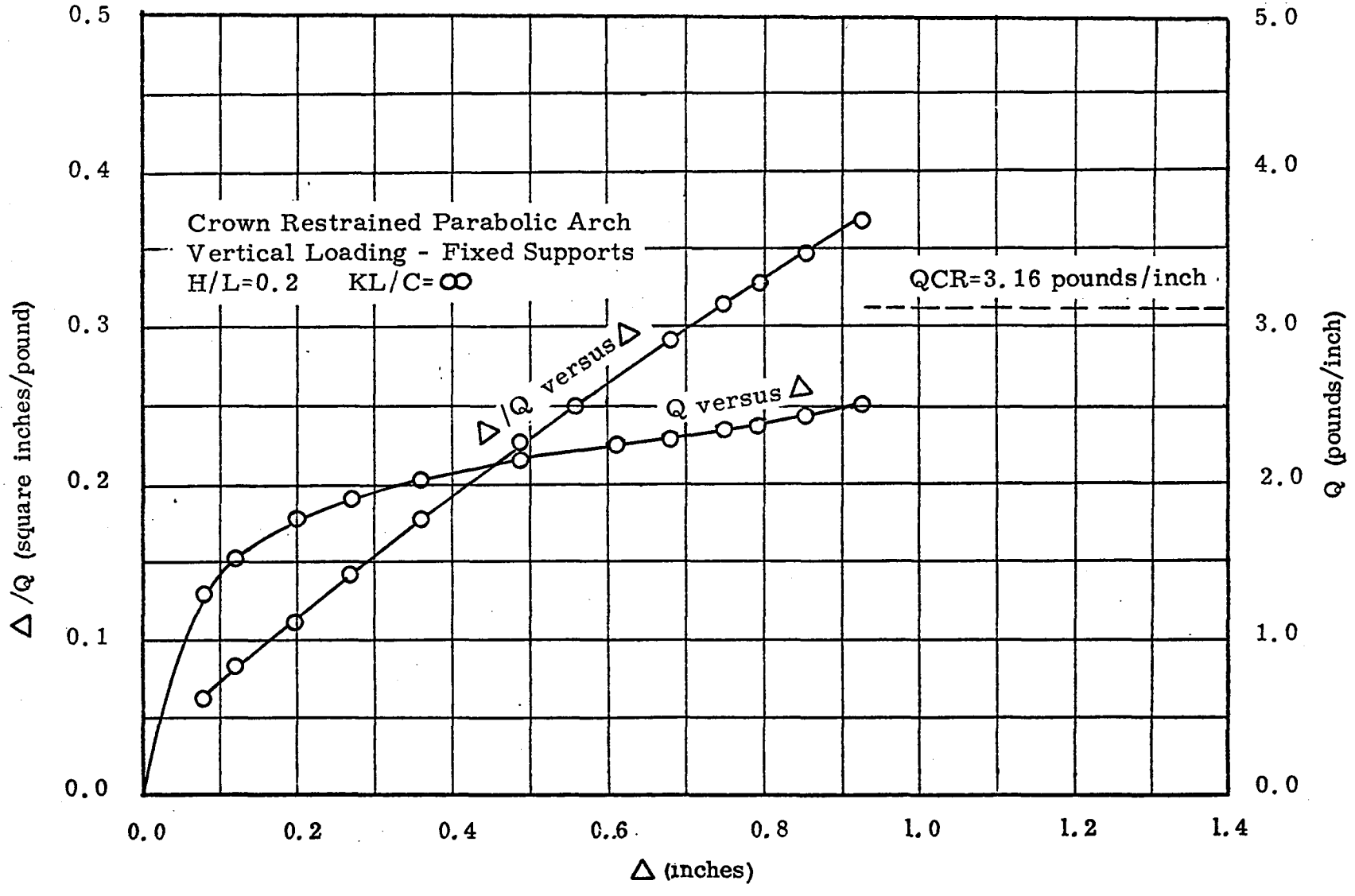

Fig. 44.-- Load-Deflection and Southwell plots for Test No. 24

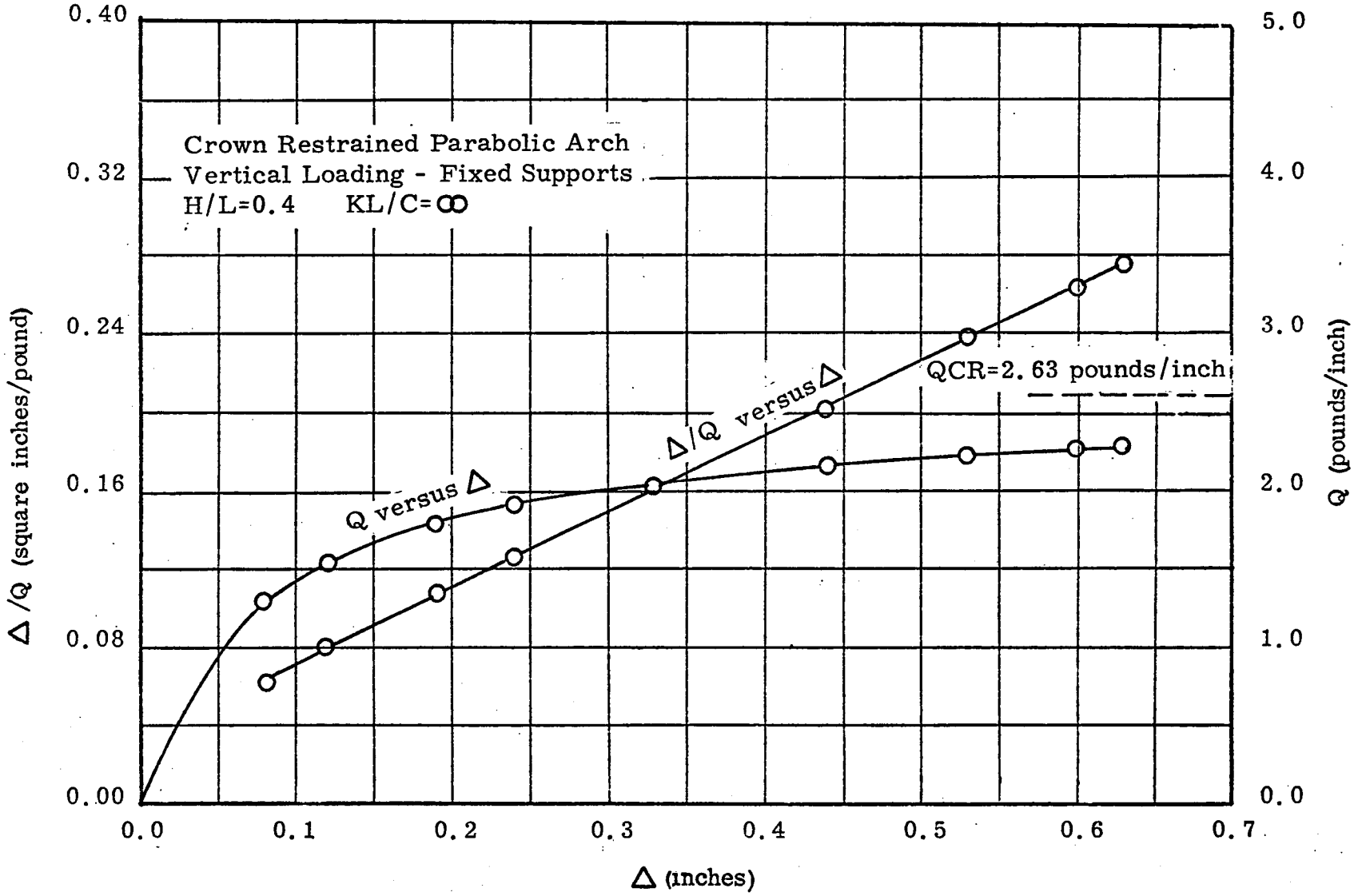

Fig. 45.--Load-Deflection and Southwell plots for Test No. 25

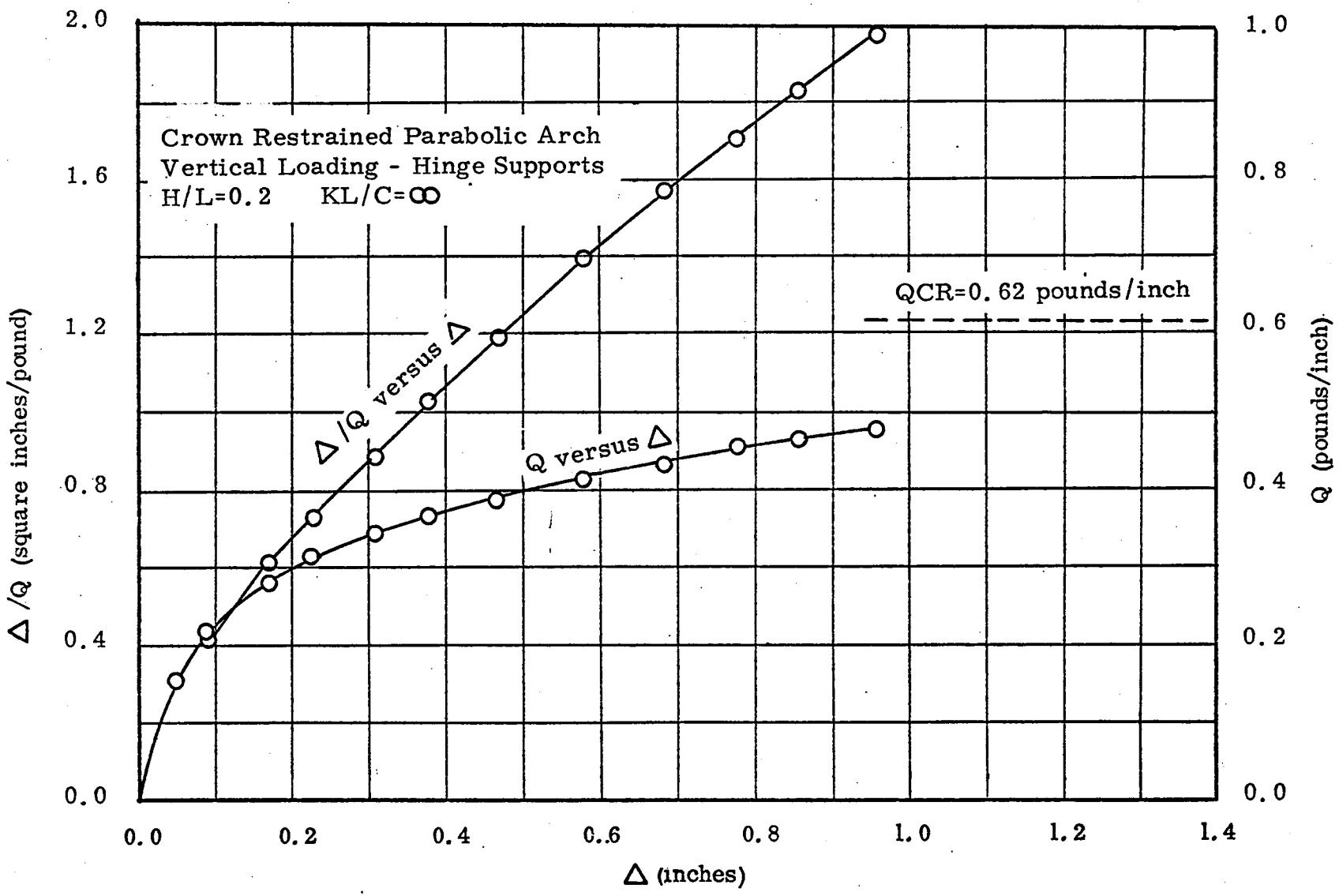

Fig. 46. -- Load-Deflection and Southwell plots for Test No. 26

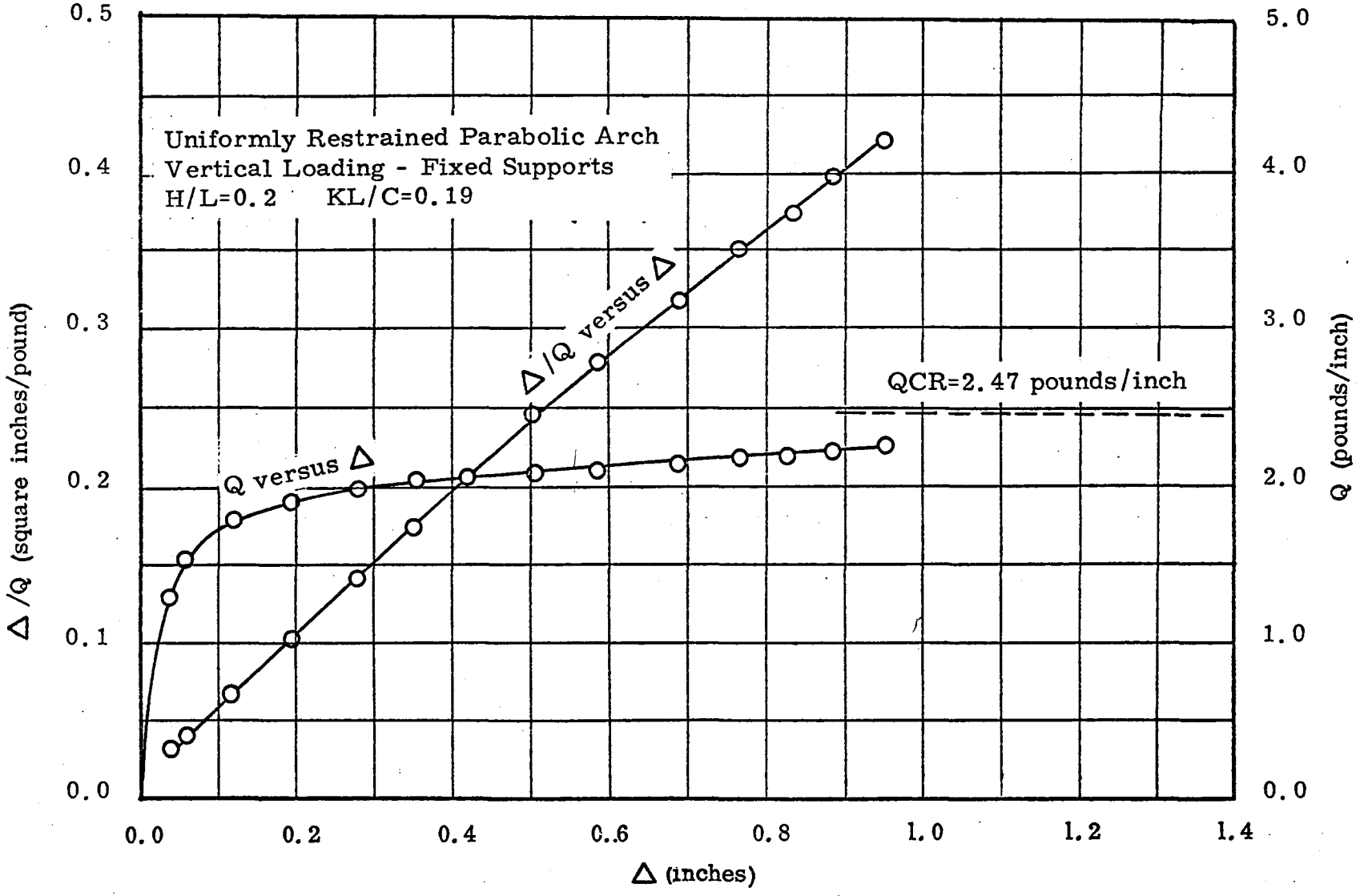

Fig. 47. -- Load-Deflection and Southwell plots for Test No. 27

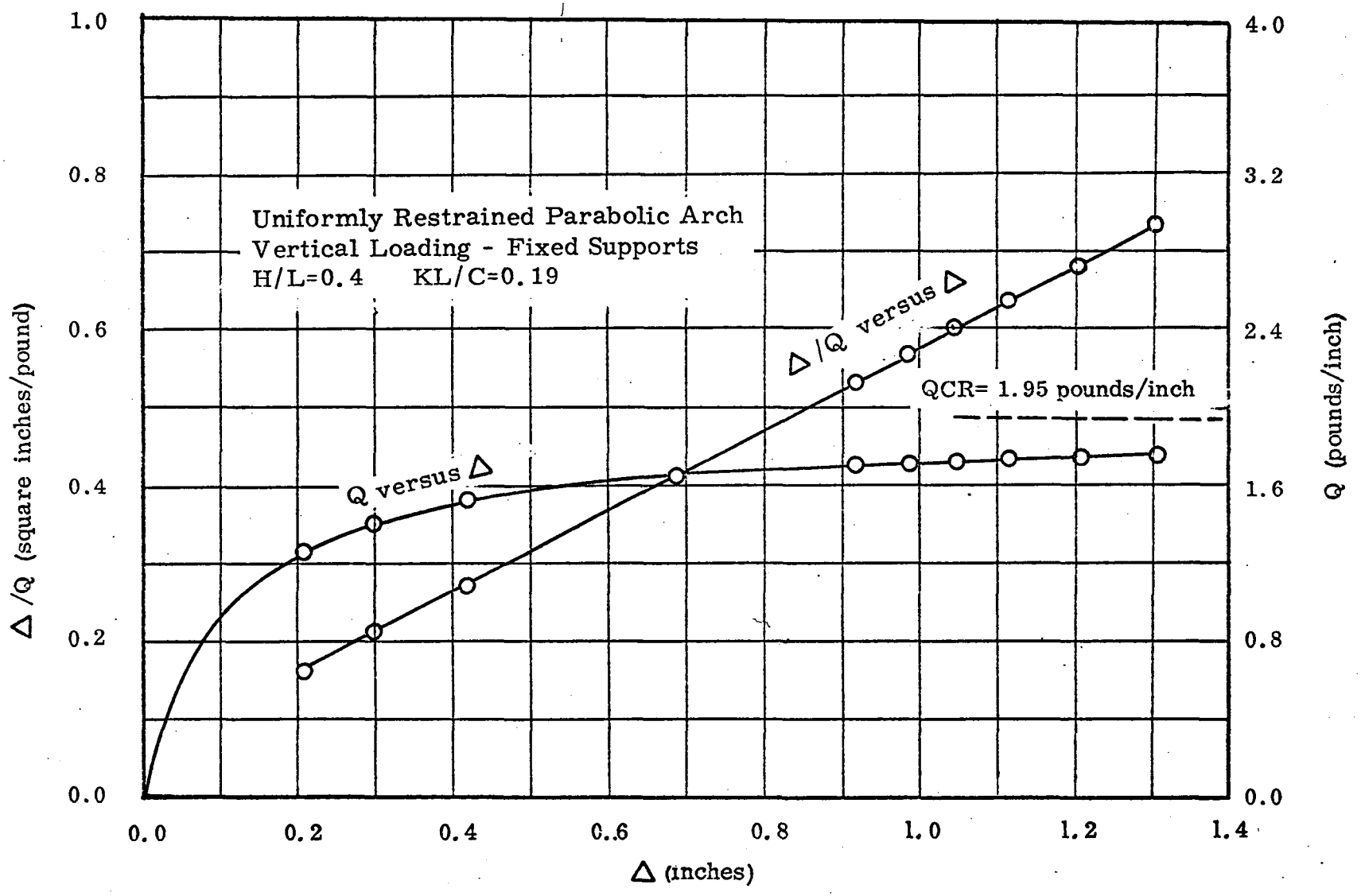

Fig. 48. -- Load-Deflection and Southwell plots for Test No. 28

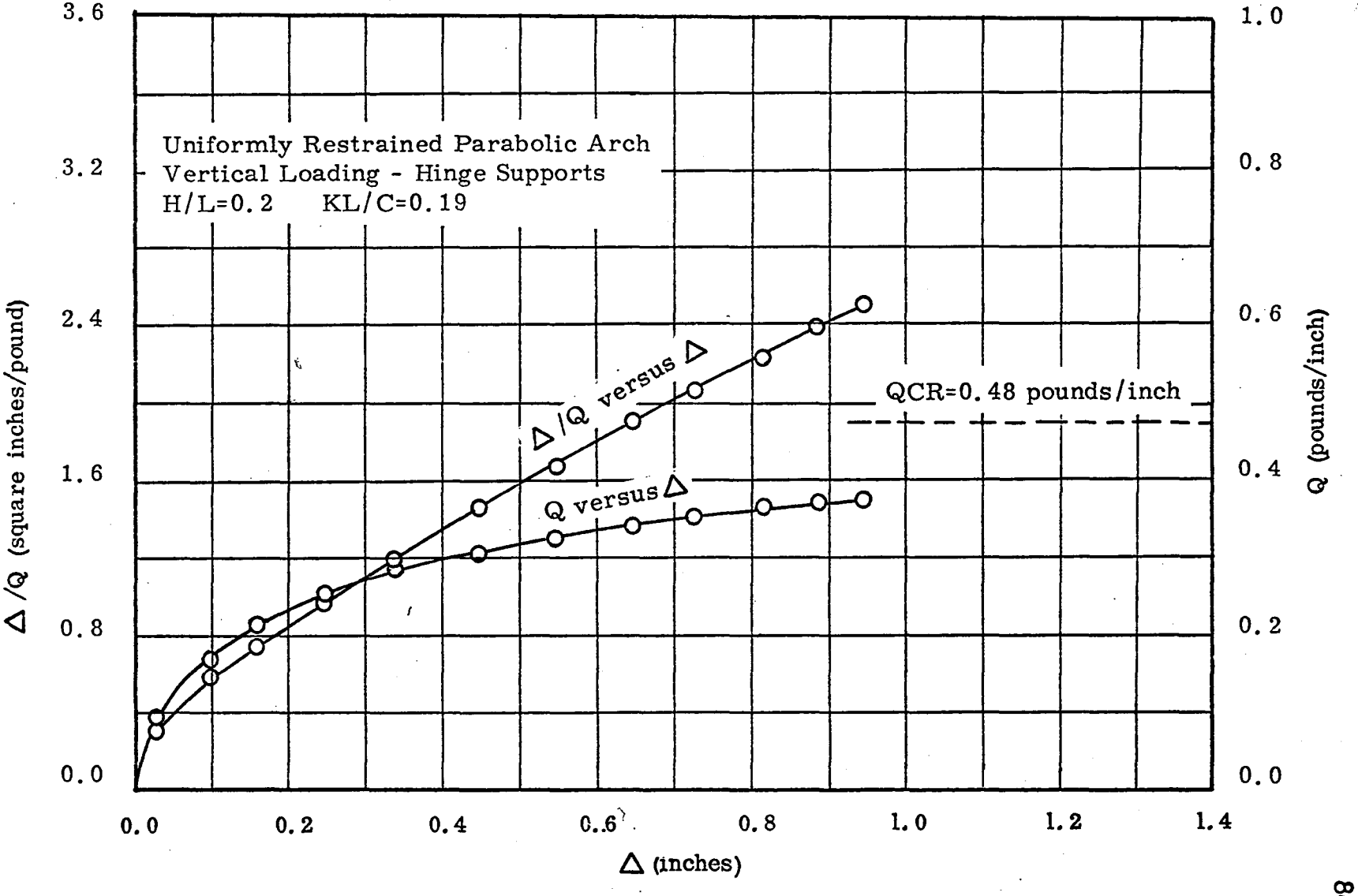

Fig. 49. -- Load-Deflection and Southwell plots for Test No. 29

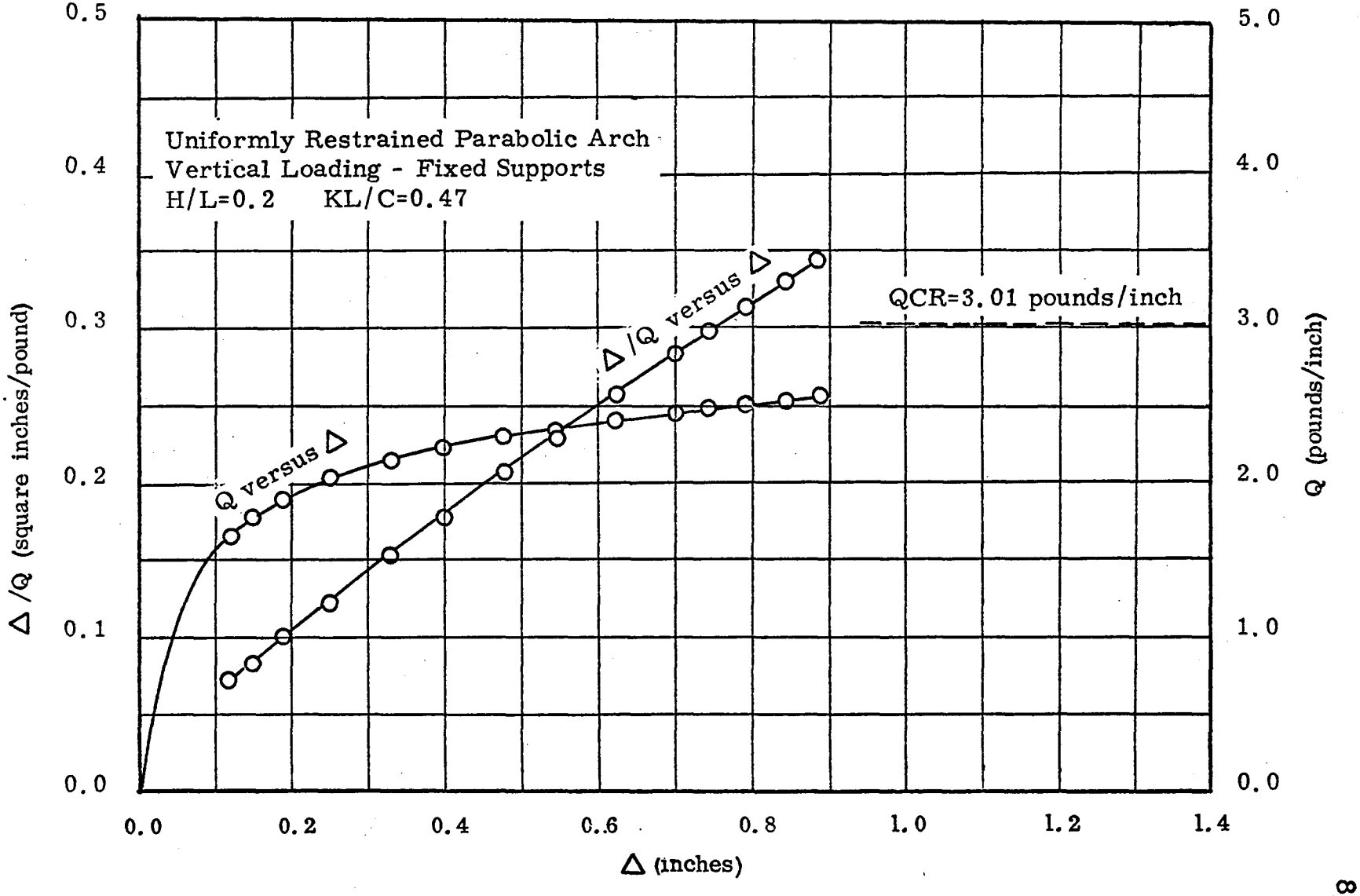

Fig. 50. -- Load-Deflection and Southwell plots for Test No. 30

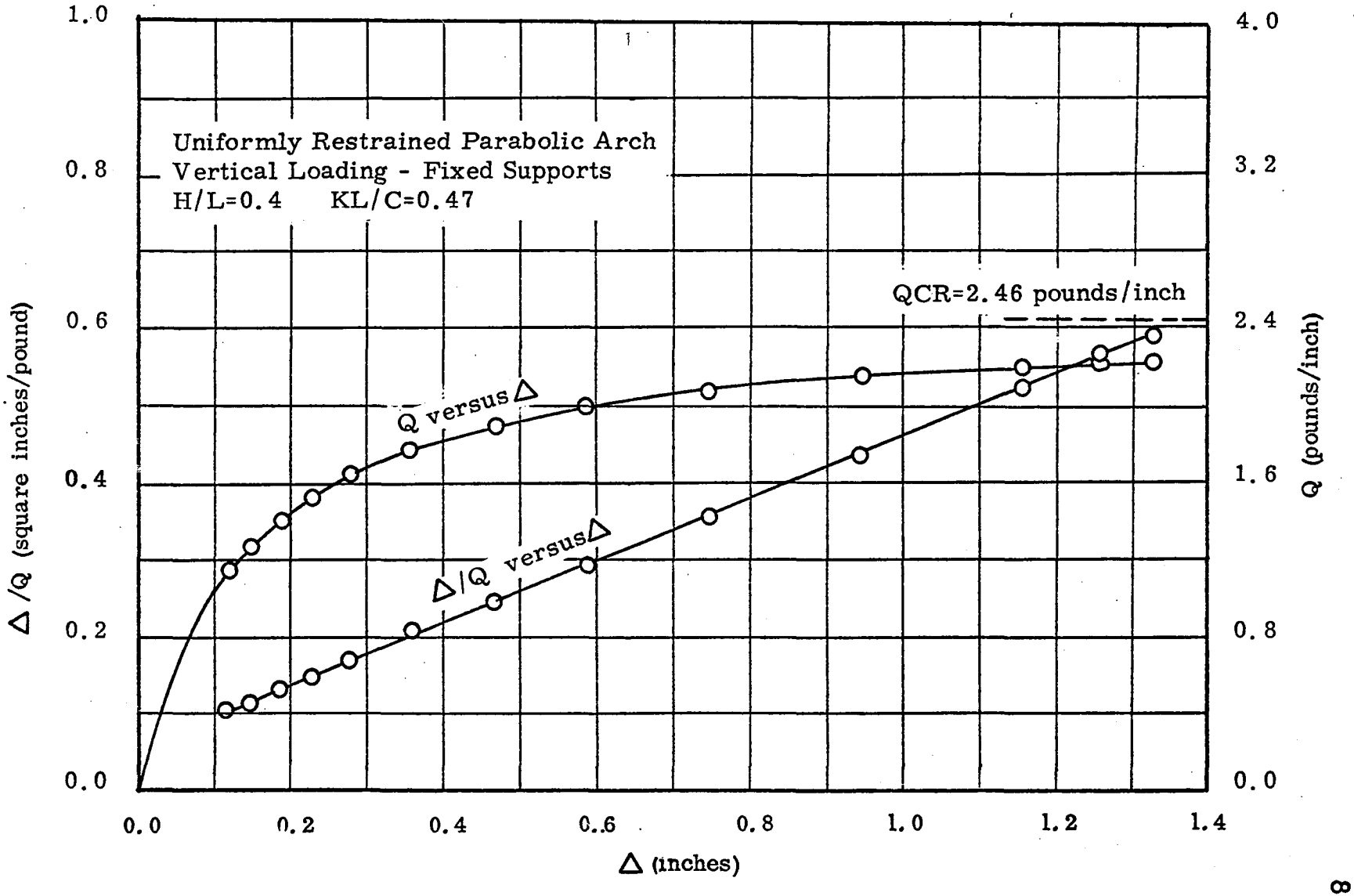

Fig. 51.--Load-Deflection and Southwell plots for Test No. 31

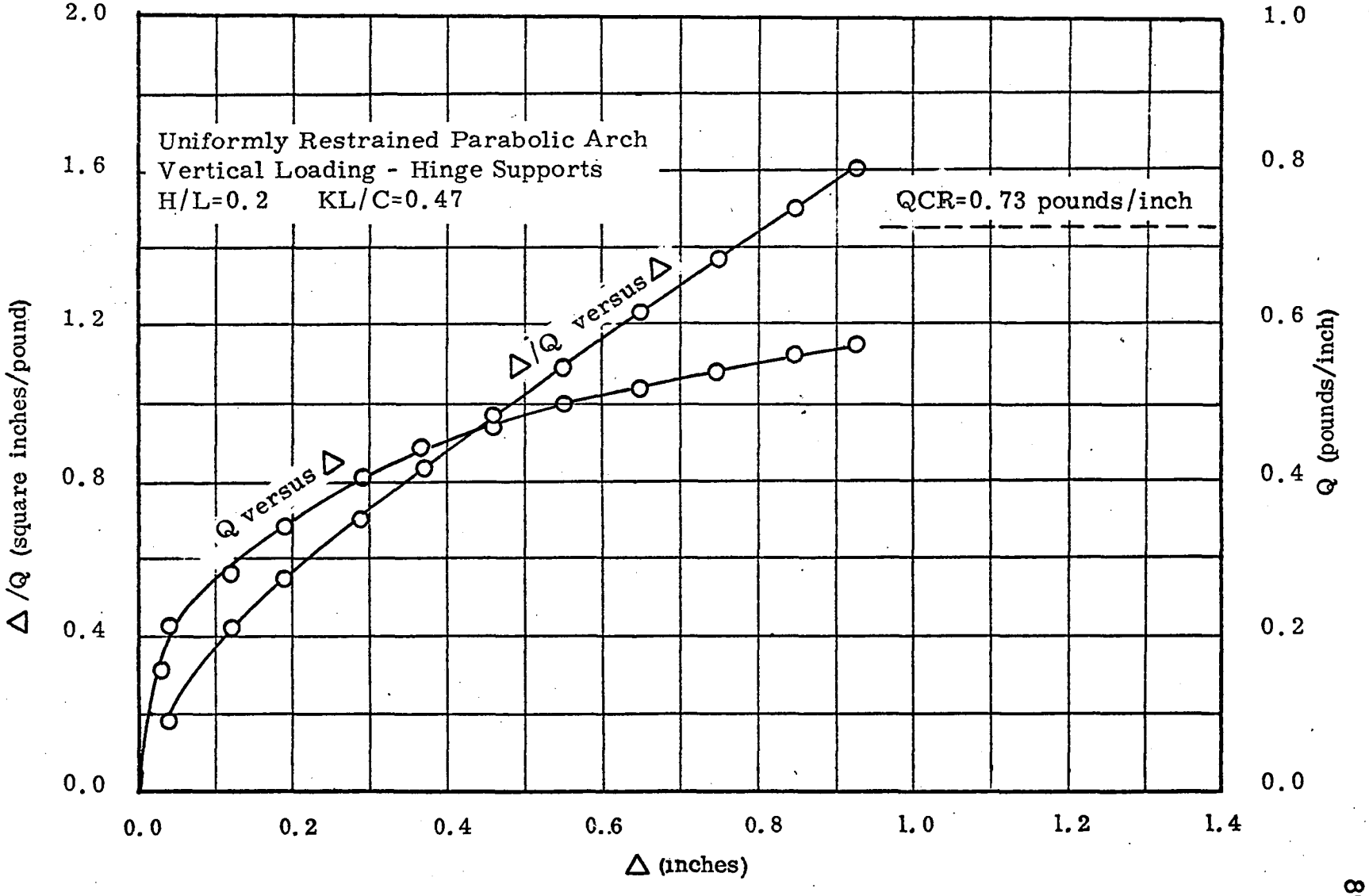

Fig. 52. -- Load-Deflection and Southwell plots for Test No. 32

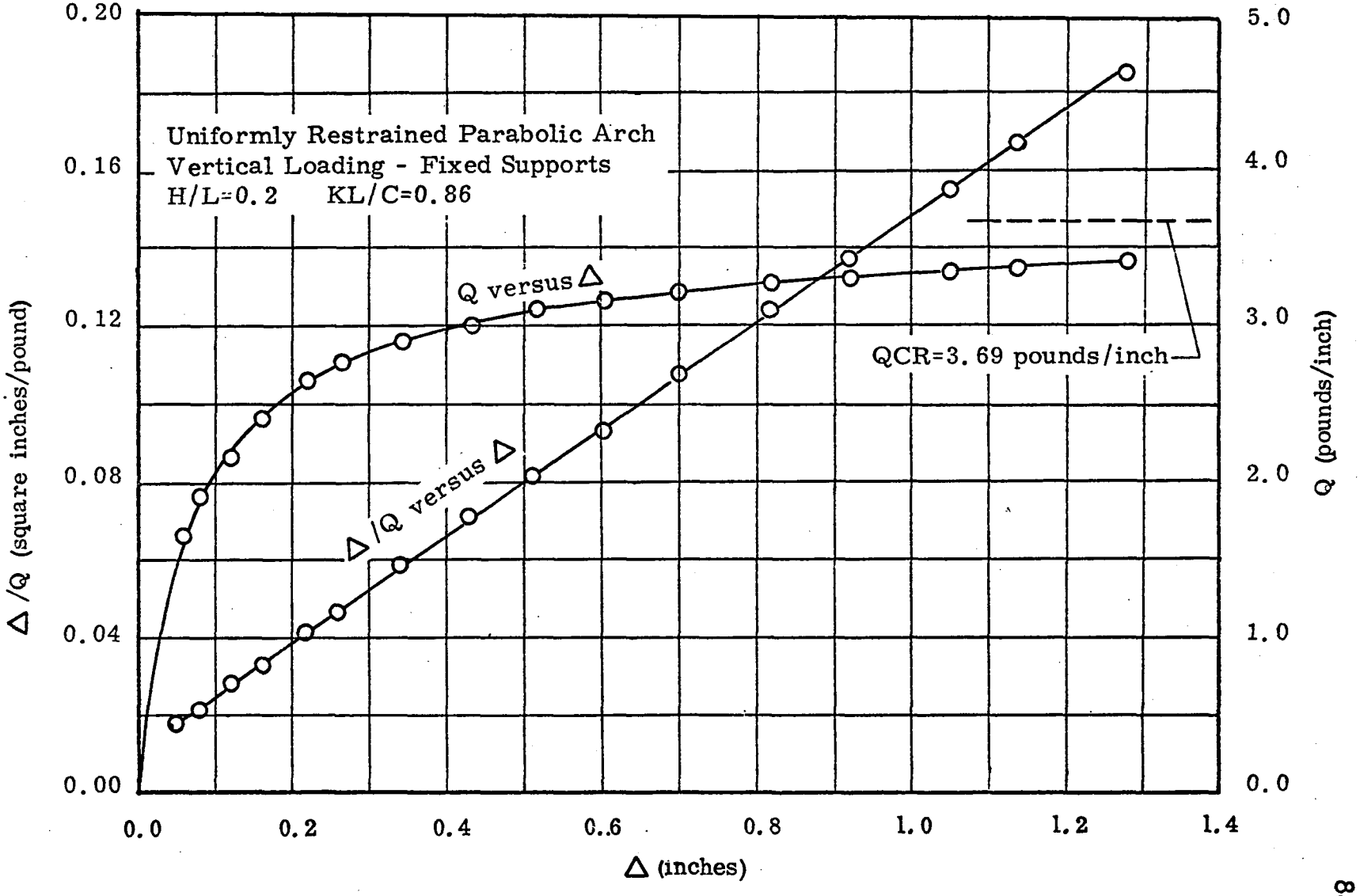

Fig. 53. -- Load-Deflection and Southwell plots for Test No. 33

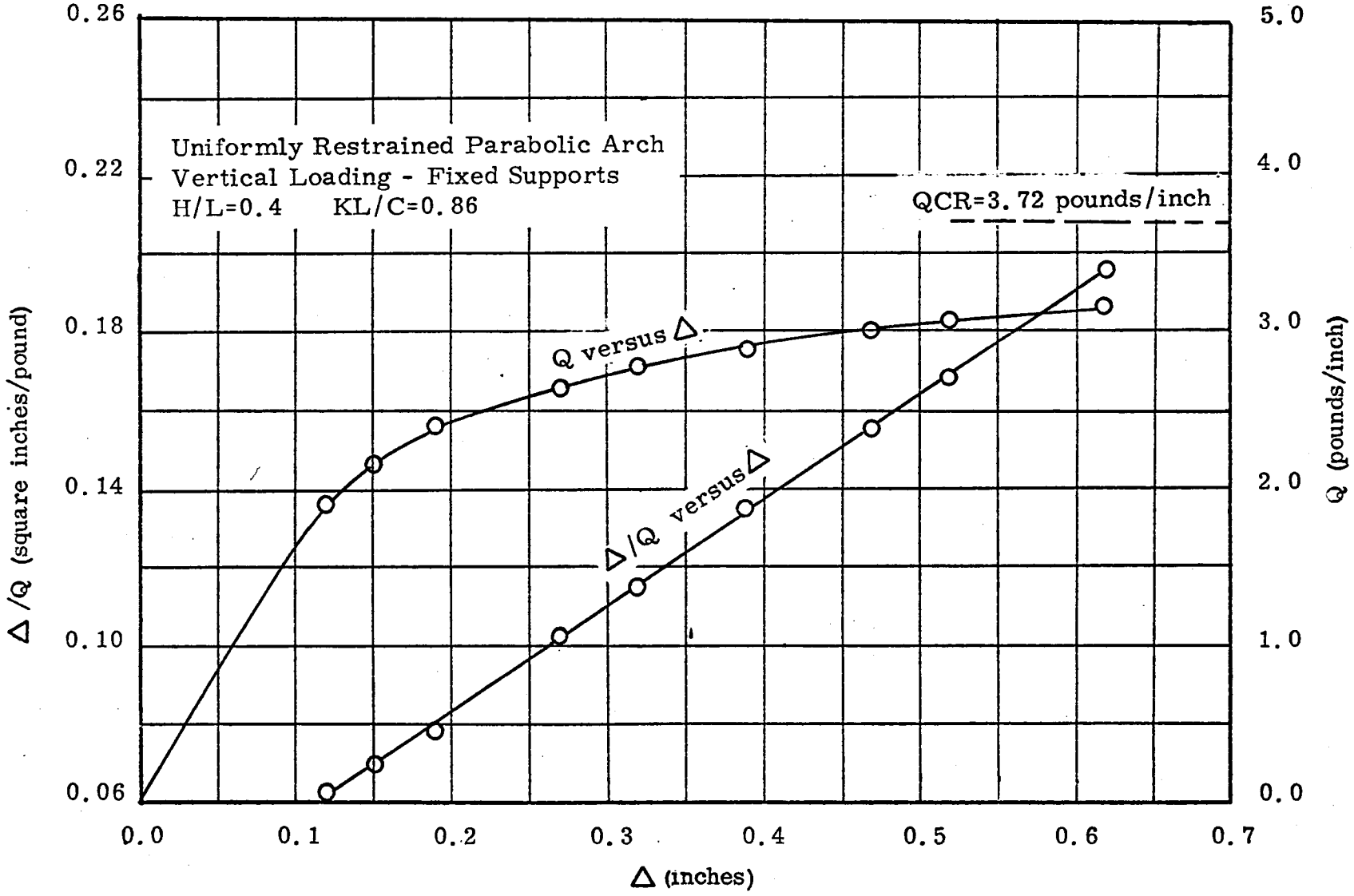

Fig. 54.--Load-Deflection and Southwell plots for Test No. 34

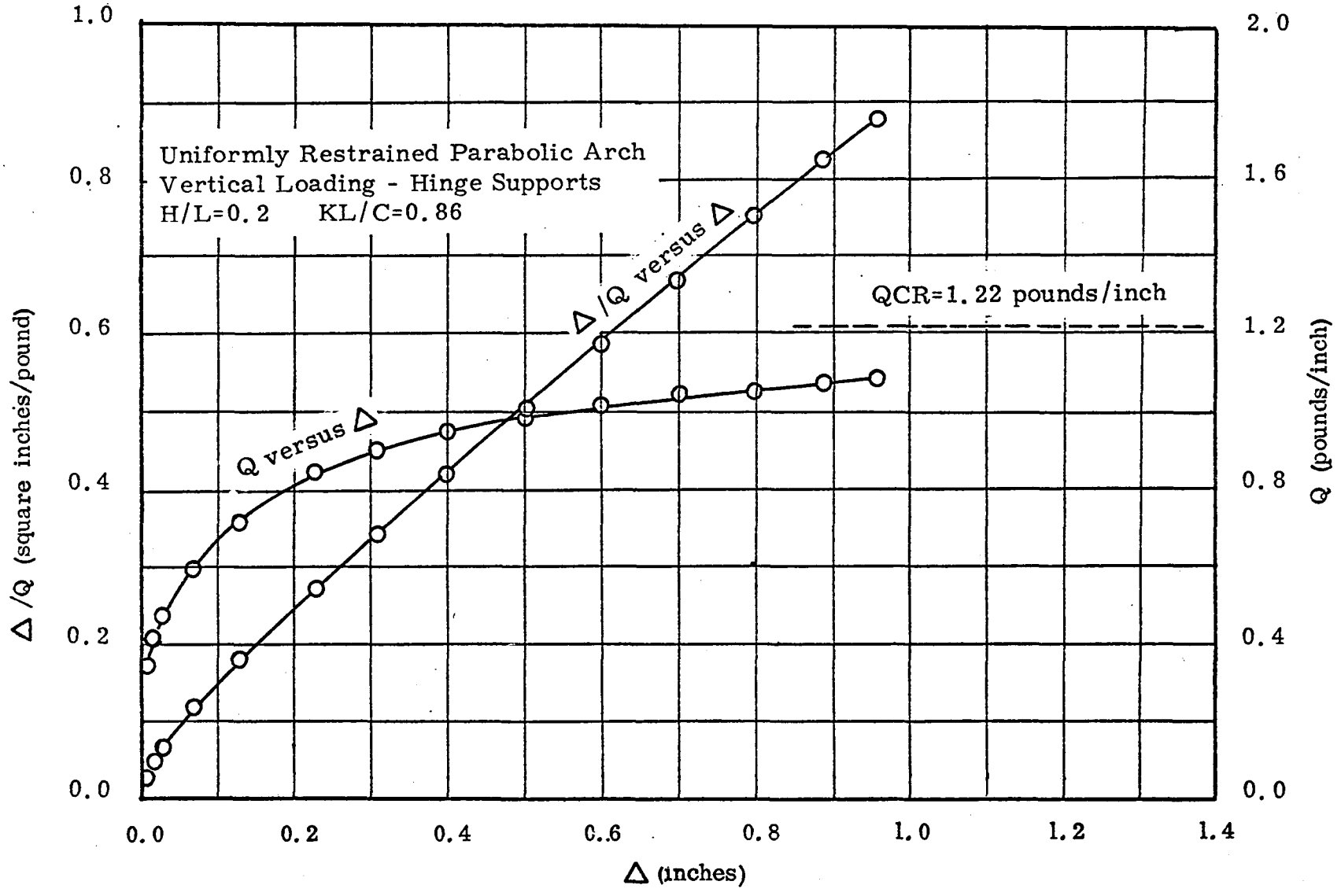

Fig. 55. -- Load-Deflection and Southwell plots for Test No. 35

APPENDIX B

"$\bar{\beta}$" TEST

"$\bar{\beta}$" TEST

The purpose of this test was to verify the variation of the angle of twist ($\bar{\beta}$), based on the theoretical approach of Chapter IV, for a vertically loaded arch with fixed end supports and a rigid restraint at the crown.

Figure 56 below indicates the variation of the lateral deflection ($\bar{v}$), slope of the lateral deflection ($\frac{d\bar{v}}{ds}$) and the angle of twist ($\bar{\beta}$) over one-half of the arch span as obtained from the theoretical solution.

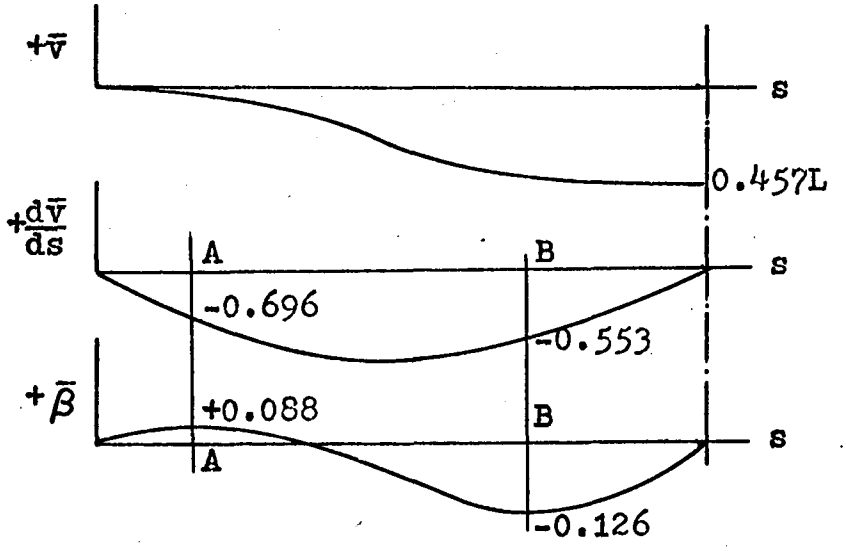

Fig. 56.--Theoretically calculated deflection, slope of deflections and angle of twist curves for Test No. 25

It can be observed that the angle of twist changes algebraic sign within one-half of the arch span. This sign change was not initially anticipated. Hence, the purpose of this test was to verify the sign change.

The experimental data necessary to accomplish the aforementioned was obtained in conjunction with arch Test No. 25.

Two mirrors were mounted on the sides of the arch. A "dot" was painted on each mirror. The location of the mirrors along the arch were such that the "dots" coincided with the points A and B of Figure 56. The angles of twist have maximum values at points A and B.

As illustrated by Figure 57, a transit and a sheet of graph paper mounted on a drawing board were placed at distance "d" perpendicular to each mirror. By observing the "dots" with a transit and also their reflected positions on the graph paper at different stages of loading, it was possible to calculate the horizontal and vertical rotations of the mirrors. The distance "d" was so large relative to the lateral deflection of the arch and the distance between the transit and the graph paper that the horizontal rotation (R_h) and the vertical rotation (R_v) can be approximated as

$$R_h = \frac{\Delta v}{2d} \quad \text{and} \quad R_v = \frac{\Delta h}{2d} \tag{16}$$

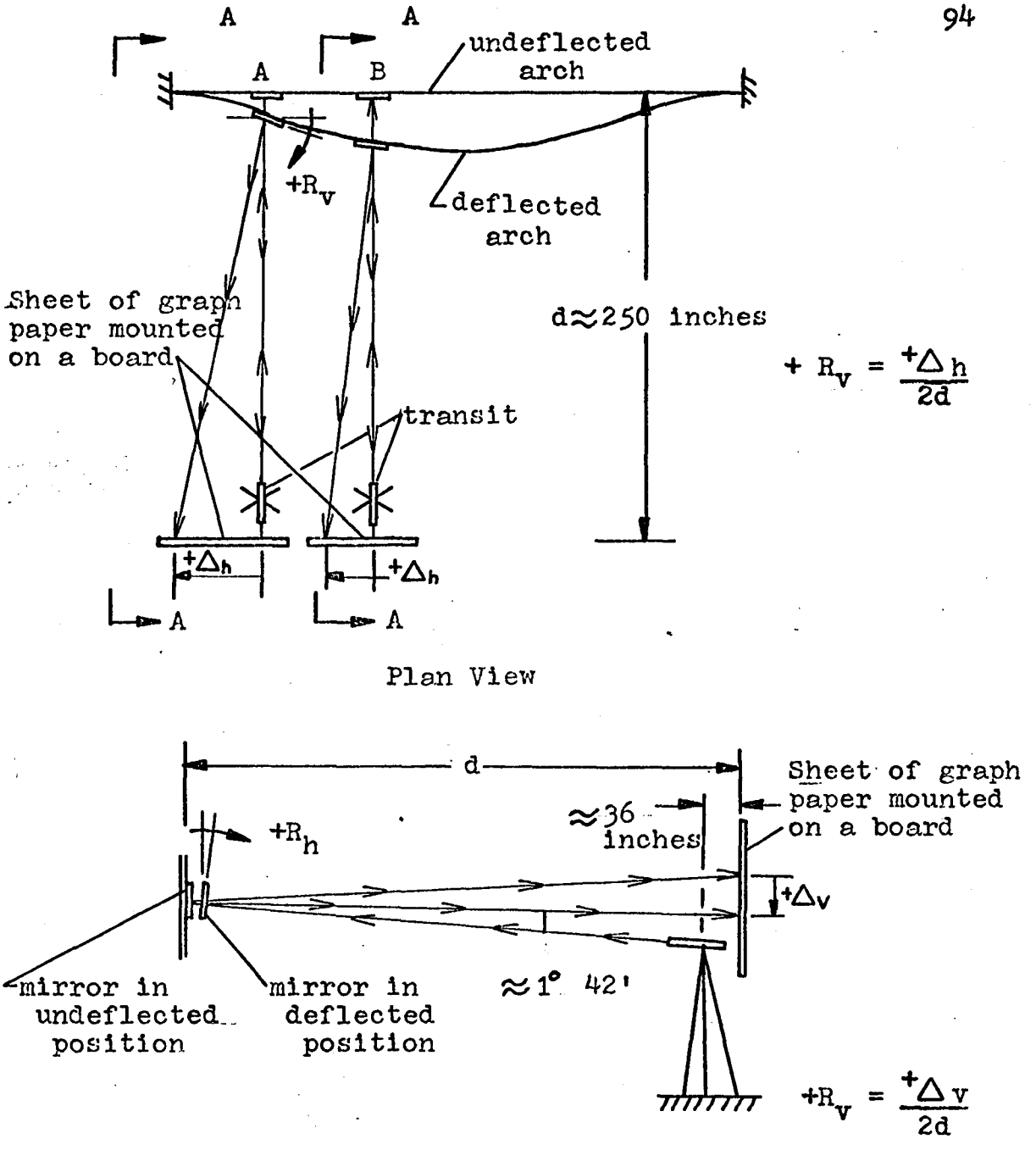

Fig. 57.--Arrangement of instrumentation to facilitate the experimental calculation of the angle of twist

In (16) Δ_h and Δ_v are the changes from the undeflected arch readings of the reflected positions of the "dots" on the graph paper in the horizontal and vertical directions, respectively.

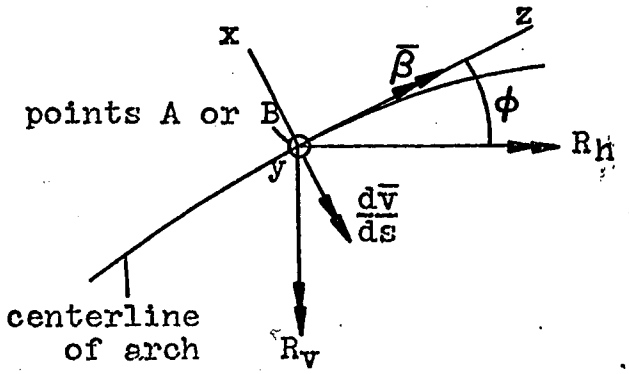

Fig. 58--Profile view of arhc centerline showing rotation at points A and B.

Once the horizontal and vertical rotations of the mirrors (or the arch cross-section at the points A and B) were known the angle of twist and the slope of the lateral deflection could be calculated. By referring to Figure 58 it was determined that

$$\begin{aligned} \bar{\beta} &= R_h \cos\phi - R_v \sin\phi \\ \frac{d\bar{v}}{ds} &= R_h \sin\phi + R_v \cos\phi \end{aligned} \qquad (17)$$

When the arch had a lateral deflection of 0.63 inches, the horizontal and vertical rotations of the arch at points A and B were calculated from (16) to be

$$\begin{aligned} R_h^a &= 0.0142 \text{ radians} \quad R_h^b = 0.0086 \text{ radians} \\ R_v^a &= 0.0139 \text{ radians} \quad R_v^b = 0.0111 \text{ radians} \end{aligned} \tag{18}$$

In (18) and henceforth superscripts "a" and "b" indicate reference to points A and B respectively. The angle in (17) and Figure 58, which is defined by the arctanϕ equal to the slope of the undeflected arch, was found to be

$$\phi^a = 51 \text{ degrees} \quad \phi^b = 22.5 \text{ degrees} \tag{19}$$

Upon the combination of (17), (18) and (19), $\bar{\beta}$ and $\frac{d\bar{v}}{ds}$ are

$$\begin{aligned} \bar{\beta}^a &= +0.0017 \text{ radians} \quad \frac{d\bar{v}^a}{ds} = -0.0197 \text{ radians} \\ \bar{\beta}^b &= -0.00365 \text{ radians} \quad \frac{d\bar{v}^b}{ds} = -0.0135 \text{ radians} \end{aligned} \tag{20}$$

The theoretical values of $\bar{\beta}$ and $\frac{d\bar{v}}{ds}$ shown in Figure 56 were based on a lateral deflection at the crown of the arch $\bar{v} = 0.457L$ where L is the arch span and equal to 59 inches. Therefore, these experimental values must be increased by the ratio 0.457L/0.63, or

$$\bar{\beta}^a = \frac{0.457(59)}{0.63}(0.0017) = +0.073 \text{ radians}$$

$$\frac{d\bar{v}}{ds}^a = \frac{0.457(59)}{0.63}(-0.0197) = -0.842 \text{ radians}$$

$$\bar{\beta}^b = \frac{0.457(59)}{0.63}(-0.00365) = -0.156 \text{ radians} \qquad (21)$$

$$\frac{d\bar{v}}{ds}^b = \frac{0.457(59)}{0.63}(-0.0135) = -0.577 \text{ radians}$$

It can be concluded that the angle of twist and the slope of lateral deflection in (21) obtained from experimental considerations check the theoretically obtained values shown on Figure 56 very favorably. The algebraic sign of the angle of twist does change within one-half of the arch span.

BIBLIOGRAPHY

1. Hencky, H., "Kippsicherheit und Acherbildung an Geschlossenen Kreisringen", Zeitschrift fur angewandt Mathematik und Meckanik, Vol. 1, 1921.

2. Timoshenko, Stephen P., "Kippsicherheit des Gekrummten Stabes mit Kreisformiger Mittellinie", Zeitschrift fur angewandt Mathematik und Meckanik, Vol. 3, 1923.

3. Timoshenko, Stephen P., and Gere, James M., "Theory of Elastic Stability", McGraw-Hill Book Company, Inc., New York, 2nd Ed., 1961, p. 315.

4. Goldberg, John and Bogdanoff, John L., "Out-of-Plane Buckling of I-Section Rings", International Association for Bridge and Structural Engineering, Vol. 22, 1962

5. Oslund, Lars, "Lateral Stability of Bridge Arches Braced with Transverse Bars", Transaction of Royal Institute of Technology, Stockholm, Sweden, 1954.

6. Stussi, F., "Lateral Buckling and Vibration of Arches", Publications of International Association for Bridges and Structural Engineering, Vol. 7, 1943-44.

7. Godden, William G., "The Lateral Buckling of Tied Arches", Institution of Civil Engineers, Proceedings, Vol. 4, Part 3, n. 2, pp. 496-515, August, 1954.

8. Fukasawa, Yasuharu, "The Buckling of Circular Arches by Lateral Flexure and Torsion UnderAxial Trust", Transactions of the Japan Society of Civil Engineers, No. 96, August, 1963.

9. Layrangues, P., "Stabilite' E'lastique de Duex Poutres ou de Deux Arcs Circulaires R'eunis par un Re'seau Continu D'entreloises Horizontales", Travaux, Vol. 47, No. 345, pp. 344-52, July-August, 1963.

10. Layrangues, P., "Stabilite' Laterale des Arcs Circulaires de Section Constante a Parois Minces, a Profil Ouvert ou Ferme'", Annales des Pont et Chausses, Vol. 133, No. 6, pp. 759-77, November-December, 1963.

11. Dabrowski, R., "Stability of Single-Girder Bridge", Rozprawy Inzynierskie, Vol. 5, Part 4, pp. 582-634, 1957.

12. Southwell, R.V., "On the Analysis of Experimental Observations in Problems of Elastic Stability", London Royal Society Proceedings A, Vol. 135, p. 601, 1932.

13. Ariaratnam, S.T., "The Southwell Method for Predicting Critical Loads of Elastic Structures", Quarterly Journal of Mechanics and Applied Mathematics, Vol. 14, Part 2, p. 137, 1961.

14. Love, A.E.H., A Treatise on the Mathematical Theory of Elasticity, Dover Publication, New York, 1944.

15. Conte, S.D., Elementary Numerical Analysis, McGraw-Hill Book Company, Inc., New York, 1965.

16. Ojalvo, Irving U. and Newman, Malcolm, "Buckling of Naturally Curved and Twisted Beams", Under Publication.

17. Carnahan, Brice, Luther, H.A. and Wilkes, James O., Preliminary Edition of Applied Numerical Methods, Vol. 1 and 2, John Wiley and Sons, Inc., New York, 1964.